UNIVERSITY OF CAPE COAST

THE STUDY OF ACOUSTIC EFFECTS IN CARBON ALLOTROPES

KWADWO ANOKYE DOMPREH

2015

UNIVERSITY OF CAPE COAST

THE STUDY OF ACOUSTIC EFFECTS IN CARBON ALLOTROPES

BY

KWADWO ANOKYE DOMPREH

Thesis submitted to the Department of Physics of the School of Physical Sciences, College Of Agriculture and Natural Sciences, University of Cape Coast, in partial fulfilment of the requirements for award of Doctor of Philosophy Degree in Physics

DECEMBER, 2015

DECLARATION

Candidate's Declaration

I hereby declare that this thesis is the result of my own original work and that no part of it has been presented for another degree in this university or elsewhere.

Candidate's Signature..... Date:.....

Name: Kwadwo Anokye Dompreh

Supervisor's Declaration

We hereby declare that the preparation and presentation of the thesis were supervised in accordance with the guidelines on supervision of thesis laid down by the University of Cape Coast.

Supervisor's Signature..... Date:.....

Name: Prof. S. Y. Mensah

Co-Supervisor's Signature..... Date:.....

Name: Dr. Raymond Edziah

ABSTRACT

Acoustic effects such as absorption/amplification of acoustic phonons, Acoustoelectric Effect (AE) and Acoustomagnetoelectric Effect (AME) were studied in Carbon Allotropes. In this thesis, the Carbon Allotropes considered are Graphene Nanoribbon (GNR), 2-dimensional Graphene sheet, and Carbon Nanotubes (CNT). The Boltzmann transport equation (BTE) and the phonon kinetic equation (PKE) were used. All results were analysed numerically and graphically presented. Using BTE for Armchair Graphene Nanoribbon (AGNR), amplification of acoustic waves (Γ/Γ_0) and acoustomagnetoelectric field (E_{same}) were studied in the presence of an external electric and magnetic fields. Γ/Γ_0 and E_{same} were found to depend on the sub-band index (p_i), the nanoribbon width (N), and the dimensionless factor ($\eta = \Omega\tau$).

Using the PKE, amplification (absorption) and AE in 2D graphene and Carbon Nanotubes (CNTs) were studied. On hypersound amplification, a mechanism due Cerenkov emission was employed where the ratio of the drift velocity (V_d) to the velocity of sound (V_s) was considered. In both materials, the dependence of amplification (absorption) on frequency (ω_q) were analysed. Here the acoustic waves were considered as phonons in the hypersound regime. In CNT, it was observed that the maximum amplification was attained as $V_d = 1.1V_s$ which occurred at $E = 51.7$ Vcm^{-1}. For $n = 2$, (where n is an integer) the absorption obtained qualitatively agree with an experimental measurement.

ACKNOWLEDGEMENTS

My heart felt gratitude goes to my Principal Supervisor, Prof. S. Y. Mensah and wife, Prof. (Mrs.) Mensah for their mentorship since my first degree right through my masters degree and upon whose guidance and advice enabled me to complete this Doctoral studies. Without their substantial direction, it would not have been possible to do this research. I will like to thank my Co-Supervisor, Dr. R. Edziah for his encouragements and advice, my head of department, Prof. M. J. Eghan, Head of Physics Department for his directions and also linking me to iThemba LABS as a junior scientist. Not forgetting, Prof. J.J. Fletcher for his advice, and Prof. David K. Essumang, the Dean of the school of Physical Sciences for his directions during my studies. I will also like to thank my parents Mr. S. K. Dinkyine (old Soldier) and Mad. Akua Twumwaa, for their support; my friends and loved ones especially Kwasi Amoafo Frimpong, Dr. Kofi Fosuhene, Mr. Anim Agyei, Mr. Kwadwo Baido and Mr. George Antwi for their support. Last but not least, my special thanks goes to my wife Ernestina Aba Ocran, and kids Akosua Animwaah, Yaa Boatemaa, and Kwame Dompreh. I would also like to thank Awo Boatemaa and kids Kwame Dompreh and Eno Baanie for their encouragement and support, Bernard Barnor, Madam Gladys Agyeiwaah Manison and all my other family members at Adomfe in the Ashanti region.

DEDICATION

To all my family members and loved ones

TABLE OF CONTENTS

LIST OF FIGURES

SYMBOLS

a	distance (m)
P	power (Js^{-1})
ω	angular frequency (rad s^{-1})
β	quantized wave vector
E_g	energy gap (eV)
E_x	electric field (V)
E_{SAME}	Acoustomagnetoelectric field (V/cm)
$\Omega\tau$	dimensionless factor
N	width of Nanoribbon (nm)
p_i	sub-band index
T	temperature (K)
V_D	drift velocity (m/s)
q	acoustic wavenumber (m^{-1})
l	mean free path
ω_q	frequency (s^{-1})
θ	angel in degrees
Γ	hypersound absorption coefficient
j	current density

H_{AA}	matrix element
$E(p)$	energy dispersion
t	nearest-neighbor hopping energy (eV)
H	Hydrogen
F	Fluorine
Cl	Chlorine
Br	Bromine
S	Sulphur
SH	thiol functional group
OH	Hydroxyl

PHYSICAL CONSTANTS

Speed of Light (c)	2.9×10^{8} ms^{-1}
Speed of Sound (V_s)	2.5×10^{5} ms^{-1}
Planck's constant ($\hbar$)	6.582×10^{-16} eVs
Boltzmann's constant (K_β)	8.617×10^{-5} eVK^{-1}
Electronic charge (e)	1.6×10^{-19} J
Deformation potential (Λ)	9 eV
Tight-binding overlapp integral (γ)	0.3 eV
Relaxation time (τ)	10^{-10} s
Chemical potential (ξ)	0.1 eV
Lattice constant (a_{c-c})	1.42 nm
Electron mobility (μ)	10^{5} cm$^2(Vs)^{-1}$
Nearest-neighbor hopping energy (t)	2.8 eV
Fermi Velocity (V_F)	10^{8} cms^{-1}

ABBREVIATIONS

AME	**A**coustoMagneto**E**lectric
GNR	**G**raphene **N**ano **R**ibbon
AGNR	**A**rmchair **G**raphene **N**anoribbon
DC	**D**irect **C**urrent
3D	**T**hree **D**imensional
CNT	**C**arbon **N**anotube
AE	**A**coustoEelectric **E**ffect
CVD	**C**hemical **V**apour **D**eposition
SiC	**S**ilicon **C**arbide
GO	**G**raphite **O**xide
ZGNR	**Z**igzag **G**raphene **N**ano **Ribbon**
SWNT	**S**ingle **W**alled **N**ano **T**ube
MWNT	**M**ulti **W**alled **N**ano **T**ube
TCF	**T**ransparent **C**onducting **F**ilms
ITO	**I**ndium **T**in **O**xide
InGaZnO	**I**ndium **G**allium **Z**inc **O**xide
FEDs	**F**ield **E**mission **D**isplays
OLC	**O**nion-**L**ike **C**arbon

CNW	**C**arbon **N**ano**W**alls
MWPECVD	**M**icrowave **P**lasma **C**hemical
Vapor	**D**eposition
RFPECVD	**R**adio-**F**requency **P**lasma
Enhanced	**C**hemical **V**apor **D**eposition
HWCVD	**H**ot-**W**ire **C**hemical **V**apor **D**epostion
EBEPECVD	**E**lectron **B**eam **E**xcited
Enhanced	**C**hemical **V**apor **D**eposition
SAW	**S**urface **A**coustic **W**aves

CHAPTER ONE

INTRODUCTION

Background

This thesis deals with the study of acoustic effects in Allotropes of Carbon in the hypersound regime having $ql >> 1$. The interactions of acoustic waves with Carbon Allotropes such as Graphene (2D), Armchair Graphene Nanoribbon (AGNR), and Carbon Nanotubes (CNT) are treated. The effects discussed are acoustic phonon amplification, acoustic phonon absorption, Acoustoelectric Effect (AE), and Acoustomagnetoelectric Effect (AME). In this chapter, a brief overview of the various forms of Carbon Allotropes, how they are produced, their energy dispersion, their physical and electrical properties. The scope, objective and organization of the thesis are also presented.

Carbon Allotropes

Among all the known elements on earth, the most versatile and unique material which is capable of forming different architectures at the nanoscale is carbon [1]. In nature, two kinds of pure free carbon known to exit are graphite and diamond [2], but nowadays different forms has been discovered [3]. The different molecular configurations that pure carbon can take are referred to as allotropes of Carbon. These are graphite, diamond, C60 fullerene [4],

Nanotube [5], Graphene [6], Carbon Nanocone [7], Nanochain [8], Graphdiyne [9], and many others.

These allotropes of carbon are determined by the possibility of carbon atoms binding to each other in different ways which gives the variety of the properties of carbon allotropes [10]. Diamond for instance, has each carbon atom covalently bounded to four equivalent neighboring carbon atoms located in the vertices's of a tetrahedron [11]. Each of the four carbon valence electrons therefore participates in the formation of four equivalent covalent bonds. This explains the high hardness and insulating properties of diamond. Graphite on the other hand, has each carbon atoms covalently bonded to three neighboring carbon atoms located at the edges of an equilateral triangle on one plane with the central carbon [12]. Three of the four valence electrons in carbon are involved in the formation of three equivalent bonds in one plane. The density of the fourth electrons are delocalized in a π-electron cloud over and under the graphite plane. This gives the conducting properties of graphite along its layers [13]. The dispersion interactions of the π-electrons ($\pi - \pi$ interaction) causes attraction between the planes of the graphite. The attraction is $\approx 1.4 \pm 0.1$ kcalmol^{-1} per carbon atom [14]. This is strong enough to keep them bound to each other, but much weaker than covalent bonding, which explains the softness of graphite [15].

Hybridization of carbon atoms

Hybridisation (or hybridization) is the concept of mixing atomic orbitals into new hybrid orbitals (with different energies, shapes, etc., than the component atomic orbitals) which is suitable for the pairing of electrons to form chemical bonds in valence bond theory [16]. Hybridization of carbon atomic orbitals into hybrid orbitals can be used to explain the properties of carbon bonding in diamond and graphite. The classification is generally based on the contribution of the *s* and *p* orbitals in hybridized orbital forming π bonds [17].

In Diamond, four valence electrons of carbon are involved in the formation of four equivalent σ-bonds in diamond. That is, one *s* and three *p* atomic orbitals form four equivalent sp^3 hybrid orbitals. In the case of graphite, one *s* and two *p* atomic orbitals form three equivalent sp^2 hybrid orbitals contributing to the formation of three equivalent σ-bonds lying in a plane and the remaining *p* orbitals are perpendicular to this plane contributing to σ-bonds [18]. Thus, diamond and graphite are designated sp^3 and sp^2 carbon allotropes, respectively [19].

sp^n Carbon Allotropes

The sp^n formulation for carbon allotropes are possible for $1 < n < 3$. That is when *n* is an integer, a pure *sp*, sp^2 and sp^3 hybridizations occurs, but if *n* is non-integer, then the allotropes have intermediate hybridization. Carbon atoms can have different hybridizations within one framework which constitute another large family of carbon allotropes with mixed hybridization [20].

Generally, infinite number of combining sp^n, sp^m, sp^l, with non-integer n, m, l

is possible. However, it is convenient to approximate the intermediate hybridizations to the nearest pure ones and consider only four different types of mixed carbon allotropes: $sp-sp^2$, $sp-sp^3$, sp^2-sp^3 and $sp-sp^2-sp^3$ as shown in Figure 1.

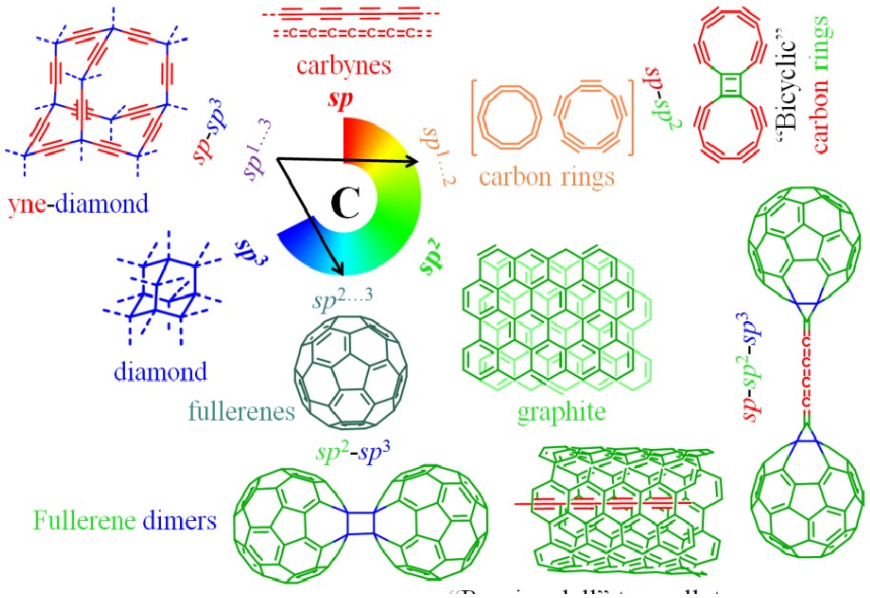

Figure 1: Schematic classification of carbon allotropes with representatives of each type [21]

Different sp^3-carbons can exist depending on their crystal structure. The most abundant conventional diamond has a face-centered cubic crystal structure (thus given the name diamond lattice). However, other crystal structures can be prepared by compressing graphite under different conditions.

Graphene

Graphene is an allotrope of carbon in the form of a two-dimensional, atomic-scale, hexagonal lattice in which one atom forms each vertex (see Figure 2).

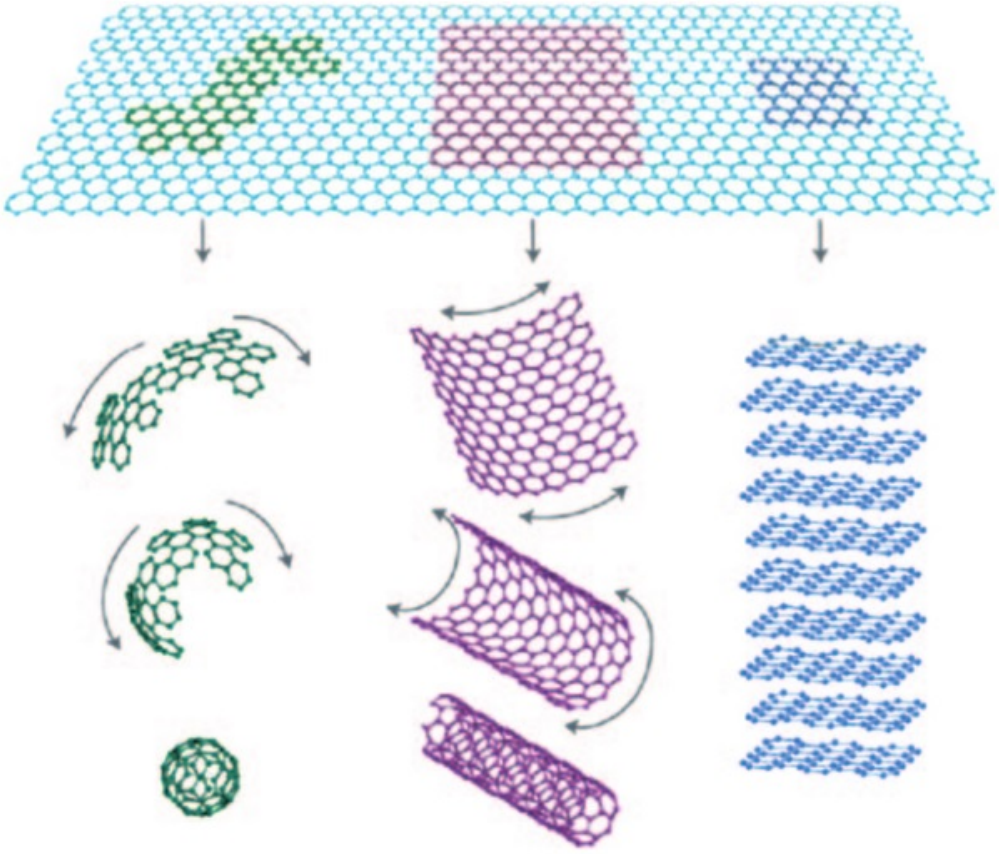

Figure 2: Graphitic forms is a 2D building material for carbon materials wrapped up into 0D buckyballs, rolled into 1D nanotubes or stacked into 3D graphite [30]

Graphene has exceptional properties for future nano-electronics [22–25]. It is an ideal two-dimensional electron gas (2D) system made up of one layer of carbon atom having a high electron mobility (μ) at room temperature with high mechanical and thermodynamic stability [26]. Several unusual phenomena

such as half-integer quantum Hall effect [27], non-zero Berry's phase [28], and minimum conductivity [29] have been observed experimentally in Graphene. It is the basic structural element of other allotropes, including graphite, charcoal, Carbon Nanotubes (CNT) and buckminsterfullerene. Graphene-based electronics has attracted much attention due to high carrier mobility in bulk graphene devices such as sub-terahertz field-effect transistors [31], infrared transparent electrodes [32] and THz plasmonic devices [33].

Electronic band structure of Graphene

In 2D systems, the most popular description of band structure is the tight-binding one, given by Wallace [34]. In Graphene, the band structure exhibits very unique features: the conduction and the valence bands are not separated by a gap, and do not overlap either. In fact, they intersect in two inequivalent points, called Dirac points in the first Brillouin zone [35]. The electron dispersion in the vicinity of the Dirac points is conical (which is the reason for the name) and not parabolic, as in most semiconductors. Hence, the group velocity is independent of the energy. The Fermi level for undoped Graphene lies exactly at the intersection points, and Graphene is a gap-less material. It's dispersion curve resembles that of ultra-relativistic particle, therefore, one can write a relativistic dynamic equation for electron excitations. Such equation can be derived from the tight-binding model [36], and the resulting equation is in fact the well known Dirac equation for massless particles.

The dispersion relation of Graphene

The structure of Graphene is in the form of a honeycomb lattice where the carbon atoms condense due to their sp^2 hybridization. The honeycomb lattice is not a Bravais lattice because two neighbouring sites are not equivalent (see figure 3a and b).

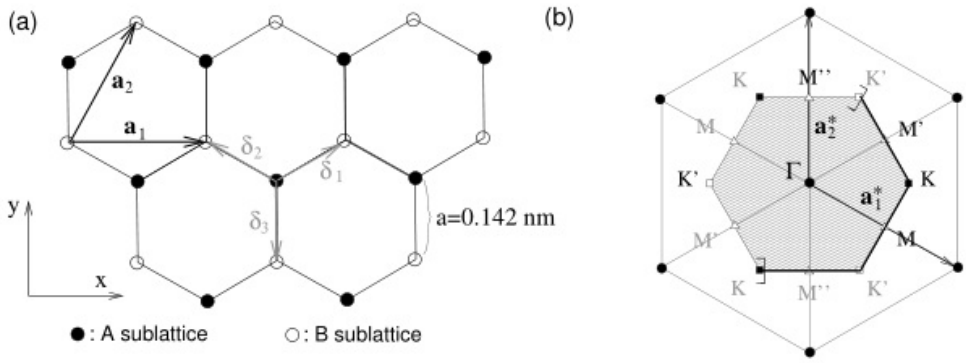

Figure 3: (a) Honeycomb lattice of Graphene. (b) Reciprocal lattice of the triangular lattice [30]

Each carbon atom in the honeycomb lattice is surrounded by three neighbours, with which it shares electrons. Three out of four valence electrons form the chemical bonds, and form a relatively low-lying band. The one, which is left, has a character of a *p* orbital, perpendicular to the Graphene plane. These electrons form the upper, valence and conductance, bands. Graphene has potential applications in single molecule gas detection due to its 2D structure, in transistors because of its high electronic quality, in integrated circuits, in transparent conducting electrodes, as well as in solar cells, ultra capacitors, and bio-devices because of its super physical properties in electric, electronic, optical, thermal, and mechanical properties [30].

In Figure 3a, the vectors δ_1, δ_2, and δ_3 connect the carbon atoms, separated by a distance $a = 0.142$ nm. The vectors a_1 and a_2 are basis vectors of the triangular Bravais lattice. Its primitive lattice vectors are a_1^* and a_2^* (see Figure 3b). The shaded region represents the first Brillouin zone (BZ), with its center Γ and the two inequivalent corners K (black squares) and K′ (white squares). In Graphene, the Hamiltonian that govern the dynamics of electrons is given by the matrix element H_{AA} as

$$H_{AA} = \int d^3 r \Phi_A^* H \Phi_A \tag{1}$$

where, Φ_A and Φ_A^* are the electronic wave function. Introducing the expression for the Bloch function Φ_A in Eqn. (1) gives

$$H_{AA} = \int d^3 r \frac{1}{\sqrt{N}} \sum_{R_A}^{N} \exp(-iR_A)^*(r - R_A) H \frac{1}{\sqrt{N}} \sum_{R'_A}^{N} \exp(-iR'_A)^*(r - R'_A) \tag{2}$$

R is the position of the center of the honeycomb lattice. Considering the nearest neighbour hopping between A atom and all B sub-lattices, and making $R_A = R'_A$ gives

$$\int d^3 r^*(r - R_A) H(r - R_A) = E_0 \tag{3}$$

where E_0 is the energy of the state where

$$H_{AA} = H_{BB} \tag{4}$$

To calculate the off-diagonal element, the definition $H_{AB} = \int d^3r \Phi_A^* H \Phi_B$ is used. By inserting the Bloch functions, the Eqn. (2) transforms to

$$H_{AA} = \int d^3r \frac{1}{\sqrt{N}} \sum_{R_A}^{N} \exp(-iR_A)^*(r - R_A) H \frac{1}{\sqrt{N}} \sum_{R'_A}^{N} \exp(-iR'_B)^*(r - R'_B)$$

$$H_{AA} = \frac{1}{N} \sum_{R_A}^{N} \sum_{R_B}^{N} \exp(-iR_A - R_B) \int d^3r^*(r - R_A) H(r - R_B) \qquad \textbf{(5)}$$

In Eqn. (5) the difference of $R_A - R_B$ appears in the exponential. The B atom has 3 nearest neighbour A atoms. The difference corresponds to 3 vectors m_l with $l = 1, 2, 3$. Therefore the matrix element with these vectors become

$$H_{AB} = \frac{1}{N} \sum_{R_B}^{N} \sum_{m_l}^{N} \exp(-ikm_l) \int d^3r^*(r - m_l) H(r) \qquad \textbf{(6)}$$

k is a unit vector. letting $\int d^3r^*(r - m_l) H(r) = -t$, where t is the hopping parameter between nearest neighbour $t = 2.8$ eV. Eqn. (6) becomes

$$H_{AB} = -t \sum_{m_l} exp(-ikm_l) = -tf(k) \qquad \textbf{(7)}$$

The $f(k)$ is the geometrical factor which can be expressed in terms of the x, y, and z axis. The off-diagonal element H_{AB} can be obtained from

$$H_{AB} = H_{AB}^* = -tf^*(k) = -tf(k) \qquad \textbf{(8)}$$

The geometric values for the vectors m_l are

$$\begin{aligned} m_1 &= ak_y \\ m_2 &= \frac{\sqrt{3}}{2}a(k_x - \frac{1}{\sqrt{3}}k_y) \\ m_3 &= \frac{\sqrt{3a}}{2}(-k_x - \frac{1}{\sqrt{3}}k_y) \end{aligned} \tag{9}$$

Inserting Eqn. (9) into the exponential part of Eqn. (7) gives

$$\begin{aligned} f(k) &= \exp(-ik_y a) + \exp(-ik_x\frac{\sqrt{3a}}{2})\exp(ik_y a/2) + \\ &\quad \exp(ik_x\frac{\sqrt{3a}}{2})\exp(ik_y a/2) \\ &= \exp(-ik_y a) + 2\exp(ik_y a/2)\cos(k_x\frac{\sqrt{3}a}{2}) \\ &= [(\exp(-ik_y a) + 2\exp(ik_y a/2)\cos(k_x\frac{\sqrt{3}a}{2})) \\ &\quad (\exp(ik_y a) + 2\exp(-k_y a/2)\cos(k_x\frac{\sqrt{3}a}{2}))]^{1/2} \\ &= [1 + 2\exp(-k_y\frac{3a}{2}\cos(k_x\frac{\sqrt{3}a}{2})) + 2\exp(ik_y\frac{3a}{2}\cos(k_x\frac{\sqrt{3}a}{2} + \\ &\quad 4\cos^2(k_x\frac{\sqrt{3}a}{2})))]^{1/2} \\ &= [1 + 4\cos^2(k_x\frac{\sqrt{3}a}{2}) + 4\cos(k_x\frac{\sqrt{3}a}{2})\cos(k_y\frac{3a}{2})]^{1/2} \end{aligned} \tag{10}$$

In deriving Eqn. (10) , $f(k) = \sqrt{|f(k)|^2}$ was utilized. The energy levels of a sheet of Graphene can be found by diagonalizing the matrix into (2×2) form where,

$$h_0 \equiv -t(1 + \exp(ika_1) + \exp(ika_2)) = -t(1 + 2\exp(ik_x a)\cos(k_y b)) \tag{11}$$

The eigenvalue is given by

$$E = \pm|h_0| = \pm t\sqrt{1 + 4\cos(k_y b)\cos(k_x a) + 4\cos^2(k_y b)} \qquad \textbf{(12)}$$

with the nearest-neighbour hopping energy $t \approx 2.8$ eV and the lattice constant $a \approx 2.46$ nm. The $\pm$ sign in Eqn. (12) correspond to the conduction and valence bands, respectively, as in Figure 4

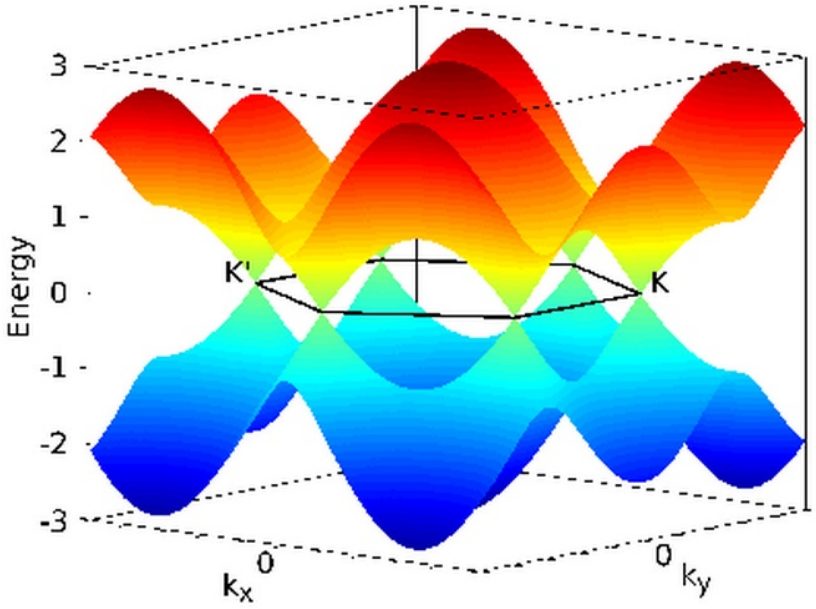

Figure 4: Graphene energy dispersion from π-bonding [37]

making $h_0(k) = 0$, the $E = 0$ at the six corners of the Brillouin zone. Therefore, $\exp(ik_x a)\cos(k_y b) = -1/2$, $k_x a = 0$, $k_y b = \pm 2\pi/3$, and $k_x a = \pi$, $k_y b = \pm\pi/3$. These points provide the states around the Fermi energy which determine the

electronic properties and can be grouped into two of three as

$$(k_x a, k_y b) = (0, -2\pi/3), (-\pi, +\pi/3), (+\pi, +\pi/3)$$

$$(k_x a, k_y b) = (0, +2\pi/3), (-\pi, -\pi/3), (+\pi, -\pi/3)$$

The reciprocal lattice showing Brillouin zone is shaded (see Figure 3b). The electric conduction is determined by the states around the Fermi energy. Therefore, it is useful to develop approximate relation that describe the regions of the $E-k$ plot around $E=0$. This can be done by replacing the expression for $h_0(k) = -\rho(1 + 2e^{ik_x a}\cos(k_y b))$ with a Taylor Expansion around $(k_x a, k_y b) = (0, \pm\frac{2\pi}{3})$, where the Energy gap is zero (note that $h_0 = 0$ at these points) as in Figure 4. In the linear regime, the valence band maximum and the conduction band minimum are degenerate at the K-point, yielding a zero energy band-gap (see Figure 5). Eqn. (12), therefore reduces to

$$E = \pm\hbar V_F |k| \tag{13}$$

(the Fermi velocity $V_F \approx 10^8\ \mathrm{ms}^{-1}$) at the Fermi level with low-energy excitation.

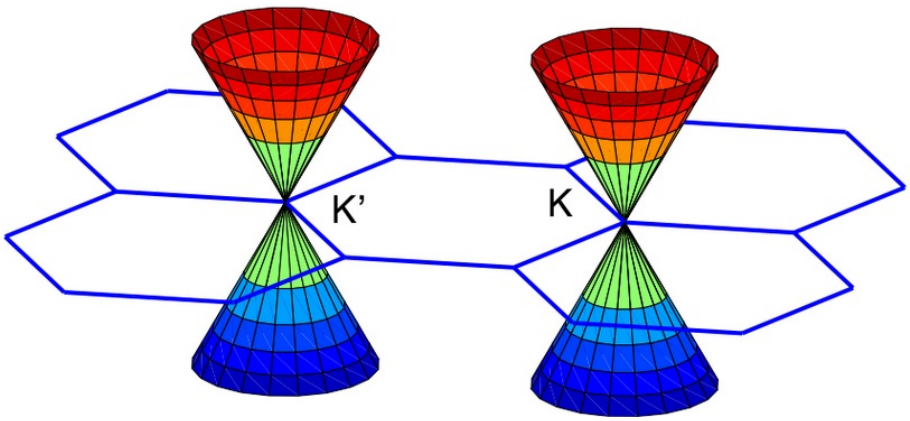

Figure 5: Valence and conduction band edges for Graphene [37]

Production of Graphene

There are various ways of producing Graphene, these involves the following: Mechanical exfoliation, epitaxial growth and chemical exfoliation.

Mechanical exfoliation

Mechanical exfoliation [38] is a process whereby Graphene flakes are produced by continuously cleaving a bulk graphite crystal with a common adhesive tape. This is then transferred onto a cleaned oxidized silicon wafer substrate with visible color. This system of producing Graphene remains the best method to provide a small amount of high-quality samples for the study of a variety of Graphene properties. Also, this technique has been used to easily obtain large size of Graphene (up to 100 μm), with high-quality that has brought enormous experimental results [39–42].

Epitaxial growth

Another method used in the industrial production of graphene is the epitaxial growth method [43]. This involves the growth of Graphene layers on metal carbides using thermal desorption of metal atoms from the carbides surface. The direct deposition on the metal surfaces is by chemical vapor deposition (CVD) [44]. A typical carbide is silicon carbide (SiC) heated to very high temperatures leads to evaporation of Si and the reformation of graphite; where the control of sublimation results in a very thin Graphene coatings over the entire surface of SiC wafers. For economical fabrication of Graphene, Aristov et al., [45] developed a method compatible with mass production. The

commercially synthesized Graphene on Cubic β-SiC/Si substrates, was a simple and cheap procedure used in mass production, but now many other types of carbide have been exploited to produce supported Graphene. For example TiC (111), TiC (410), and TaC (111).

From this method, metal surfaces can efficiently be used as catalyze decomposition of hydrocarbons into graphitic materials which support the growth of Graphene on metallic surfaces by CVD. Even though epitaxial growth is for large-scale area, it is difficult to control morphology, adsorption energy, and high-temperature process.

Chemical exfoliation

Chemical exfoliation deals with the insertion of reactants in the interlayer space of graphite to weaken the Van der Waals cohesion [46]. During the process of chemical exfoliation, the graphite flakes are first forced upon oxidative intercalation of potassium chlorate ($KCLO_3$) in concentrated sulphuric and nitric acid which received carbon sheets with hydroxyl and carboxyl moieties. This suspension is known as graphite oxide (GO). The GO is highly dispersible in water, and can be easily deposited onto SiO_2 substrates. The precipitate of GO obtained is sonicated to form separated Graphene oxide sheet which undergoes another reduction process to form Graphene sheet.

In this chemical exfoliation process, when $KClO_3$ is used, it generates a lot of chlorine dioxide gas which emits a great deal of heat, making the mixture, highly hazardous. Hummers and Offeman (1958) [47] reported a technique based on chemical exfoliation where, graphite is dispersed into a mixture of

concentrated sulfuric acid, sodium nitrate, and potassium permanganate in contrast to $KClO_3$ [48] but H_2O_2 has to be used eliminate MnO_2 generated from $KMnO_4$. They further tried using m – CPBA [49] as an oxidant but the same problem was encounted. Chandra et al., [50] used a novel synthetic procedure for oxidation acidified dichromate, to get high quality and stable aqueous dispersed graphene sheets. Using different reductants such as hydrazine [51], dimethylhydrazine [52], hydroquinone [53], and $NaBH_4$ [54], under alkaline conditions [55] or with thermal methods [56], when GO′s are deposited, the chemical reduction of GO was accompanied by the elimination of epoxy and carboxyl groups. Due to the hazardous nature of the reductants, there are lots of interests on green routes to speed de-oxygenation of Graphene oxide. One of such techniques was introduced by Wakeland et al., [56] which describes the synthesis of Graphene from GO using urea as expansion reducing agent heated in an inert gas environment (N_2) for a very short time to a moderate temperature (600^oC). Chen et al., [57] with the assistance of microwaves in a mixed solution of N, N-dimethylacetamide, and water ($DMAc/H_20$) achieved thermal reduction of Graphene oxide (GO) to Graphene.

Electronic properties of Graphene and Graphite

The electronic properties of Graphene, and graphite are determined by the bonding π- and anti-bonding π^*-orbitals that form wide electronic valence and conduction bands [5]. Theoretical calculations show that the π-band overlap in graphite disappears as the layers are further separated over their equilibrium

distance in graphite. This leads to decoupled Graphene layers that can be described as a zero-gap semiconductor.

The π-band electronic dispersion for Graphene near the six corners of the 2D hexagonal Brillouin zone is found to be linear. Thus, "cones" of carriers (holes and electrons) appear in the corners of a 2D Brillouin zone whose points touch at the Fermi energy. In Graphene, most of the experimental research focuses on the electronic properties. This is mostly utilized in designing Graphene transistors with the ability to continuously tune the charge carriers from holes to electrons. This is an example of the gate dependence in single layer Graphene. This effect is most pronounced in the thinnest samples whereas samples from multiple layers show much weaker gate dependence due to screening of the electric field by the other layers. At low temperatures and also, high magnetic fields, the exceptional mobility of Graphene allows for the observation of the quantum hall effect for both electrons and holes [5]. Due to its unique band structure, the Graphene quantum Hall effect exhibits a subtle difference from the conventional quantum Hall effect in that plateaus occur at half integers of $\frac{4e^2}{\hbar}$. For more practical applications, one would like to utilize the strong gate dependence of Graphene for either sensing or transistor applications. Unfortunately, Graphene has no band gap and correspondingly resistivity changes are small. Therefore, a Graphene transistor by its very nature is plagued by a low on/off ratio. However, one way around this limitation is to carve Graphene into narrow ribbons. By shrinking the ribbon the momentum of charge carriers in the transverse direction becomes quantized which results in the opening of a band gap.

Fullerene

Fullerene belongs to zero-dimensional carbon nanomaterials. Fullerenes are spherically shaped molecules with carbon atoms located at the corner of a polyhedral structure consisting of pentagons and hexagons [58]. It is referred to as "buckyball" due to its shape and was named after Richard Buckminster Fuller. In a Laser spectroscopy experiments, fullerenes were discovered in 1985, by researchers at Rice University. Kroto et al., [59] used laser vaporization of carbon in an inert atmosphere to produce microscopic amounts of fullerenes. However, Kretschmer et al., [60] produced isolable quantities of C60 by using an arc to vaporize graphite. Alekseyev and Dyuzhev [61], further, explained the formation of fullerene in an arc discharge and the problems associated with arc discharge calculations to the immediate fullerene molecule assembly.

Research in fullerene formation has become a field of intense study in the last two decades with a variety of fullerene derivatives with unique properties produced. Howard et al., (1991 and 1992) [62, 63], developed a method of synthesis of fullerenes in combustion and observed fullerenes C60 and C70 from benzene/oxygen flames whilst, Xie et al., (1999) [64] synthesized fullerenes C60 and C70 via microwave plasma from chloroform at low-pressure argon atmosphere. This method by [65] opened a new way to large quantity and low-cost production of fullerenes, various perchlorinated intermediates of fullerenes, and the perchlorinated carbon clusters. In 1993, Taylor et al., [66] synthesised C60 and C70 by pyrolysis of naphthalene at $1,000^0$ C. From this method, closed fullerene cages can be prepared from

well-defined aromatic fragments. Koshio et al., [65], in 2002 used pyrolysis method to produce fullerene. In 2009, a new method by Chen and Lou [67] was reported. Here, they revealed that, C60 can be synthesized from the reduction of CO_2 via metallic lithium or $MgCO_3$ at 700^0 C, *ca*. 100 MPa. Applications of fullerene include their use in medicine to produce the specific antibiotics and drugs for certain cancers particularly melanoma. On the other hand, due to their specific properties, fullerenes have had great applications in the field of superconductivity.

Fullerence structures

Fullerence structures (Fs) with incorporated iron atoms were reported by Koprinarov et al., [68]. These were obtained via d.c arc discharge between carbon electrodes in air and ferrocene gas mixture ambient. This method made fullerene creation easier and increased the product quantity. Richter et al., [69] also, devised a novel method of fullerene production by using acetylene/oxygen/argon flat flames by adding chlorine and burning at low pressure. These and many other chemical syntheses of fullerenes also have been reported [70].

Graphene Nanoribbon (GNR)

Graphene ribbons (GNRs) are a few nanometres in width ($\leq$ 50 nm) and are one of the many carbon nanostructures based materials which have been extensively studied [71–84]. These GNRs are geometrically terminated Graphene, having their electronic structure modelled by imposing appropriate

boundary conditions. They are one-dimensional structures with hexagonal two dimensional carbon lattices, which are stripes of Graphene. GNR's exist in two forms: Armchair and Zigzag . GNRs with Armchair edges (AGNR) can be either metallic or semiconducting depending on their widths [85, 86] and that GNRs with "zigzag" edges (ZGNR) are metallic with peculiar edge states on both sides of the ribbon regardless of their widths [87, 88]. The Armchair Graphene Nanoribbon (AGNR) and Zigzag Graphene Nanoribbon (ZGNR) (see Figure 6), with well-defined width have being extensively studied using the tight-binding approach [89–91] and edge functionalization method in Density Functional Theory (DFT) [93].

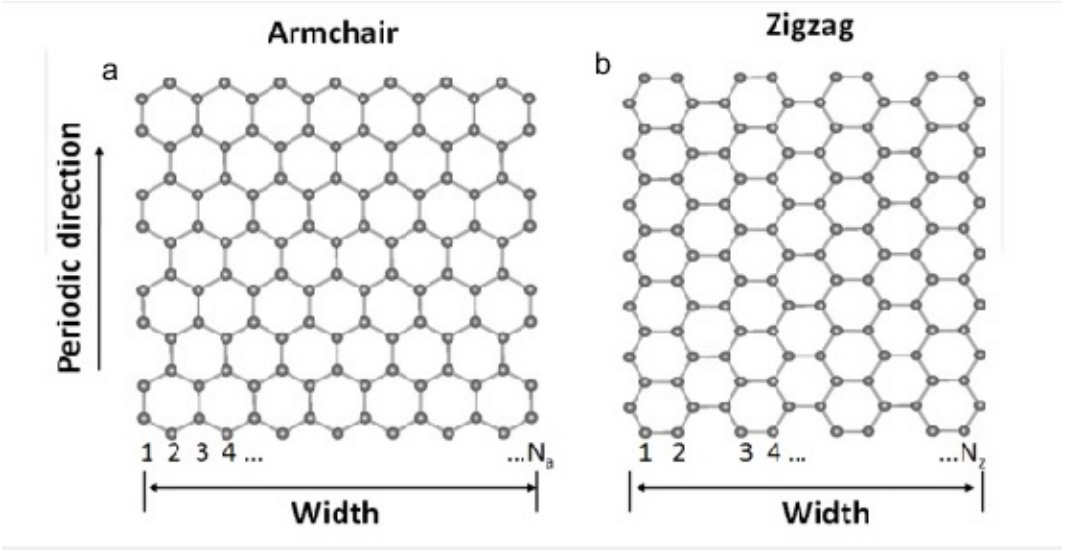

Figure 6: Graphene Nanoribbon edges showing (a) Armchair edge and (b) Zigzag edge [90]

Mostly, -H, -F, -Cl, -Br, -S, -SH and -OH are used to engineer the band gap so as to utilize the various properties of GNRs for electronic applications. Although the tight-binding approximation based on π-states of carbon can accurately describe the energy dispersion of the carbon sheet, a careful

consideration of edge effects in GNRs is required to determine their band structures accurately [94, 95]. Recent ab-initio calculations [96–98] reveal that all GNRs with hydrogen-passivated armchair or zigzag-shaped edges have nonzero direct bandgaps. The gap size decreases as the width of the GNR increases, approaching zero in Graphene in the limit of infinite width.

Energy dispersion of Graphene Nanoribbon

The energy dispersion relation $\varepsilon(\vec{p})$ for GNRs band near the Fermi point is expressed [37] as

$$\varepsilon(\vec{p}) = \frac{E_g}{2}\sqrt{[(1+\frac{\vec{p}^2}{\hbar^2\beta^2})]} \tag{14}$$

where the energy gap $E_g = 3ta_{c-c}\beta$, with β being the quantized wave vector given as

$$\beta = \frac{2\pi}{a_{c-c}\sqrt{3}}\left(\frac{p_i}{N+1} - \frac{2}{3}\right) \tag{15}$$

The p_i is the subband index, N the number of dimmer lines which determine the width of the AGNR, $a_{c-c} = 1.42$ Å is the carbon-carbon (c-c) bond length, $t = 2.7$ eV is the nearest neighbor (c-c) tight-binding overlap energy.

Carbon Nanotubes (CNT)

Carbon Nanotubes (CNT) (also known as a buckytube) discovered by Iijima [99] is a member of the fullerene structural family and are emerging as important materials for electronic applications. Due to the remarkable electrical and mechanical properties [100–102] which are attributed to its unusual band structures [103–105], the π-bonding and anti-bonding (π^*)

energy band of CNT crosses at the Fermi level in a linear manner [106–108]. CNT occur by wrapping Graphene into cylinders and are categorized as single-walled nanotubes (SWNTs) and multi-walled nanotubes (MWNTs) (see Figure 7).

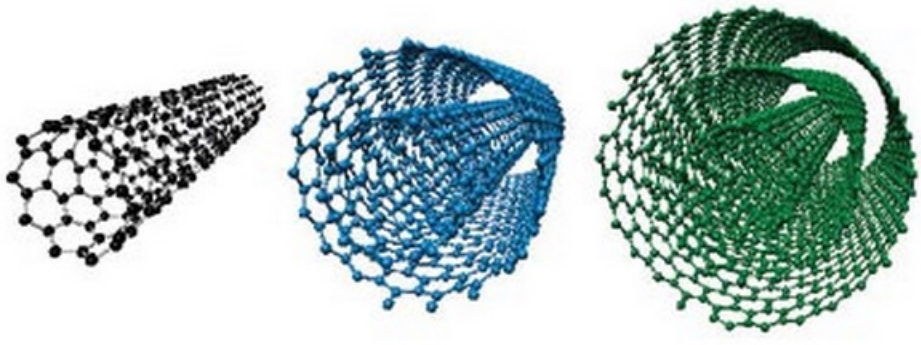

Figure 7: One, two and three walls of Carbon Nanotube [109]

The SWNTs can be formed in three different designs: Armchair, Chiral, and Zigzag depending on the way the Graphene is wrapped into a cylinder. A SWNT's structure is represented by a pair of indices (n, m) called the chiral vector (see Figure 8).

The metallic and semi-conducting Single-Walled Carbon Nanotube (SWCNT) have been proposed as the most viable materials to develop high performance thin films to completely eliminate the use of critical metals in electronic devices such as: i) Indium in transparent conducting films (TCF, indium oxide doped by tin, ITO) and ii) Indium and Gallium as semiconductor InGaZnO ($a - IGZO$) in thin film field effect transistors ($TFTs$) for applications in optoelectronic [112, 113]. The unusual band structure [114] of CNT, coupled

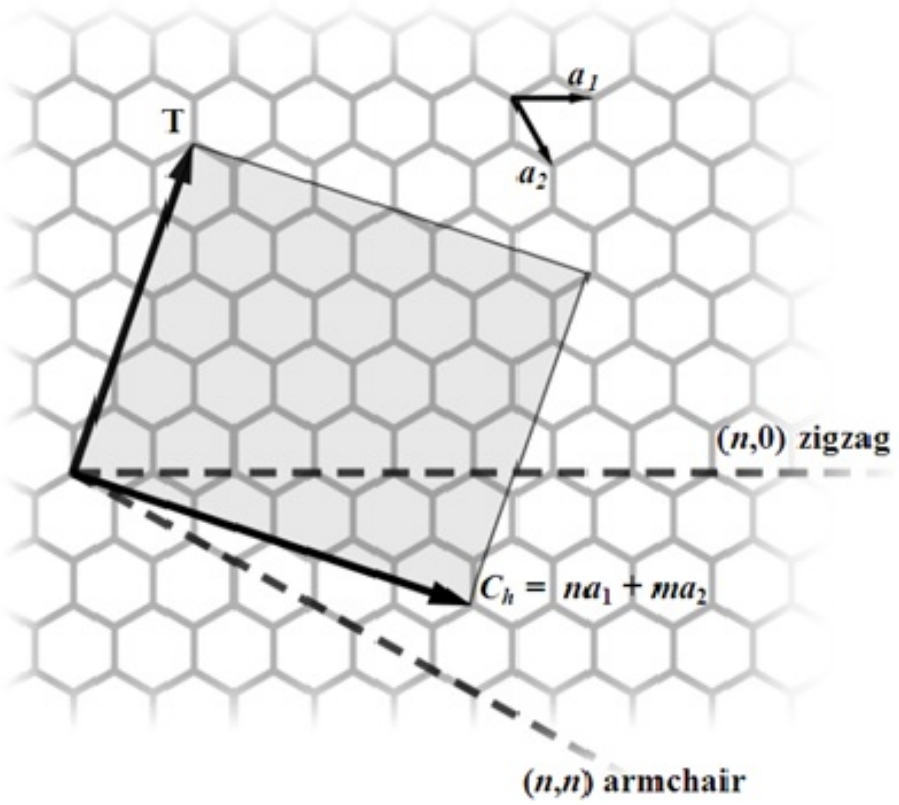

Figure 8: The (n,m) denotes the nanotube naming scheme. T denotes the tube axis, and a_1 and a_2 are the unit vectors of Graphene in real space [109]

with large electron densities and high drift velocities (with electron mobility of $\mu \approx 10^5\ cm^2/Vs$) at room temperatures opens a way for employing carrier control processes rather than direct electrical control. From the tight-binding approach, the dispersion law for Zigzag CNT is given as

$$E(p) = \pm\gamma_0\sqrt{1+4\cos(ap_z)\cos(\frac{as\Delta p_\phi}{\sqrt{3}})+4\cos^2(\frac{as\Delta p_\phi}{\sqrt{3}})} \qquad \textbf{(16)}$$

In view of the transverse quantization of the quasi-momentum, its transverse component can take m discrete values, $p_\phi = s\Delta p_\phi = \pi\sqrt{3}s/am(s = 1,...,m)$ and we used $E(s\Delta p_\phi, p_z) \equiv E_s(p_z)$ in both equations. As different from p_ϕ, we assume p_z continuously varies within the range $0 \leq p_z \leq 2\pi/a$ which corresponds to the model of infinitely long $CN(L = \infty)$. In the linear

approximation, the energy dispersion $\varepsilon(\vec{p})$ relation is given as

$$E(p_z) = \varepsilon_0 \pm \frac{\sqrt{3}}{2\hbar}\gamma_0 b(\vec{p} - \vec{p}_0) \tag{17}$$

The ε_0 is the electron energy in the Brillouin zone at momentum p_0, b is the lattice constant , γ_0 is the tight-binding overlap integral ($\gamma_0 = 2.54$ eV). The $\pm$ sign indicates that in the vicinity of the tangent point, the bands exhibit mirror symmetry with respect to each point. For Armchair CNT, the dispersion relation yields

$$E(p_z) = \pm\gamma_0\sqrt{1 + 4\cos(\frac{v\pi}{n})\cos(\frac{k\sqrt{3}a_{cc}}{2}) + 4\cos^2(\frac{k\sqrt{3}a_{cc}}{2})} \tag{18}$$

Here $\gamma_0 \approx 3.0$ eV is the overlapping integral, $a = \frac{3b}{2\hbar}$, $b = 0.142$ nm is the $c-c$ bond length. The $-$ and $+$ signs correspond to the valence and conduction bands, respectively. At the Fermi points, the conduction and valence band cross each other , therefore when $v = 0$, $k_F = \pm 2\pi/3\sqrt{3}a_{cc}$ which gives the metallic nature to the armchair nanotube. Making the substitution, $k = k_t + 3k_0/2$ gives

$$E = \pm t_0(1 - 2\cos(\frac{k_t\sqrt{3}a_{cc}}{2})) \tag{19}$$

where, $k_0 = 2k_F/3\sqrt{3}a_{cc} \approx 1.7 \times 10^{10}$ m^{-1}.

Properties of Carbon Nanotubes

The structure and properties of Carbon nanotubes (CNTs), have great applications in very wide areas of science and technology including nano-technology [115], electronics [116], optics [117], materials science, and architecture [118]. The structural applications of CNTs cover a wide ranges of industries such as clothes, sports equipment such as stronger and lighter tennis rackets, bike, various kinds of balls, combat jacket like combat jackets, concrete as the increase of the tensile strength, polyethylene, the possibility of the space elevator, synthetic muscles in medical science and sports, high tensile strength fibers, applications in the build of bridges, ultrahigh-speed flywheels, and applications in fire protection [118–120].

In electromagnetic field, the applications of CNTs are grouped in respect of their uses in chemical nanowires, conductive films, electric motor brushes, magnets, optical ignition, their applications to produce light bulb filament (as an alternative for tungsten filaments), the applications relating to their fine superconductivity properties, in display screens such as field emission displays (FEDs), the applications in industrial transistor and the electromagnetic antenna [121, 122]. Other applications of CNTs are in respect of their chemical applications, including air pollution filters, biotech containers, hydrogen storage, water filtration, and the mechanical applications such as using them as the faster oscillators, nanotube membrane, slick surface, carbon nanotube actuators, infrared detector, radiometric standard, and their application as the thermal radiation for space satellites [123, 124]. It is worth noting that the wide range of applications of CNTs mentioned is due to their unique mechanical,

electrical, thermal, and optical properties which are briefly introduced in this section.

Strength of Carbon Nanotube

Carbon nanotubes (CNTs) are the strongest materials known. This is is due to the covalent sp^2 bonds between the individual carbon atoms. Yu et al., (2000) [125] tested the tensile strength of a multiwalled carbon nanotube (MWCNT) to access up to 63 GPa. The specific strength is defined as the material's strength (force per unit area at breaking point) divided by its density. Considering the low density of CNTs (1.3 to 1.4 gcm^3), the specific strength of CNTs is obtained up to $kNmkg^{-1}$ which is the the best of the known materials.

Electrical properties of Carbon Nanotubes

The electrical properties of a nanotube strongly depend on its structure due to the symmetrical and exceptionally electronic structure of Graphene [126–128]. Lu and Chen [129], reported armchair nanotubes to be metallic otherwise, is semiconducting with a very small band. (5,0) SWNTs is a semiconductor; but, due to the curvature effects in small diameter carbon nanotubes, it is metallic. Zigzag and chiral SWNTs with small diameters that are expected to be metallic have actually a finite gap [129].

Zhou et al., [130] suggested SWNTs can show excellent electronic properties such as the carrier mobility about 104 $cm^2V^{-1}s^{-1}$ which is higher than that of silicon. Dai et al., [131], explained that CNTs can carry an electrical current density of about 200 Acm^{-2}. Such a current density is three orders of magnitude

higher than a typical metal, for example, Cu or Al [132]. In 2006, Pierson [134] noted that the electrical properties of multiwalled carbon nanotubes (MWNTs) exhibit superconductivity with a transition temperature as high as 12 K which is approximately 30 times greater than that for ropes of SWNTs or for MWNTs with noninterconnected shells [134].

Onion-like Carbons

Carbon onions are spherically closed carbon shells which owe their name to the concentric layered structure resembling that of an onion. Carbon onions are sometimes called carbon nano-onions (CNOs) or OLC. In 1992, the quasispherical particles of carbon soot and tubular graphitic structures were radiated by intense electron-beam were reported by Ugarte [71]. In 1997, Harris and Tsang [135] observed fullerene-like structure which were close to carbon nano-particles when they used heat treatment to study the structure of two typical nongraphitizing carbons. From this model, nongraphitizing carbons were proposed which were different from the other representatives of the carbon family such as graphite, fullerenes, and nanotubes [135]. These OLCs have three to eight closed graphitic shell structures with the hollow core. Their outer diameters are in the range of $20-100$ nm. They are polyhedral nanoparticles which exhibit a well aligned concentric and high degree of symmetry structure. Such quasispherical shape, nanometer size, and surface specificity of OLCs have attracted enormous attention. Zhao et al., [136] reported a technique for a large quantity of synthesis of OLCs using carbonization of the solid-state catalyst of *PF* resin as the carbon resource and

ferric nitrate as the precursor at 1000^0 C. Iancu et al., [138] further synthesized OLCs using Fe/Al_2O_3 as catalyst by chemical vapor deposition (CVD) at a relatively low temperature (400^0 C) and efficiently avoided the growth of CNTs whilst Pervolaraki et al., [137] synthesized high-purity OLCs in high yields from coal by radio frequency plasma.

Carbon Nanofibers

Carbon nanofibers (CNFs) are composed of stacked and curved Graphene layers from a quasi-one-dimensional (1D) filament [139]. CNFs have cylindrical or conical nanostructures. Carbon nanofibers (CNFs) are composed of stacked and curved Graphene layers from a quasi-one-dimensional (1D) filament which are cylindrical or conical nanostructures. CNFs diameters vary from a few to hundred nanometers, while their lengths ranges from less than a micrometer to millimeters. Generally, CNFs can be synthesized through the traditional vapor growth methods such as cocatalyst deoxidization process [139], catalytic combustion technique [140], plasma-enhanced chemical vapor deposition [141], hot filament-assisted sputtering [142], ultrasonic spray pyrolysis [143], and ion beam irradiation [144].

Carbon Nanowalls

Carbon nanowalls (CNWs) consist of vertical aligned Graphene sheets standing on the substrates, form two-dimensional wall structure with large surface areas and sharp edges with thickness ranges from a few nm to a few tens nm [145, 146]. Different synthesis methods of CNWs based on

plasma-enhanced chemical vapor deposition techniques have been explored. The main approaches are as follows.

- Microwave plasma-enhanced chemical vapor deposition (MWPECVD).
- Radio-frequency plasma-enhanced chemical vapor deposition (RFPECVD) (RF inductively coupled plasma (ICP) and RF capacitively coupled plasma (CCP)).
- Hot-wire chemical vapor deposition (HWCVD).
- Electron beam excited plasma-enhanced chemical vapor deposition (EBEPECVD).

Hiramatsu et al. [145] using MWPECVD discovered CNWs by using NiFe-catalyze substrate (Si, SiO_2/Si, sapphire) preheated to about $650 - 700^o$ C in hydrogen plasma; the mixtures of CH_4 and H_2 were utilized as flow gases. The well-controlled MWPECVD synthesis process induced further studies to search more flexible control of the growth of CNWs [147].

Diamond and Graphite

Diamond is known to be one of the hardest materials, while graphite is soft enough and is thus used for making pencils. About the property of color, diamond is considered transparent while graphite is an opaque material and black. Graphite is a good conductor but diamond has a low electrical conductivity. On the other hand, diamond is normally referred to as being a highly thermal conductive, while graphite is considered as the most thermodynamically stable material [148].

Studies on Carbon Allotropes

There are several approaches of investigating the properties of carbon allotropes. These includes tight-binding calculations [146], density functional theory (DFT) calculations [148], and many-electron Greens function approach [149]. The most popular ones are based on the various ab-initio computations [150–152], molecular dynamics (MD) [153, 154], Cauchy-Born rule [155] and the so-called braced-truss models [156, 157]. Apart from the methods described, which are used mainly for understanding the electronic , magnetic and electrical properties of carbon allotropes, the understanding of acoustic effects resulting from the electron-phonon interaction is limited. Despite this limitation, a few experimental works on acoustic effects in carbon allotropes have been carried out.

Objectives and scope of study

Main Objectives

Among the numerous methods used in studying the properties of carbon allotropes is the interaction between electrons and phonons [158–160]. Such interaction in carbon allotropes offers very interesting phenomena which have important applications in areas related to electronics, spintronics, composites, medicine and many others. This research provides the theoretical treatment of acoustic effects of electron-phonon interaction in carbon allotropes and concentrates on novel one- and two-dimensional layered carbon (sp^2 hybridized) including 2D Graphene and Graphene nanoribbons as well as carbon nanotubes.

To date, there is no theoretical frame work for analyzing the acoustic properties of materials such as 2D Graphene, Graphene Nanoribbon, and Carbon Nanotubes. The need to study acoustic effects in Carbon allotropes are due to the applications derived from the electron - phonon interactions in the material. It includes (I) generation of high-frequency electric oscillation, (II) phonon spectrometer, (III) a non-destructive testing of microstructure and also for acoustic scanning systems.

Experimental studies of acoustic effect in Carbon Allotropes have yielded a range of different and conflicting results but the theoretical effort to explain the results obtained is lacking. This thesis is focused on explaining theoretically the acoustic effect in the above mentioned Carbon allotropes. This is achieved by studying the electron-phonon interaction in the materials where the acoustic wave is considered as monochromatic phonon of frequency (ω_q) in the short-wave region $ql >> 1$ (q is the acoustic wavenumber, l is the electron mean free path). Effect such as Amplification (absorption) of hypersound [160], Acoustoelectric Effect (AE) [161–171], Acoustomagnetoelectric effect (AME) [172–177], and Acoustothermal Effect [178] are studied in the samples and the results obtained compared to experimental results.

Specific Objectives

The objective for this thesis is to provide the theoretical framework that can lead to the attainment of SASER in 2D Graphene, AGNR, and CNT. From this study, the hypersound absorption (amplification) in Graphene, CNT in the

regime $ql >> 1$ (q is the acoustic wave number and l is the electron mean free path) is considered where the acoustic wave is considered as a flow of monochromatic phonons of frequency (ω_q). The main mechanism for understanding the acoustic effect in these materials is the phenomenon of electron-phonon interactions which leads to the exchange of energy and momentum between the carrier charges (electrons) and phonon. The Boltzmann transport equation is utilized in understanding the dynamics of the interactions in the materials. The resulting equations are numerically analyzed and graphically presented.

Organization Of Thesis

In chapter one, the introduction of carbon allotropes was outlined. This includes the synthsis, the preparation and the production of carbon allotropes such as Graphene, carbon nanotube and Graphene nanoribbon. The energy dispersion of these materials were also discussed. Chapter two also discusses the electron-phonon interaction and the fundamentals of the theoretical methods that were used in deducing the main kinetic equation. Chapter three deals with acoustic effects such as Acoustoelectric and Acoustomagneto electric effect and absoprtion/ amplification of in AGNR, 2D Graphene and Carbon Nanotube. The results and discussion with conclusions drawn are presented in chapters four and five.

CHAPTER TWO

LITERATURE REVIEW

Electron-Phonon Interaction

Electron-phonon interactions in bulk and low-dimensional semiconductors has been studied extensively in the past two decades with much attention focused on the effect such as acoustic and optical amplification of phonons [179, 180]. The confinement of electrons and phonons in nano-structured materials affects the electron transport, inelastic light scattering and many other properties including the response of the electronic system to electromagnetic waves. Electron-phonon interactions are important to the properties of carbon allotropes because activities such as:

- ballistic transport,
- superconductivity,
- excited-state dynamics,
- Raman spectra and phonon dispersions are dependent on it.

In two, one and zero dimensional systems such as superlattice [181–183], quantum wire [184–186], nanorodes [187, 188] and quantum wells [189, 190], it is well established that phonons (quantum of lattice vibration) provide the principal channel of energy transfer between the electrons and their surroundings. The main energy exchange is dependent on the relaxation time τ

where, the net transfer rate is determined by the rate at which energy flows out of the electron gas by phonon emission and the rate at which energy flows into the electron gas by phonon absorption from the lattice [191, 192]. The energy exchange between longitudinal acoustic phonons with electrons causes deformation potential scattering in the material which is due to electrons undergoing inelastic scattering [193, 194].

Graphene is a 2D system, which is very informative when compared with the more standard 2D material that has been studied extensively since the development of heterostructure and the discovery of the quantum Hall effect. In metallic systems, there are two main kinds of excitations: electron-hole pairs and collective modes such as plasmons [194]. Electron-hole pairs are incoherent excitations of the Fermi sea and a direct result of Pauli's exclusion principle. That is, an electron inside the Fermi sea with momentum k is excited outside the Fermi sea to a new state with momentum $k+q$, leaving a hole behind. The energy associated with such an excitation is simply: $\omega = \varepsilon_{k+q} - \varepsilon_k$ and for states close to the Fermi surface ($k \approx k_F$) their energy scales linearly with the excitation momentum, $\omega_q \approx V_F q$.

In a system with non-relativistic dispersion such as normal metals and semiconductors, the electron-hole continuum is made out of intra-band transitions only and exists even at zero energy since it is always possible to produce electron-hole pairs with arbitrarily low energy close to the Fermi surface. In systems with relativistic-like dispersion, such as Graphene, these excitations change considerably, especially when the Fermi energy is at the Dirac point. In this case, the Fermi surface shrinks to a point and hence

intra-band excitations disappear and only inter-band transitions between the lower and upper cones can exist. Therefore, neutral Graphene has no electron-hole excitations at low energy, instead each electron-hole pair has energy and hence the electron-hole occupies the upper part of the energy versus momentum diagram. If the chemical potential is moved away from the Dirac point then intra-band excitations are restored and the electron-hole continuum of Graphene shares features of the 2D and undoped Graphene. As the chemical potential is raised away from the Dirac point, Graphene resembles more and more as 2D material.

Bosons and Fermions

Bosons

In quantum mechanics, a boson is a particle that follows the Bose-Einstein statistics [195–197]. They are made up of fundamental particles such as photons, gluons, W and Z bosons, the Higgs Bosons and some quasiparticles such as Cooper pairs, plasmons and phonons. They have an integer spin ($s = 0$, 1, 2, etc) and a symmetric wave function ψ. The statistics of bosons do not restrict the number of them that occupy the same quantum state. The elementary bosons are force carriers that function as the 'glue' that holds matter together [197].

Fermions

These are particles characterized by Fermi-Dirac statistics which obey the Pauli exclusion principle [198]. These includes all quarks and Leptons as well as composite particles made of an old number such as baryons, atoms and nuclei. Fermions can be elementary particle such as electron or composite particles as protons [199, 200]. They posses conserved baryon or lepton quantum numbers with half-integer spin.

The Hamiltonian of the System

The Hamiltonian describing the electron-phonon system can be represented as the sum of the individual Hamiltonian of electron (el), phonon (ph), coulomb $(coul)$ and their interactions (int) [201–204]. This is expresed mathematically [205, 206] as

$$H = H_{el}^{0} + H_{ph}^{0} + H_{coul}^{0} + H_{int}^{0} \tag{20}$$

where

$$H_{el}^{0} = \sum_{\vec{k}\vec{\sigma}} \varepsilon_{\vec{k}} a_{\vec{k}\vec{\sigma}}^{\dagger} a_{\vec{k}\vec{\sigma}}^{\dagger} \tag{21}$$

$$H_{ph}^{0} = \sum_{\vec{k}\vec{\lambda}} \omega_{\vec{k}\vec{\lambda}} \left(a_{\vec{k}\vec{\lambda}}^{\dagger} b_{\vec{k}\vec{\lambda}} + \frac{1}{2} \right) \tag{22}$$

$$H_{coul}^{0} = \frac{1}{2} \sum_{\vec{k}\vec{k}'\vec{q}} V(\vec{q}) \left(a_{\vec{k}'+\vec{q}\vec{\sigma}'}^{\dagger} a_{\vec{k}\vec{\sigma}}^{\dagger} a_{\vec{k}+\vec{q}\vec{\sigma}} a_{k'\sigma'} \right) \tag{23}$$

$$H_{int}^{0} = \sum_{\vec{k}\vec{k}'\vec{\sigma}\vec{\lambda}} g_{\vec{k}\vec{k}'} a_{\vec{k}\vec{\sigma}}^{\dagger} a_{\vec{k}'\vec{\sigma}} \left(b_{-\vec{q}\vec{\lambda}}^{\dagger} + b_{\vec{q}\vec{\lambda}} \right) \tag{24}$$

$b^{\dagger}_{\vec{k}\vec{\lambda}}$ creates a phonon with wave vector $\vec{q} = \vec{k}' - \vec{k}$ and polarization $\vec{\lambda}$ and $g \propto M^{-\frac{1}{2}}$ is the bare electron-phonon coupling. The second-quantization representation [207–210] of the H^0_{el} in Eqn. (21) can be expressed in terms of the momentum-spin (i.e. $\alpha = k, \sigma$) single-particle basis. The single-particle basis function is given as

$$\Phi_{\alpha}(x) = \Phi_{k\sigma}(r, s) = \frac{1}{\sqrt{\Omega}} e^{\mathbf{k}\cdot\mathbf{r}} \delta_{s\sigma} \tag{25}$$

The kinetic energy operator in Eqn. (21) is a single-particle operator and the second-quantization representation is given as

$$H^0_{el} = \sum_{\alpha,\alpha'} \alpha' \frac{p^2}{2m} \alpha a^{\dagger}_{\alpha'} a_{\alpha} \tag{26}$$

where the matrix element

$$\alpha' \frac{p^2}{2m} \alpha = \int x \Phi^*_{\alpha'}(x) \left(-\frac{\hbar^2}{2m} \nabla^2 \right) \Phi_{\alpha}(x) \tag{27}$$

using the Bloch function for $\Phi_{\alpha'}$, Eqn. (26) can be expressed as

$$\begin{aligned}
\alpha' \frac{p^2}{2m} \alpha &= \sum_s \int^3 r \left(\frac{1}{\sqrt{\Omega}} e^{-i\tilde{\mathbf{k}}'\cdot\mathbf{r}} \delta_{\vec{s}\vec{\sigma}'} \right) \left(-\frac{\hbar^2}{2m} \nabla^2 \right) \left(\frac{1}{\sqrt{\Omega}} e^{\tilde{\mathbf{k}}\cdot\mathbf{r}} \delta_{\vec{s}\vec{\sigma}} \right) \\
&= \sum_s \int^3 r \left(\frac{1}{\sqrt{\Omega}} e^{-i\tilde{\mathbf{k}}'\cdot\mathbf{r}} \delta_{\vec{s}\vec{\sigma}'} \right) \left(-\frac{\hbar^2 k^2}{2m} \right) \left(\frac{1}{\sqrt{\Omega}} e^{\mathbf{k}\cdot\mathbf{r}} \delta_{\vec{s}\vec{\sigma}} \right) \\
&= \frac{\hbar^2 k^2}{2m} \left(\frac{1}{\Omega} \int^3 r e^{(\tilde{\mathbf{k}} - \tilde{\mathbf{k}}')\cdot\mathbf{r}} \right) \left(\sum_s \delta_{\vec{s}\vec{\sigma}'} \delta_{\vec{s}\vec{\sigma}} \right) \\
&= \frac{\hbar^2 \vec{k}^2}{2m} \delta_{\vec{k}\vec{k}'} \delta_{\vec{\sigma}\vec{\sigma}'}
\end{aligned} \tag{28}$$

substituting Eqn. (28) in Eqn. (26) gives

$$H_{el}^{0} = \sum_{\vec{k}\vec{\sigma}} \frac{\hbar^2 \vec{k}^2}{2m} a_{\vec{k}\vec{\sigma}}^{\dagger} a_{\vec{k}\vec{\sigma}} \delta_{\vec{k}\vec{k}'} \delta_{\vec{\sigma}\vec{\sigma}'} \tag{29}$$

The Quantized Theory Of Phonons

For a one dimensional model of a crystal lattice, the equilibrium position x_i for the atoms are shown [211,212] in the Figure (9). The Hamiltonian of the system

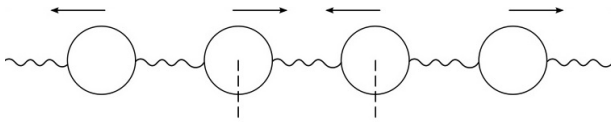

Figure 9: Equilibrium positions of atoms in a one-dimensional crystal lattice [214]

of atoms is

$$H = \sum_{i} \frac{p_i^2}{2m} + \frac{K}{2} \sum_{i} (x_i - x_{i+1})^2 \tag{30}$$

where $[x_i, p_i] = \delta_{nm}$. Diagonalizing the Hamiltonian in normal modes using Fourier series such as

$$\hat{x}_i = \frac{1}{N} e^{ka} \hat{x}_k, \tag{31}$$

$$\hat{x}_{i+1} = \sum_{n} e^{ka} \hat{x}_{-k} \tag{32}$$

From Eqn. (31) and (32)

$$\frac{K}{2} \sum_{i} (x_i - x_{i+1})^2 = \frac{K}{2} \sum_{\vec{k}} \hat{x}_k \hat{x}_{-\vec{k}} \left(2 - e^{\vec{k}a} - e^{-\vec{k}a}\right) \tag{33}$$

$$= \frac{m}{2} \sum_{\vec{k}} \omega_{\vec{k}}^2 \hat{x}_{\vec{k}} \hat{x}_{-\vec{k}} \tag{34}$$

where $\omega_{\vec{k}}^2 = \frac{2K}{m}(1-\cos k)$. In the $\vec{k}$ basis, the Hamiltonian becomes

$$H = \frac{1}{2m}\sum_{\vec{k}} \hat{p}_{\vec{k}}\hat{p}_{-\vec{k}} + \frac{m}{2}\sum_{\vec{k}} \omega_{\vec{k}}^2 \hat{x}_{\vec{k}}\hat{x}_{-\vec{k}} \tag{35}$$

with $\left[\hat{x}_{\vec{k}}, \hat{p}_{\vec{k}'}\right] = \delta_{\vec{k}\vec{k}'}$. The raising and lowering operators can be written as

$$b_k = \left(\frac{m\omega_{\vec{k}}}{2}\right)^{\frac{1}{2}}\left(\hat{x}_{\vec{k}} - \frac{\hat{p}_{-\vec{k}}}{m\omega}\right) \tag{36}$$

$$b_{\vec{k}}^{\dagger} = \left(\frac{m\omega_{\vec{k}}}{2}\right)^{\frac{1}{2}}\left(\hat{x}_{-\vec{k}} - \frac{\hat{p}_{\vec{k}}}{m\omega}\right) \tag{37}$$

From Eqn. (36) and (37), the Hamiltonian Eqn. (35) can be written as

$$H_{ph} = \sum_{\vec{k}\lambda} \omega_{\vec{k}\lambda} b_{\vec{k}\lambda}^{\dagger} b_{\vec{k}\lambda} \tag{38}$$

The Electron-Phonon Coupling (H_{int})

For an ion localised at position $\mathbf{R}_i$ at a displacement $\mathbf{u}_i$ from its equilibrium position $\mathbf{R}_i^0$, the interaction energy of the electronic charge density with the ions is

$$H_{int} = \sum_{i\vec{\sigma}} \int^3 r \Psi_{\vec{\sigma}}^{\dagger}(\mathbf{r})\Psi_{\vec{\sigma}}(\mathbf{r})V(\mathbf{r}-\mathbf{R}_i) \tag{39}$$

For small amplitude vibrations, Eqn. (39) can be expressed in powers of $\mathbf{u}_i$,

$$H_{int} = \sum_{i\vec{\sigma}} \int^3 r \Psi_{\vec{\sigma}}^{\dagger}(\mathbf{r})\Psi_{\vec{\sigma}}(\mathbf{r})V(\mathbf{r}-\mathbf{R}_i^0) + \sum_{i\vec{\sigma}} \int^3 r \Psi_{\vec{\sigma}}^{\dagger}(\mathbf{r})\Psi_{\vec{\sigma}}(\mathbf{r})\mathbf{u}_i \cdot \nabla_{\mathbf{R}_i} V(\mathbf{r}-\mathbf{R}_i)|_{\mathbf{R}_i^0} + \cdots \tag{40}$$

Expanding the field operators $\Psi_{\vec{\sigma}}$ in terms of Bloch waves

$$\Psi(\mathbf{r}) = \sum_{\vec{k}} a_{\vec{k},\vec{\sigma}} \Psi_{\vec{k}}(\mathbf{r}) \tag{41}$$

where

$$\Psi_{\vec{k}\vec{\sigma}} = e^{\tilde{\mathbf{k}}\cdot\mathbf{R}_i^0} \Psi_{\vec{k}}(\mathbf{r})$$

Performing a shift by a Bravais lattice vector and using the periodicity of $\nabla_{\mathbf{R}_i^0} V(\mathbf{r}-\mathbf{R}_i^0)$

$$\begin{aligned}
&\int^3 r \Psi^*_{\vec{k}'\vec{\sigma}}(\mathbf{r}) \Psi_{\vec{k}\vec{\sigma}}(\mathbf{r}) \nabla_{\mathbf{R}_i^0}(\mathbf{r}-\mathbf{R}_i^0) \\
&\qquad = \int^3 r \Psi^*_{\vec{k}'\vec{\sigma}}(\mathbf{r}+\mathbf{R}_j^0) \Psi_{\vec{k}\vec{\sigma}}(\mathbf{r}+\mathbf{R}_j^0) \nabla_{\mathbf{R}_i^0} V(\mathbf{r}-\mathbf{R}_i^0) \\
&\qquad = e^{(\tilde{\mathbf{k}}-\tilde{\mathbf{k}}'\cdot\mathbf{R}_j^0)} \underbrace{\int^3 r \Psi^*_{\vec{k}'\vec{\sigma}}(\mathbf{r}) \Psi_{\vec{k}\vec{\sigma}}(\mathbf{r}) \nabla_{\mathbf{R}_i^0}(\mathbf{r}-\mathbf{R}_i^0)}_{W_{\vec{k}\vec{k}'}}
\end{aligned} \tag{42}$$

Second-quantizing the displacement u in Eqn. (40) gives

$$u_i(t) = \frac{1}{\sqrt{NM}} \sum_{k\lambda} Q_\lambda(\mathbf{k},t) e^\lambda(\mathbf{k}) e^{\mathbf{k}\cdot\mathbf{R}_i^0} \tag{43}$$

where

$$Q_\lambda(\tilde{\mathbf{k}}) = \frac{1}{\sqrt{2\omega_\lambda(\tilde{\mathbf{k}})}} \left(b_\lambda(\tilde{\mathbf{k}}) + b^\dagger(-\tilde{\mathbf{k}}) \right) \tag{44}$$

Interaction Hamiltonian can be written as

$$H_{int} = \sum_{kk'\sigma} a^{\dagger}_{k'\sigma} a_{k\sigma} \sum_{j} W_{kk'} e^{(\mathbf{k}-\mathbf{k}')\cdot\mathbf{R}^0_j} \frac{1}{\sqrt{NM}} \sum_{k\lambda} Q_{\lambda}(\mathbf{k}) e^{\lambda}(\mathbf{k}) e^{\mathbf{k}\cdot\mathbf{R}^0_j} \tag{45}$$

$$= \sum_{kk'\sigma} \sum_{\lambda} a^{\dagger}_{k'\sigma} a_{k\sigma} \left(W_{kk'} e^{\lambda}(\mathbf{q}) \right) Q_{\lambda}(\mathbf{q}) \sqrt{\frac{N}{M}}$$

$$= \sum_{kk'\sigma} g_{kk'\lambda} a^{\dagger}_{k'\sigma} a_{k\sigma} \left(b_{\lambda}(\mathbf{k}) + b^{\dagger}_{\lambda}(-\mathbf{k}) \right) \tag{46}$$

where $\vec{k}$ is the momentum conservation interpreted as

$$\tilde{\mathbf{k}} = \mathbf{k} - \mathbf{k}' + \mathbf{G} \tag{47}$$

G being a vector of reciprocal lattice ($\tilde{\mathbf{k}}$ lies in the 1st Brillouin zone). The electron-phonon coupling constant is

$$g_{kk'\lambda} = \left(W_{kk'} e^{\lambda}(\tilde{\mathbf{k}}) \right) \sqrt{\frac{N}{2M\omega^{im}_{pl}(\tilde{\mathbf{k}})}} \tag{48}$$

Landau Quantization

The electron states in the presence of a magnetic field $\tilde{\mathbf{H}}$ are described by the Schrödinger equation [215–218].

$$\frac{1}{2m} \left(\vec{p} - e\vec{A}c \right)^2 \Psi_r = E\Psi_r, \qquad \vec{A} = (0, \vec{H}_x, 0)$$

From Eqn. (20) the Hamiltonian is expressed in momentum space as, ignoring the spin,

$$H = \sum_{\vec{p}} \frac{(\vec{p} - e\vec{A}c)^2}{2m} a_p^{\dagger} a_p + \sum_k \omega_k (b_k^{\dagger} b_k) + \sum_{p,k} g_{pk} a_{p+k}^{\dagger} a_k (b_{p,k} + b_{p,k}^{\dagger}) \qquad \textbf{(49)}$$

The General Quantum Equation

The general quantum equation for statistical average value of the electron particle number operator (or the electron distribution function) [219–221] is

$$n_{\vec{p}}(t) = \left\langle a_{\vec{p}}^{\dagger} a_{\vec{p}} \right\rangle_t = S_{\vec{p}} \left(a_{\vec{p}}^{\dagger} a_{\vec{p}} \rho(t) \right) \qquad \textbf{(50)}$$

where $S_{\vec{p}}$ is the trace and $\rho(t)$ is the statistical operator. The derivative of the density matrix over time is expressed as

$$\frac{\partial n_{\vec{p}}}{\partial t} = S_{\vec{p}} \left(a_{\vec{p}}^{\dagger} a_{\vec{p}} \frac{\partial \rho(t)}{\partial t} \right) \qquad \textbf{(51)}$$

Using the Heisenberg equation [222, 223]

$$\frac{\partial \rho}{\partial t} = [H, \rho] = (H\rho - \rho H) \qquad \textbf{(52)}$$

This describes the evaluation of the quantum system. Substituting Eqn. (52) into Eqn. (51) gives

$$\begin{aligned} \frac{\partial n_{\vec{p}}}{\partial t} &= S_{\vec{p}} \left(a_{\vec{p}}^{\dagger} a_{\vec{p}} \rho H - a_{\vec{p}}^{\dagger} a_{\vec{p}} H \rho \right) \\ &= S_{\vec{p}} \left[\left(a_{\vec{p}}^{\dagger} a_{\vec{p}} H - a_{\vec{p}}^{\dagger} a_{\vec{p}} H \right) \rho \right] \end{aligned} \qquad \textbf{(53)}$$

The initial condition in the case of a pure state may be expressed with $\rho_t = t$. This gives

$$\frac{\partial n_{\vec{p}}}{\partial t} = \left\langle \left[H, a^{\dagger}_{\vec{p}} a_{\vec{p}} \right] \right\rangle_t \tag{54}$$

The Hamiltonian in Eqn. (52) can be substituted into Eqn. (54) and using the algebra of the commutator gives

$$\left[a^{\dagger}_{\vec{p}'} a_{\vec{p}'}, a^{\dagger}_{\vec{p}} a_{\vec{p}} \right] = a^{\dagger}_{\vec{p}'} a_{\vec{p}'} a^{\dagger}_{\vec{p}} a_{\vec{p}} - a^{\dagger}_{\vec{p}} a_{\vec{p}} a^{\dagger}_{\vec{p}'} a_{\vec{p}'}, \tag{55}$$

$$a^{\dagger}_{\vec{p}'} a_{\vec{p}'} a^{\dagger}_{\vec{p}} a_{\vec{p}} = a^{\dagger}_{\vec{p}\vec{p}'} \left(\delta_{\vec{p}'} - a^{\dagger}_{\vec{p}} a_{\vec{p}'} \right) a_{\vec{p}}$$

using the identity $a_{\vec{p}'} a^{\dagger}_{\vec{p}} + a^{\dagger}_{\vec{p}} a_{\vec{p}'} = \delta_{\vec{p}\vec{p}'}$,

$$\delta_{\vec{p}\vec{p}'} a^{\dagger}_{\vec{p}'} a_{\vec{p}} - a^{\dagger}_{\vec{p}} \left(\delta_{\vec{p}\vec{p}'} - a_{\vec{p}} a^{\dagger}_{\vec{p}'} \right) a_{\vec{p}'} = a^{\dagger}_{\vec{p}} a_{\vec{p}} a_{\vec{p}'} a_{\vec{p}'} a_{\vec{p}'} \tag{56}$$

$$\begin{aligned} \left[a^{\dagger}_{\vec{p}} a_{\vec{p}}, a^{\dagger}_{\vec{p}'+k} a_{\vec{p}'} \right] &= a^{\dagger}_{\vec{p}} a_{\vec{p}} a^{\dagger}_{\vec{p}'+k} a_{\vec{p}'} - a^{\dagger}_{\vec{p}'+k} a_{\vec{p}'} a^{\dagger}_{\vec{p}} a_{\vec{p}} \\ &= \delta_{\vec{p}\vec{p}'+k} a^{\dagger}_{\vec{p}} a_{\vec{p}'} - a^{\dagger}_{\vec{p}'+k} a^{\dagger}_{\vec{p}} a_{\vec{p}'} a_{\vec{p}} - a^{\dagger}_{\vec{p}'+\vec{k}} a_{\vec{p}'} a^{\dagger}_{\vec{p}} a_{\vec{p}} \\ &= \delta_{\vec{p}\vec{p}'+k} a^{\dagger}_{\vec{p}} a_{\vec{p}'} - \delta_{\vec{p}\vec{p}'} a^{\dagger}_{\vec{p}'+k} a_{\vec{p}} + a^{\dagger}_{\vec{p}'+\vec{k}} a_{\vec{p}'} a^{\dagger}_{\vec{p}} a_{\vec{p}} - a^{\dagger}_{\vec{p}'+k} a_{\vec{p}'} a^{\dagger}_{\vec{p}} a_{\vec{p}} \end{aligned} \tag{57}$$

$$\frac{\partial n_{\vec{p}}}{\partial t} = \sum_{\vec{p},\vec{k}} g_{\vec{p},\vec{k}} \left[a^{\dagger}_{\vec{p}+\vec{k}} a_{\vec{p}} \left(b_{\vec{k}} + b^{\dagger}_{-\vec{k}} \right)_t - a^{\dagger}_{\vec{p}} a_{\vec{p}-\vec{k}} \left(b_{\vec{k}} + b^{\dagger}_{-\vec{k}} \right)_t \right] \tag{58}$$

The time-dependent Schrödinger equation [224, 225]

$$\hat{H}\Psi(t) = \frac{\partial}{\partial t}\Psi \tag{59}$$

But the operators remain independent of time. The solution of Eqn. (59) is

$$\Psi(t) = e^{-\hat{H}t}\Psi(0) \tag{60}$$

The exponential of an operator is defined by the Taylor expansion

$$e^{\hat{H}t} = 1 - \hat{H}t + \frac{1}{2}\left(-\hat{H}t\right)^2 + \cdots + \frac{1}{n!}\left(-\hat{H}t\right)^n + \cdots \tag{61}$$

If Ψ_E is an eigenstate of the Hamiltonian, $\hat{H}\Psi_E = E\Psi_E$. Then the operator solution simplifies

$$\Psi_E = e^{-Et}\Psi_E(0) \tag{62}$$

To calculate the expectation value of a state as the system evolves in time, the expectation value will change

$$\begin{aligned} F(t) &= \Psi(t)\hat{F}\Psi(t) \\ &= \Psi(0)\underbrace{e^{\hat{H}t}\hat{F}e^{-\hat{H}t}}_{\hat{F}(t)}\Psi(0) \end{aligned} \tag{63}$$

In the Schrödinger equation, the states have the time dependence. In the Heisenberg approach, the states remain time-independent at the expense of the operator acquiring dependence. The differential of $\hat{F}(t)$ gives

$$\frac{\partial F(t)}{\partial t} = (\hat{H}\hat{F} - \hat{F}\hat{H}) \tag{64}$$

It is convenient to introduce a correlation operator F

$$F_{p_1,p_2,q}(t) = a^{\dagger}_{p_1} a_{p_2} b_{q_t} \tag{65}$$

which satisfies

$$\frac{\partial n_p}{\partial t} = \sum_k C_k \left\{ F_{p+k,p,k}(t) + F^*_{p,p+k,-k}(t) - F_{p,p-k,k}(t) - F^*_{p-k,p,-k}(t) \right\} \tag{66}$$

Apart from the relaxation contribution due to phonon-phonon collisions, a driving force is introduced by electron-phonon interaction

$$\frac{\partial F_{p_1,p_2,q}(t)}{\partial t} = \frac{1}{\hbar} \left[a^{\dagger}_{p_1} a_{p_2} b_q, \hat{H} \right]_t \tag{67}$$

From Eqn. (67) the algebra of the operators

$$\begin{aligned}
[a^{\dagger}_{p_1} a_{p_2}, a^{\dagger}_p a_p] &= a^{\dagger}_{p_1} a_{p_2} a^{\dagger}_p a_p - \delta_{p_1 p} a^{\dagger}_p a_{p_2} + a^{\dagger}_p a_{p_2} + a^{\dagger}_{p_1} a^{\dagger}_p a_p a_p \\
&= -\delta_{p_1 p} a^{\dagger}_p a_{p_2} + \delta_{p_1 p_2} a^{\dagger}_{p_1} a_p && (68) \\
&= \frac{}{2m} \left[\left(p_1 - \frac{e}{c} A(t) \right)^2 - \left(p_2 - \frac{e}{c} A(t) \right)^2 \right] a^{\dagger}_{p_1} a_{p_2} b_{q_t} && (69) \\
&= \frac{}{2m} \left[p_1^2 - p_2^2 - (p_1 - p_2, A(t)) \frac{2e}{c} \right] a^{\dagger}_{p_1} a_{p_2} b_{q_t} && (70) \\
&= \left[\varepsilon_{p_1} - \varepsilon_{p_2} - (p_1 - p_2, A(t)) \frac{e}{mc} \right] a^{\dagger}_{p_1} a_{p_2} b_{q_t} && (71) \\
&= \left[\varepsilon_{p_1} - \varepsilon_{p_2} - (p_1 - p_2, A(t)) \frac{e}{mc} \right] F_{p_1,p_2,q} && (72)
\end{aligned}$$

where $\varepsilon_p = \frac{p^2}{2m}$. Substituting Eqn. (72) into Eqn. (67) gives

$$\frac{\partial F_{p_1,p_2,q}(t)}{\partial t} = \left[\varepsilon_{p_1} - \varepsilon_{p_2} - \omega_q - (p_1 - p_2, A(t))\frac{e}{mc}\right] F_{p_1,p_2,q}(t) + \sum_{p_3} C_{-q} a^{\dagger}_{p_1} a^{\dagger}_{p_3-q} a_{p_2} a_{p_3 t} + \sum_{q_1} C_{q_1}\left[a^{\dagger}_{p_1+q_1} a_{p_2}\left(b_q + b^{\dagger}_{-q}\right) b_{q_t} - a^{\dagger}_{p_1} a_{p_2} b_q \left(b_q + b^{\dagger}_{-q}\right)_t\right] \quad (73)$$

$$a^{\dagger}_{p_1+q_1} a_{p_2} b_{-q_1} b_q \quad = a_{p_1+q_1} a_{p_2} b^{\dagger}_{-q} b_q \quad (74)$$

$$a^{\dagger}_{p_1} a^{\dagger}_{p_3-q} a_{p_2} a_{p_3} \quad = \delta_{p_1 p_3} n_{p_1} \delta_{p_2, p_3-q} n_{p_2} \quad (75)$$

The phonon occupation number [226, 227] is given as $N_q(t) = b^{\dagger}_q b_{q_t}$ with $F_{p,p-k,k}$, where $p_1 - p_2 = \pm k$

$$(p_1 - p_2, A(t)) \implies \left(k, \frac{E_o}{\Omega}\right)\cos(\Omega t) \quad (76)$$

$$E(t) = E_0 \sin(\Omega t) = -\frac{1}{c}\frac{A}{t} \quad (77)$$

Letting $\Phi(t) = \left(\varepsilon_{p+k} - \varepsilon_p - \omega_k - \frac{e}{m}\frac{k}{\Omega} E_o \cos(\Omega t)\right)$, Eqn. (73) reduces to

$$\frac{\partial F}{\partial t} = \Phi(t) F(t) + [\ldots] \quad (78)$$

$\frac{\partial F}{\partial t} = \Phi(t) F(t)$ grouping like terms gives $\frac{\partial F}{F(t)} = \Phi(t)\partial t$

$$F(t) = C(t) \exp\left\{\int_{\infty}^{t'_1} \Phi(t)\, t\right\} \quad (79)$$

Differentiating Eqn. (79)

$$F'(t) = C'(t)\exp\left\{\int_{\infty}^{t_1'}\Phi(t)t\right\} + C(t)\Phi(t)\exp\left\{\int_{\infty}^{t_1'}\Phi(t)t\right\} \tag{80}$$

$$C'(t)\exp\left\{\int_{\infty}^{t_1'}\Phi(t)t\right\} + C(t)\Phi(t)\exp\left\{\int_{\infty}^{t_1'}\Phi(t)t\right\} = \Phi(t)C(t)\exp\left\{\int_{\infty}^{t_1'}\Phi(t)t\right\} + [\ldots] \tag{81}$$

$$C'(t) = \exp\left\{-\int_{\infty}^{t_1'}\Phi(t)t\right\}[\ldots]$$
$$C(t) = \int_{-\infty}^{t}\exp\left\{-\int_{\infty}^{t_1'}\Phi(t)t\right\}[\ldots]\,t \tag{82}$$

From Eqn. (82)

$$F(t) = \int_{-\infty}^{t}[\ldots]\exp\left\{\int_{-\infty}^{t}\Phi(t)t - \int_{-\infty}^{t_1}\Phi(t)t\right\} \tag{83}$$

The exponential part of Eqn. (83) can be expanded as

$$\exp\left\{\int_{-\infty}^{t}\Phi(t)t\right\} = \exp\left\{\left(\varepsilon_{p+k}t - \varepsilon_p t - \omega_k t - \frac{e}{m}\frac{k_o E_o}{\Omega^2}\sin(\Omega t) + \delta t\right)\right\}$$
$$= \exp\left\{\left(\varepsilon_{p+k} - \varepsilon_p - \omega_k + \delta\right)t\right\}\exp\left\{-\frac{e}{m}\frac{k_o E_o}{\Omega^2}\sin(\Omega t)\right\}$$
$$= e^{\left(\varepsilon_{p+k}-\varepsilon_p-\omega_k+\delta\right)t}\sum_s J_s(a)e^{-s\Omega t} \tag{84}$$

since $e^{z\sin(\Omega t)} = \sum_{l=-\infty}^{\infty} J_l(z)e^{l\Omega t}$

$$\exp\left\{-\int_{-\infty}^{t}\Phi(t)t\right\} = \exp\left\{-\left(\varepsilon_{p+k}t - \varepsilon_p t - \omega_k t - \frac{e}{m}\frac{k_o E_o}{\Omega^2}\sin(\Omega t) + \delta t\right)\right\}$$
$$= \exp\left\{-\left(\varepsilon_{p+k} - \varepsilon_p - \omega_k + \delta\right)t\right\}\exp\left\{-\frac{e}{m}\frac{k_o E_o}{\Omega^2}\sin(\Omega t)\right\}$$
$$= e^{-\left(\varepsilon_{p+k}-\varepsilon_p-\omega_k+\delta\right)t}\sum_l J_l(a)e^{s\Omega t} \quad \textbf{(85)}$$

Taking the product of Eqn. (84) and Eqn. (85)

$$\exp\left\{\int_{-\infty}^{t}\Phi(t)t\right\}\cdot\exp\left\{-\int_{-\infty}^{t}\Phi(t)t\right\} = \sum_{s,l}J_s(a)J_l(a)exp(-s\Omega t)exp(l\Omega t)\times$$
$$exp\left(\varepsilon_{p+k} - \varepsilon_p - \omega_k + \delta\, t\right) - \left(\varepsilon_{p+k} - \varepsilon_p - \omega_k + \delta\, t\right)$$

simplifies to

$$= \sum_{s,l}J_s(a)J_l(a)exp((l-s)\Omega t)exp(\left(\varepsilon_{p+k} - \varepsilon_p - \omega_k + \delta\right)t)$$
$$exp(-\left(\varepsilon_{p+k} - \varepsilon_p - \omega_k + \delta\right)t) \quad \textbf{(86)}$$

Solving the operations in Eqn. (83)

$$i\sum_{q_1}c_q[\langle a^+_{p_1+q_1}a_{p_2}(b_{q_1} + b^+_{-q})b_q\rangle_t - \langle a^+_{p_1}a_{p_2-q}b_q(b_{q_1} + b^+_{-q_1})\rangle_t] \quad \textbf{(87)}$$

$$i\sum_{q_1}c_q[\langle a^+_{p_1+q_1}a_{p_2}b^+_{-q}b_q\rangle_t - \langle a^+_{p_1}a_{p_2-q}b_q b^+_{-q}\rangle_t] \quad \textbf{(88)}$$

Assuming that $\langle b_q b_q\rangle = 0$

$$i\sum_{q_1}c_q[\langle a^+_{p_1+q_1}a_{p_2}\rangle\langle b^+_{-q_1}b_q\rangle - \langle a^+_{p_1}a_{p_2-q}\rangle\langle b_q b^+_{-q}\rangle] \quad \textbf{(89)}$$

$$i\sum_{q_1} c_q[n(t')\delta_{p_1+q_1,p_2}N_q(t) - n(t')\delta_{p_1,p_2-q}(N_q(t')+1)] \tag{90}$$

$$\sum_{q} c_q[n_{p+q}(t')N_q(t) - n_{p_1-q_1}(t')(N_{q_1}(t)+1)] \tag{91}$$

$$i\sum c_{-q}n_p\delta_{p_1,p_3}\delta_{p_2,p_3-q}n_{p_2} \tag{92}$$

$$i\sum c_{-q}[n_{p_1}n_{p_1-q}] \tag{93}$$

Therefore the driving force equation becomes

$$\begin{aligned}\frac{\partial F_{p,p+k,k}(t)}{\partial t} = i[\varepsilon_{p+q} - \varepsilon_p - \omega_k - \frac{e}{mc}(p_{p+k} - p_p, A(t))] \\ F_{p+k,p,k}(t') + i\sum_k c_k[n_p(t')(1-n_{p+k}(t'))N_k(t') \\ -n_{p+k}(t')(1-n_p(t'))(N_k(t)+1)]\end{aligned} \tag{94}$$

where

$$\begin{aligned}F(t) = i\sum_k c_k \sum_{s,l} J_s(a,k)J_e(a,k)e^{i(l-s)\Omega t}\int_{-\infty}^{t} dt'\{[n_p(t') \\ \times(1-n_{p+k}(t'))N_k(t')n_{p+k}(t')(1-n_p(t')(N_k(t')+1))] \\ \times exp[i(\varepsilon_{p+k} - \varepsilon_p - \omega_k - l\Omega + i\delta)(t-t')]\}\end{aligned} \tag{95}$$

Substituting Eqn. (95) into Eqn. (73) gives the quantum kinetic equations as

$$\frac{\partial N_q(t)}{\partial t} = -\sum_k |\, c_k \,|^2 \sum_{s,l} J_s(a.k) J_l(a.k) e^{(i(l-s)\Omega t)} \int_\infty^t dt' \{[n_p(t') \times (1-n_{p+k}(t'))N_k(t') - n_{p+k}(t')(1-n_p(t'))(N_k(t)H)]\}$$

$$exp[i(\varepsilon_{p+k} - \varepsilon_p - \omega_k - l\Omega + i\delta)(t-t')] + [n_p(t')(1-n_{p+k}(t')) \times (N_k(t')+1) - n_{p+k}(t')(1-n_p(t'))(N_k(t'))]$$

$$exp[i(\varepsilon_{p+k} - \varepsilon_p - \omega_k - l\Omega + i\delta)(t-t')] - [n_{p-k}(t')(1-n_p(t')) \times (N_k(t') - n_p(t')(1-n_{p-k}(t'))(N_k(t')+1)] \quad \textbf{(96)}$$

Considering the average phonon occupation number to be $N_q(t) = \langle b_q^+ b_q \rangle_t$

$$\frac{\partial N_q(t)}{\partial t} = -\sum_k |\, c_k \,|^2 \sum_p \sum_{s,l} J_s(a.q) J_l(a.q) e^{(l-s)\Omega t} \int_{-\infty}^t dt' \{n_p(t') \times [1-n_{p+q}(t')]N_q(t') - n_{p+q}(t')[1-n_p(t')][N_q(t')+1] \times expi(\varepsilon_{p+k} - \varepsilon_p - \omega_k - l\Omega + i\delta)(t-t')\} \quad \textbf{(97)}$$

The electron occupation number transform in a Fourier series [228] as

$$n_p(\omega) = \int_{-\infty}^{+\infty} n_p(t) e^{+i\omega t} dt \quad \textbf{(98)}$$

Thus

$$\frac{\partial n_p(\omega)}{\partial t} = +i\omega n_p(\omega) \quad \textbf{(99)}$$

The quantum kinetic equation for electron distribution [230,231] is given as

$$-i\omega n_p(\omega) = i\sum \mid c_k \mid^2 \sum_{l=-\infty}^{\infty} J_l^2(a,k)\{[n_{p+k}(\omega)(N_k+1) - n_p(\omega)N_k] \times[\Delta_1^{(+)} - \Delta_1^{(-)}] + [n_{p-k}(\omega)N_k - n_p(\omega)(N_k+1)][\Delta_2^{(+)} - \Delta_2^{(-)}]\} \quad (100)$$

where

$$\Delta^{(+)} = (\varepsilon_{p+k} - \varepsilon_p - \omega_k \pm \omega - l\Omega \mp i\delta)^{-1} \quad (101)$$

$$\Delta^{(-)} = (\varepsilon_{p-k} - \varepsilon_p + \omega_k \mp \omega - l\Omega \pm i\delta)^{-1} \quad (102)$$

With the time Fourier transform, the electron occupation number is

$$n_p(t) = \int_{-\infty}^{\infty} n_p(\omega) e^{-i\omega t} \frac{d\omega}{2\pi} \quad (103)$$

with $\omega \approx \frac{1}{\tau} \Rightarrow \omega \approx 1$. For a quasi-classical case where $\Omega\tau \gg 1$, gives $\Omega \gg \omega$. Therefore, the electron quantum kinetic equation becomes

$$\frac{\partial n_p(t)}{\partial t} = 2\pi\sum_k \mid c_k \mid^2 \sum_{l=-\infty}^{\infty} J_l^2(a,k)\{[n_{p+k}(N_k+1) - n_p N_k]\delta(\varepsilon_{p+k} - \varepsilon_p - \omega_k - l\Omega) + [n_{p-k}N_k - n_p(N_k+1)]\delta(\varepsilon_{p+k} - \varepsilon_p + \omega_k - l\Omega)\} \quad (104)$$

The rate of change of the electron occupation number is proportional to the occupation of the electron

$$\frac{\partial n_p(t)}{\partial t} = st[n_p(t)] \quad (105)$$

where *st* is the collision integral.

Boltzmann Distribution Function

A distribution-function $f(k,r,t)$ is the probability of occupation of an electron at time t at r with wavevectors lying between k, $k+dk$. Under equilibrium ($E = B = \nabla_r f = \nabla_T f = 0$, i.e., no external electric (E) or magnetic (B) field and no spatial and thermal gradients), the distribution function is found from quantum-statistical analysis to be given by the Fermi-Dirac function for fermions -

$$f_0(\varepsilon) = \{1 + exp(\frac{\varepsilon_k - \mu}{K_\beta T})\} \tag{106}$$

where ε_k is the energy of the electron, μ is the Fermi energy, and k_β is the Boltzmann constant. Any external perturbation drives the distribution function away from the equilibrium; the Boltzmann-transport equation (BTE) governs the shift of the distribution function from equilibrium. It may be written formally as [232]

$$\frac{\partial f}{\partial t} = \frac{F_t}{\hbar} \cdot \nabla_k f(k) + v \cdot \nabla_r f(k) + \frac{\partial f}{\partial t} \tag{107}$$

where on the right hand side, the first term reflects the change in distribution function due to the total field force $F_t = E + v \times B$, the second term is the change due to concentration gradients, and the last term is the local change in the distribution function. Since the total number of carriers in the crystal is constant, the total rate of change of the distribution is identically zero by Liouville's theorem. Hence the local change in the distribution function is written as

$$\frac{\partial f}{\partial t} = \frac{\partial f}{\partial t}|_{coll} = \frac{F_t}{\hbar} \cdot \nabla_k f(k) + v \cdot \nabla_r f(k) + \frac{\partial f}{\partial t} \tag{108}$$

The $\frac{\partial f}{\partial t}|_{coll}$ is the collision term where the first term has been split off from the field term since collision effects are not easily described by fields. The second term is due to applied field only and the third is due to concentration gradients. Denoting the scattering rate from state $k \rightarrow k'$ as $S(k,k')$, the collision term is given by

$$\frac{\partial f(k)}{\partial t}|_{coll} = \sum_{k}^{'}[S(k',k)f(k')[1-f(k)] - S(k,k')f(k)[1-f(k')]] \qquad \textbf{(109)}$$

Figure (10) provides a visual representation of the scattering processes that form

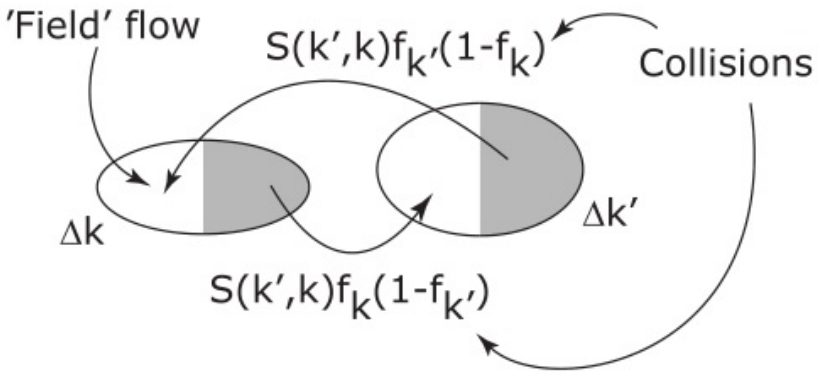

Figure 10: Scattering term of Boltzmann transport equation depicting the inflow and outflow of the distribution function [233]

the collision term. The increase of the distribution function in the small volume Δk by particles flowing in by the field term is balanced by the net flow out by the two collision terms. At equilibrium ($f = f_0$), the principle of detailed balance enforces the condition

$$S(k',k)f_0(k')[1-f_0(k)] = S(k,k')f_0(k)[1-f_0(k')]$$

which translate into

$$S(k',k)exp(\frac{\varepsilon_k}{K_\beta T}) = S(k,k')exp(\frac{\varepsilon_{k'}}{K_\beta T}) \tag{110}$$

In the special case of elastic scattering, $\varepsilon_k = \varepsilon'_k$, and as a result, $S(k',k) = S(k,k')$ irrespective of the nature of the distribution function. Using this, one rewrites the collision term as

$$\frac{\partial f(k)}{\partial t}|_{coll} = \sum_k{}' S(k',k)f(k') - f(k) \tag{111}$$

The collision equation can be written as

$$\frac{f(k)}{dt} + \frac{f(k)}{\tau(k)} = \sum_k{}' S(k,k')f(k') \tag{112}$$

where the scattering time $\tau(k)$ is defined as

$$\frac{1}{\tau(k)} = \sum_k{}' S(k,k')$$

A particle prepared in state $|k\rangle$ at time $t = 0$ by an external perturbation will be scattered into other states $|k'\rangle$ due to collisions, and the distribution function in that state will approach the equilibrium distribution exponentially fast with the time constant $\tau_q(k)$ upon the removal of the applied field. The scattering time $\tau_q(k)$ may be viewed as a lifetime of the particle in the state $|k\rangle$. Let us now assume that the external fields and gradients have been turned on for a long time. They have driven the distribution function to a steady state value f from f_0. The perturbation is assumed to be small, i.e., distribution function is assumed not to

deviate far from its equilibrium value of f_0. Under this condition, it is common practice to assume that

$$\frac{\partial f}{\partial t} = \frac{\partial f}{\partial t}|_{coll} = -\frac{f - f_0}{\tau} \tag{113}$$

where τ is a time scale characterizing the relaxation of the distribution. This is the relaxation time approximation, which is crucial for getting a solution of the Boltzmann transport equation. When the distribution function reaches a steady state, the Boltzmann transport equation may be written as

$$\frac{\partial f}{\partial t} = -\frac{f - f_0}{\tau} - \frac{F_t}{\hbar} \cdot \nabla_k f(k) - v \cdot \nabla_r f(k) = 0 \tag{114}$$

where the relaxation time approximation to the collision term has been used. In the absence of any concentration gradients, the distribution function is given by

$$f(k) = f_0(k) - \tau \frac{F_t}{\hbar} \cdot \nabla_k f \tag{115}$$

Using the definition for the velocity $v = \frac{\partial \varepsilon_k}{\partial k}$ the distribution function become

$$f(k) = f_0(k) - \tau F_t \cdot v \frac{f(k)}{\partial \varepsilon} \tag{116}$$

and since the distribution function is assumed to be close to f_0, we can make the replacement $f(k) \to f_0(k)$, whence the distribution function

$$f(k) = f_0(k) - \tau F_t \cdot v \frac{f_0(k)}{\partial \varepsilon} \tag{117}$$

is the solution for the Boltzmann transport equation for a perturbing force F_t. The electron-phonon interaction can be considered in three cases:

- the interaction through the piezo-electric coupling,
- the interaction through the deformation potential and
- the interaction through the polar scattering.

Generally, we consider the interaction irrespective of the coupling type. Therefore, considering f_k as the distribution function of the conduction electrons and that of the phonons as N_q where q is the wave number vector of the phonons. The distribution functions f_k and N_q are assumed to obey the following equations:

$$\frac{\partial f_k}{\partial t} = -\frac{eF}{\hbar}\left(\frac{\partial f_k}{\partial k_x}\right) + \left(\frac{\partial f_k}{\partial t}\right)_c \tag{118}$$

and

$$\frac{\partial N_q}{\partial t} = \left(\frac{\partial N_q}{\partial t}\right)_c + \left(\frac{\partial N_q}{\partial t}\right)_p \tag{119}$$

where F is the intensity of the electric field applied in the $-x$ direction, and e is the absolute value of the electronic charge. Here, the collision term $(\frac{\partial f_k}{\partial t})_c$ is given by

$$\begin{aligned}\left(\frac{\partial f_k}{\partial t}\right)_c = \frac{2\pi}{\hbar}\sum_q C_q^2\{f_{k+q}(N_q+1) - f_k N_q\}\delta(\varepsilon_{k+q} - \varepsilon - \hbar\omega_q) + \\ \frac{2\pi}{\hbar}\sum_q C_q^2\{f_{k-q}N_q - f_k(N_q+1)\}\delta(\varepsilon_{k-q} - \varepsilon + \hbar\omega_q)\end{aligned} \tag{120}$$

where C_q is a quantity characterizing the interaction between the conduction. electrons and phonons with the wave number q and the angular frequency ω_q. The explicit form of C_q will be given afterwards. On the other hand, the collision term $(\frac{\partial N_q}{\partial t})_c$ is given by

$$(\frac{\partial N_q}{\partial t})_c = (\frac{2\pi}{\hbar})\sum_k C_q^2\{f_{k+q}(N_q+1) - f_k N_q\}\delta(\varepsilon_{k+q} - \varepsilon_k - \hbar\omega_q) \qquad \textbf{(121)}$$

Considering the electrical conductivity, the distribtution function is assumed to be

$$f_x(k) = f_0(\varepsilon) - \hbar v(\varepsilon,t)k_x\frac{\partial f_0}{\partial \varepsilon}$$

where $f_0(\varepsilon)$ is the Maxwell's distribution function given as

$$f_0(\varepsilon) = (2\pi)^3 n_c(\hbar/2 * k_\beta T)^{3/2} exp(-\varepsilon/k_\beta T)$$

Further, the $v(\varepsilon)$ is related to the drift velocity of the electrons through the following equation :

$$v_d = \frac{1}{6\pi^2 n_e}(\frac{2m*}{\hbar^2})^3\int_0^\infty \varepsilon^3 v(\varepsilon)(-\frac{df_0}{d\varepsilon})d\varepsilon \qquad \textbf{(122)}$$

CHAPTER THREE

ACOUSTIC EFFECT

In this chapter, the theory underlying acoustic effect in Carbon Allotropes will be treated. This includes acoustic phonon amplification and Acoustomagnetoelectric effect (AME) in AGNR, Amplification and Acoustoelectric Effect (AE) in Graphene, hypersound absorption and acoustoelectric effect in CNT.

Background of acoustic effects in materials

Acoustic effect in semiconductor materials have been considered in many works [234–238]. This was first observed by Hutson, et al., [239, 240] who amplified radio-frequency ultrasound in CdS. By using a strong piezoelectric coupling between electrons and elastic waves in CdS, amplification was achieved. In semiconductor materials, it is known that, when an acoustic phonon passes through a semiconductor, it may interact with various elemental excitations which may lead to amplification or absorption of phonons. An amplification of acoustic phonons occurs when there is energy loss from the charge carriers to the phonons, but vice-versa, attenuation occurs which leads to acoustic wave absorption [241, 242]. Among the variety of nonequilibruim effects that can cause amplification or absorption of phonons are the drift velocity of the charge carriers, application of an external bias, temperature

difference and chemical concentration. For velocity change, when drift velocity of the charge carriers exceeds the velocity of sound, leads to amplification but when it is less attenuation occurs. This effect is referred to as Cerenkov effect [244, 245]. Akin to Cerenkov acoustic-phonon emission, when the drift velocity of electrons V_D exceeds the sound velocity (V_s) of the host material [246] it causes amplification of the acoustic-phonons but when $V_D < V_s$, causes absorption of acoustic-phonons. This has been ultilised experimentally to confirm the breakdown of quantum Hall effect [247], the generation of coherent phonon-polariton radiation [248], and large acoustic gain in coherent phonon oscillators in semiconductors [249–256]. Furthermore, the emission and absorption of acoustic-phonons is used to provide detailed information on the excitation and relaxation mechanisms in semiconductors via deformation potential, where the effect of interactions can be used to determine the physical properties of the material.

Acoustic phonon amplification in Graphene Nanoribbon (GNR)

The idea of acoustic wave amplification in bulk material was theoretically predicted by Tolpygo and Uritskii (1956) [257], and Weinreich [258] and in N-Ge by Pomerantz [167]. Hypersound generation in bulk [252] and low-dimensional materials such as Superlattices [253–257], Cylindrical Quantum Wire [258], and Quantum Wells [259] has been studied. In low-dimensional systems, the acoustic wave amplification (absorption) was studied theoretically and experimentally [260–263]. Recently the study of acoustic effect in semiconductor nanostructure materials has been extended to

(CNT) and graphene with few experimental work carried out [264–268]. These carbon based materials have interesting properties as well as an excellent combination of electronic, optoelectronic, and thermal properties compared to conventional rigid silicon which makes them excellent systems for application in electronic and optoelectronic systems. Graphene [270–272] is a single-atom sheet of graphite. The most interesting property of graphene is its linear energy dispersion $E = \pm\hbar V_F|k|$ (the Fermi velocity $V_F \approx 10^8$ ms^{-1}) at the Fermi level with low-energy excitation. Graphene-based electronics has attracted much attention due to high carrier mobility in bulk graphene devices such as sub-terahertz field-effect transistors [273], infrared transparent electrodes [274] and THz plasmonic devices [275]. In particular, acoustic-phonons providing terahertz (10^{12} Hz) hypersonic sources can lead to the attainment of phonon laser or SASER [276, 277] in graphene via Cerenkov effect which is an intense field of research. Following the works of [269, 278], Zhao et al., [279] proposed the possibility of attaining Cerenkov acoustic-phonon emission in graphene whilst Insepov et al., [280], performed experimentally the surface acoustic wave amplification by D.C voltage supply in Graphene. Under an external bias, this effect is also observed to occur in semiconductors. Other

effects such as absorption of acoustic phonons [281, 282]; Acoustoelectric Effect (AE) [283–289]; Acoustomagnetoelectric Effect (AME) [290–294]; Acoustothermal Effect [295] and Acoustomagnetothermal Effect [296]. The concept of sound generation by the electron drift comes from the modification of the electron-phonon interaction form factor due to change of the phonon modes structure [297]. In GaAs/AlAs superlattice, phonon amplification occurs under an external source of non-equilibrium phonons. A possible evidence for phonon amplification can be observed in phonon assisted transport measurement where a resonance-like emission of terahertz acoustic phonons occurs. This observation suggests the possibility to develope an electrically pumped high-intensity source of terahertz coherent acoustic phonon based on a superlattice structure. Such a device, which could be called a SASER (sound amplification by stimulated emission of radiation), would have potential applications in photon optics, phonon spectroscopy, and acoustical imaging of nanostructures [299]. The general kinetic equation becomes

$$\begin{aligned} -\{eE &+ \omega_H[p,h]\}\frac{\partial f_p}{\partial p} = 2\pi\sum_k |\, C_k\,|^2\,\{[f_{p+k}(N_k+1) - f_p N_k] \\ \delta(\varepsilon_{p+k} &- \varepsilon_p - \hbar\omega_q) + [f_{p-k}N_k - f_p(N_k+1)]\delta(\varepsilon_{p-k} - \varepsilon_p + \hbar\omega_q)\} \\ &+ \frac{\pi\Lambda^2\bar{W}}{\rho S^3} \times \{(f_(p+q) - f_p)\delta(\varepsilon_{p+q} - \varepsilon_p - \hbar\omega_q) \\ &+ (f_{p-q} - f_p)\delta(\varepsilon_{p-q} - \varepsilon_p + \hbar\omega_q)\} \end{aligned} \tag{123}$$

For small deviations of the distribution function from the equilibrium state the collision term when the external field is not zero thus becomes

$$-\{eE+\omega_H[p,h]\}\frac{\partial f_p}{\partial p}=-\frac{f_p-f_0(\varepsilon_p)}{\tau(\varepsilon_p)}+\frac{\pi\varepsilon^2\bar{W}}{\rho S^3}\{(f_{p+q}-f_p)$$
$$\delta(\varepsilon_{p+q}-\varepsilon_p-\hbar\omega_q)+(f_{p-q}-f_p)\delta(\varepsilon_{p-q}-\varepsilon_p+\hbar\omega_q)\} \quad \textbf{(124)}$$

To calculate for the amplification of acoustic waves in AGNR, the method developed in [46] was adopted, where the sound flux ($\vec{W}$), d.c. electric field ($\vec{E}$) and a constant magnetic field ($\tilde{\mathrm{H}}$) are considered mutually perpendicular to the plane of the AGNR. The acoustic wave is considered in the hypersound regime $ql >> 1$ (q is the acoustic wavenumber and l is the mean free path of an electron). To solve for the partial current generated in the AGNR, the Boltzmann kinetic equation

$$-\left(e\vec{E}\frac{\partial f_{\vec{p}}}{\partial \vec{p}}+\Omega[\vec{p},\vec{H}],\frac{\partial f_{\vec{p}}}{\partial \vec{p}}\right)=-\frac{f_{\vec{p}}-f_0(\varepsilon_{\vec{p}})}{\tau(\varepsilon_{\vec{p}})}+\frac{\pi\xi^2\vec{W}}{\rho V_s^3}\times$$
$$\left\{[f_{\vec{p}+\vec{q}}-f_{\vec{p}}]\delta(\varepsilon_{\vec{p}+\vec{q}}-\varepsilon_{\vec{p}}-\hbar\omega_{\vec{q}})+[f_{\vec{p}-\vec{q}}-f_{\vec{p}}]\delta(\varepsilon_{\vec{p}-\vec{q}}-\varepsilon_{\vec{p}}+\hbar\omega_{\vec{q}})\right\} \quad \textbf{(125)}$$

is employed. Here, ξ is the constant of deformation potential, e the electronic charge, $\vec{E}$ is the constant electric field produced by the acoustic wave in the open-circuited field, $\omega_{\vec{q}}$ is frequency, $\vec{W}$ is the density of the acoustic flux, ρ is the density of the sample and $\vec{p}$ the characteristic quasi-momentum of the electron. The relaxation time is $\tau(\varepsilon_{\vec{p}})$ and the cyclotron frequency, $\Omega=\frac{\mu H}{c}$. Where μ is the mobility, c is the speed of light, $\hbar$ is the planck constant, $f_0(\varepsilon)$ is the equilibrium function of the electron distribution, and $\vec{q}$ is the acoustic wavenumber of the sound. The energy dispersion relation $\varepsilon(\vec{p})$ for AGNRs

band near the Fermi point is expressed [300] as

$$\varepsilon(\vec{p}) = \frac{E_g}{2}\sqrt{[(1+\frac{\vec{p}^2}{\hbar^2\beta^2})]} \tag{126}$$

where the energy gap $E_g = 3ta_{c-c}\beta$, with β being the quantized wave vector given as

$$\beta = \frac{2\pi}{a_{c-c}\sqrt{3}}\left(\frac{p_i}{N+1} - \frac{2}{3}\right) \tag{127}$$

The p_i is the subband index, N the number of dimmer lines which determine the width of the AGNR, $a_{c-c} = 1.42$ Å is the carbon-carbon (c-c) bond length, $t = 2.7$ eV is the nearest neighbor (c-c) tight-binding overlap energy. The distribution function $f_p(\varepsilon)$ is expressed by Taylor expansion as

$$f_{\vec{p}} = f_0(\varepsilon) - \vec{p}f_1(\varepsilon) + ... \tag{128}$$

The $f_1(\varepsilon) = \vec{\chi}(\varepsilon)\frac{\partial f_0}{\partial \varepsilon}$ is the perturbative part. The $\vec{\chi}(\varepsilon)$ characterises the deviation of the f_p from its equilibruim and is determined from the Boltzmann kinetic equation. Multiplying the Eqn. (125) by $\vec{p}\delta(\varepsilon - \varepsilon_{\vec{p}})$ and summing over $\vec{p}$ reduces the Boltzmann kinetic equation to

$$\frac{\vec{R}(\varepsilon)}{\tau(\varepsilon)} + \Omega\left[\vec{H}, \vec{R}(\varepsilon)\right] = \vec{\Lambda}(\varepsilon) + \vec{S}(\varepsilon) \tag{129}$$

where $\vec{R}(\varepsilon)$ is the partial current density given as

$$\vec{R}(\varepsilon) \equiv e\sum_{\vec{p}} \vec{p}f_{\vec{p}}\delta(\varepsilon - \varepsilon_{\vec{p}}) \tag{130}$$

with $\vec{\Lambda}(\varepsilon)$ and $\vec{S}(\varepsilon)$ given as

$$\vec{\Lambda}(\varepsilon) = -e\sum_{\vec{p}}\left(\vec{E}, \frac{\partial f_{\vec{p}}}{\partial \vec{p}}\right)\vec{p}\,\delta(\varepsilon - \varepsilon_{\vec{p}}) \tag{131}$$

$$\begin{aligned}\vec{S}(\varepsilon) = \frac{\pi\xi^2\vec{W}}{\rho V_s^3}\sum_{\vec{p}}\vec{p}\,\delta(\varepsilon \;-\; & \varepsilon_{\vec{p}})\{[f_{\vec{p}+\vec{q}} - f_{\vec{p}}]\delta(\varepsilon_{\vec{p}+\vec{q}} - \varepsilon_{\vec{p}} - \hbar\omega_{\vec{q}}) \\ & + \;[f_{\vec{p}-\vec{q}} - f_{\vec{p}}]\delta(\varepsilon_{\vec{p}-\vec{q}} - \varepsilon_{\vec{p}} + \hbar\omega_{\vec{q}})\}\end{aligned} \tag{132}$$

Considering $\vec{p} \to -\vec{p}$, $f_{\vec{p}} \to f_0(\varepsilon_{\vec{p}})$, by transforming the summation into integrals and integrating gives

$$\vec{\Lambda}(\varepsilon) = \vec{E}\left(\frac{2\hbar^2\beta^2}{\hbar\vec{q}}\alpha - \frac{\hbar\vec{q}}{2}\right)\frac{\partial f_0}{\partial\varepsilon}\frac{\Theta\left(1-\alpha^2\right)}{\sqrt{1-\alpha^2}} \tag{133}$$

$$\vec{S}(\varepsilon) = \frac{2\pi\vec{W}\phi}{\rho V_s\alpha}\left(\frac{2\hbar^2\beta^2}{\hbar q}\alpha - \frac{\hbar q}{2}\right)\frac{\Theta\left(1-\alpha^2\right)}{\sqrt{1-\alpha^2}}\frac{1}{f_0(\varepsilon)}\frac{\partial f_0}{\partial\varepsilon} \tag{134}$$

where $\alpha = \frac{\hbar\omega_q}{E_g}$, $\zeta = \frac{E_g^2\alpha^2}{2V_s^2}f_0(\varepsilon_{\vec{p}})$ and Θ is the Heaviside step function represented as

$$\Theta(1-\alpha^2) = \begin{cases} 1 & \text{if } (1-\alpha^2) > 0 \\ 0 & \text{if } (1-\alpha^2) < 0 \end{cases}$$

Substituting Eqn. (131) and Eqn. (132) into Eqn. (125) and solving for $\vec{R}(\varepsilon)$ gives

$$\vec{R}(\varepsilon) = \{\frac{2\pi\zeta}{\rho V_s \alpha}\left(\frac{2\hbar\beta^2}{q}\alpha - \frac{\hbar q}{2}\right)\frac{1}{f_0(\varepsilon)}\frac{\partial f_0}{\partial \varepsilon}$$
$$\{\vec{W}\tau(\varepsilon) + \vec{\Omega}[\vec{h},\vec{W}]\tau^2(\varepsilon) + \Omega^2\vec{h}(\vec{h},\vec{W})\tau^3(\varepsilon)\} + \left(\frac{2\hbar\beta^2}{q}\alpha - \frac{\hbar q}{2}\right)\frac{\partial f_0}{\partial \varepsilon}$$
$$\{\vec{E}\tau(\varepsilon) + \Omega[\vec{h},\vec{E}]\tau^2(\varepsilon) + \Omega^2\tau^3\vec{h}(\vec{h},\vec{E})\}\}\frac{\Theta(1-\alpha^2)}{\sqrt{1-\alpha^2}}\{1+\Omega^2\tau^2(\varepsilon)\}^{-1} \quad \textbf{(135)}$$

which can be written as $\vec{R}(\varepsilon) = \vec{\chi}(\varepsilon)\frac{\partial f_0}{\partial \varepsilon}$. In the linear approximation of $\vec{E}$, $\vec{\chi}(\varepsilon)$ reduces to

$$\vec{\chi}(\varepsilon) = \{\vec{E}\tau(\varepsilon) + \Omega[\vec{h},\vec{E}]\tau^2(\varepsilon)\}\left(\frac{2\hbar\beta^2}{q}\alpha - \frac{\hbar q}{2}\right)\{1+\Omega^2\tau^2(\varepsilon)\}^{-1} \quad \textbf{(136)}$$

The integral of $\vec{R}(\varepsilon)$ gives the total current density $\vec{j}$ as

$$\vec{j} = -\int_0^\infty \vec{R}(\varepsilon)d\varepsilon \quad \textbf{(137)}$$

Averaging Eqn. (136) over energy, the $\vec{j}$ in the y-direction is

$$\vec{j}_y = \{\langle\frac{\tau(\varepsilon)}{1+\Omega^2\tau^2(\varepsilon)}\rangle\vec{E}_y - \Omega\langle\frac{\tau^2(\varepsilon)}{1+\Omega^2\tau^2(\varepsilon)}\rangle[\vec{h},\vec{E}]_y\}\left(\frac{2\hbar\beta^2}{q}\alpha - \frac{\hbar q}{2}\right) \quad \textbf{(138)}$$

Here, the sound is considered propagating along the Ox axis and the magnetic field $\tilde{H}$ parallel to the Oz axis. For $j = 0$ (i.e the sample open), solving for $\vec{E}_y$ in

Eqn. (138) and substituting into Eqn. (136) for $\langle\langle\vec{\chi}(\varepsilon)\rangle\rangle_y$ yields

$$\langle\langle\vec{\chi}(\varepsilon)\rangle\rangle_y = \Omega\vec{E}_x[\langle\langle\frac{\tau(\varepsilon)}{1+\Omega^2\tau^2(\varepsilon)}\rangle\rangle\frac{\langle\frac{\tau^2(\varepsilon)}{1+\Omega^2\tau^2(\varepsilon)}\rangle}{\langle\frac{\tau(\varepsilon)}{1+\Omega^2\tau^2(\varepsilon)}\rangle} - \langle\langle\frac{\tau^2(\varepsilon)}{1+\Omega^2\tau^2(\varepsilon)}\rangle\rangle] \left(\frac{2\hbar\beta^2}{q}\alpha - \frac{\hbar q}{2}\right) \quad \textbf{(139)}$$

E_x is the electric field in the x-direction. In Eqn. (138 and 139), the averages used are expressed as

$$\langle\frac{\tau^k(\varepsilon)}{1+\Omega^2\tau^2(\varepsilon)}\rangle = -\int_0^\infty(\frac{\tau^k(\varepsilon)}{1+\Omega^2\tau^2(\varepsilon)})\frac{\partial f_0}{\partial\varepsilon}d\varepsilon$$

$$\langle\langle\frac{\tau^k(\varepsilon)}{1+\Omega^2\tau^2(\varepsilon)}\rangle\rangle = -\frac{2\pi}{f_0(\varepsilon)}\int_0^\infty(\frac{\tau^k(\varepsilon)}{1+\Omega^2\tau^2(\varepsilon)})\frac{\partial f_0}{\partial\varepsilon}d\varepsilon$$

where $k = 1,2,3$ and $f_0 = [1 + exp(\frac{1}{k_BT}(\varepsilon - \varepsilon_F))]^{-1}$ is the Fermi-Dirac distribution function. ε_F is the Fermi energy, k_B the Boltzmann constant and T the absolute temperature.

Sound Absorption in GNR

The general formula for the electronic sound absorption coefficient $(\Gamma(q))$ has the form

$$\Gamma(q) = \Gamma_0[1 - \frac{(q,\langle\langle\vec{\chi}(\varepsilon)\rangle\rangle)}{qV_s}] \quad \textbf{(140)}$$

where Γ_0 is the absorption coefficient in the absence of external fields, V_s is the speed of sound. Inserting Eqn. (139) into Eqn. (140) gives the sound

amplification ($\Gamma_\perp$) perpendicular to the electric current ($\vec{j}_y$) as

$$\Gamma_\perp = \Gamma_0\{1 - \frac{\Omega\vec{E}_x}{V_s}[\langle\langle\frac{\tau(\varepsilon)}{1+\Omega^2\tau^2(\varepsilon)}\rangle\rangle\frac{\langle\frac{\tau^2(\varepsilon)}{1+\Omega^2\tau^2(\varepsilon)}\rangle}{\langle\frac{\tau(\varepsilon)}{1+\Omega^2\tau^2(\varepsilon)}\rangle} - \langle\langle\frac{\tau^2(\varepsilon)}{1+\Omega^2\tau^2(\varepsilon)}\rangle\rangle] \left(\frac{2\hbar\beta^2}{q}\alpha - \frac{\hbar q}{2}\right)\} \quad \textbf{(141)}$$

The Eqn. (141) is a general expression for the calculation of the sound amplification in AGNR.The relaxation time τ is dependant on energy and is given as

$$\tau = \frac{3\sqrt{\pi}}{4}\tau_0(\frac{\varepsilon}{k_BT})^v$$

where τ_0 is a constant, and for acoustic phonons, $v = -1/2$. At low temperatures, the Fermi-Dirac distribution function reduces to $f_0 = exp(-\varepsilon/k_BT)$ (considering $\varepsilon_F = 0$) and ulitising the expression

$$\int_0^\infty \frac{x^{v-1}exp(-\mu x)}{x+\varphi}dx = \varphi^{v-1}exp(\varphi\mu)\Gamma(v)\Gamma(1-v,\varphi\mu)$$

Eqn. (141) simplifies to

$$\Gamma_\perp/\Gamma_0 = [1 - \frac{9\pi}{8V_s}\Omega E_x\tau_0^2 exp(\phi^2)\{\frac{9\pi}{16}\frac{\Gamma(-3/2,\phi^2)\Gamma(-1/2,\phi^2)}{\Gamma(-2,\phi^2)} - \Gamma(0,\phi^2)\}\left(\frac{2\hbar\beta^2}{q}\alpha - \frac{\hbar q}{2}\right)] \quad \textbf{(142)}$$

where $\phi = \frac{3\sqrt{\pi}}{4}\Omega\tau_0$ and $\Gamma(n,m)$ is gamma function (where n, m are integers).

Acoustomagnetoelectric Effect in GNR

Acoustomagnetoelectric Effect (AME) in semiconductors and their related materials deals with the appearance of a d.c electric field in the Hall direction when the material is placed in a magnetic field H with the sample on open circuit. This interaction is treated as that between the sound wave and the field which leads to a collective drift of acoustically bunched electrons. The study of AME in semiconductors and its related materials have generated lot of interest recently . AME in materials such as Superlattices [301–303], Quantum Wires [304], CNT [305] deals with appearance of a d.c electric field in the Hall direction when the sample is on open circuit. Studies have shown that the propagation of acoustic waves causes the transfer of energy and momentum to the conducting electrons [303]. The AME was predicted by Grinberg and Kramer [306] for bipolar semiconductors and experimentally observed in Bismuth by Yamada [307]. By applying the sound flux ($\vec{W}$), electric current ($\vec{j}$), and magnetic fields ($\tilde{\mathrm{H}}$) perpendicularly to the sample, it is interesting to note that, with the sample opened in direction perpendicular to the Hall direction, can leads to a non-zero AME [308]. Mensah et. al., [301] studied these effect in superlattice in the hypersound regime, Bau et. al., [309] studied the AME of cylindrical quantum wires. Also, AME effect in mono-polar semiconductor for both weak and quantizing field were studied [310]. Experimentally, AME has been observed in n-InSb [311], and in graphite [312] for $ql << 1$. In this thesis, AME in graphene nanoribbon is studied where the Boltzmann kinetic equation is used to study the SAME in GNR. This is achieved by applying sound flux ($\vec{W}$) to the GNR sample in the presence of

electric field ($\vec{E}$) and magnetic fields ($\tilde{\mathrm{H}}$). With the sample open ($j=0$), give the E_{SAME} in GNR.

The configuration for suface acoustomagnetoelectric field in GNR will be considered with the acoustic phonon $\vec{W}$, the magnetic field $\tilde{\mathrm{H}}$ and the measured E_{SAME} lying in the same plane. Based on the method developed in [313], the partial current density generated in the sample is solved from the Boltzmann transport equation given in Eqn. (125). The Eqn. (136) can further be simplified with the following substitutions $g=1/1+\Omega^2\tau(\varepsilon)^2$, $\gamma_k \equiv \langle g\tau(\varepsilon)^k\rangle$, and $\eta \equiv \langle\langle g\tau(\varepsilon)^k\rangle\rangle$ where $k=1,2,3$. This yields

$$\vec{j}=\frac{\Delta\Gamma_0}{\rho V_s\alpha}\frac{\Theta(1-\alpha^2)}{\sqrt{1-\alpha^2}}\left\{\eta_1\vec{W}+\Omega\eta_2[\vec{h},\vec{W}]+\Omega^2\eta_3\vec{h}(\vec{h},\vec{W})\right\}+ \Delta\frac{\Theta\left(1-\alpha^2\right)}{\sqrt{1-\alpha^2}}\left\{\gamma_1\vec{E}+\gamma_2\Omega[\vec{h},\vec{E}]+\Omega^2\gamma_3\vec{h}(\vec{h},\vec{E})\right\} \quad \textbf{(143)}$$

With the sample opened ($\vec{j}=0$), and ignoring higher powers of Ω gives

$$\gamma_1\vec{E}_x-\gamma_2\Omega\vec{E}_y = -\gamma_1\vec{E}_\alpha \quad \textbf{(144)}$$

$$\gamma_2\Omega\vec{E}_x+\gamma_2\Omega\vec{E}_y = -\gamma_2\Omega\vec{E}_\alpha \quad \textbf{(145)}$$

where $E_\alpha=\frac{\Gamma_0}{\rho S\alpha}$. Making the $\vec{E}_y$ the subject of the equation yields

$$\vec{E}_y=\vec{E}_\alpha\Omega\left\{\frac{\eta_1\gamma_2-\eta_2\gamma_1}{\gamma_1^2+\gamma_2^2\Omega^2}\right\} \quad \textbf{(146)}$$

substituting the expressions for $\eta_1, \eta_2, \gamma_1, \gamma_2$ into Eqn. (146), with $\vec{E}_y = \vec{E}_{SAME}$ gives

$$\vec{E}_{SAME} = \vec{E}_\alpha \Omega \left\{ \frac{\langle \frac{\tau(\varepsilon)^2}{1+\Omega^2\tau(\varepsilon)^2} \rangle \langle \langle \frac{\tau(\varepsilon)}{1+\Omega^2\tau(\varepsilon)^2} \rangle \rangle - \langle \langle \frac{\tau(\varepsilon)^2}{1+\Omega^2\tau(\varepsilon)^2} \rangle \rangle \langle \frac{\tau(\varepsilon)}{1+\Omega^2\tau(\varepsilon)^2} \rangle}{\langle \frac{\tau(\varepsilon)}{1+\Omega^2\tau(\varepsilon)^2} \rangle^2 + \langle \frac{\tau(\varepsilon)^2}{1+\Omega^2\tau(\varepsilon)^2} \rangle^2 \Omega^2} \right\} \quad \textbf{(147)}$$

In Eqn. (146), the following averages were used

$$\langle .... \rangle = -\int_0^\infty (....) \frac{\partial f_0}{\partial \varepsilon} d\varepsilon$$
$$\langle \langle .... \rangle \rangle = -\frac{2\pi}{f_0(\varepsilon)} \int_0^\infty (....) \frac{\partial f_0}{\partial \varepsilon} d\varepsilon$$

where $f_0 = [1 - exp(-\frac{1}{kT}(\varepsilon - \varepsilon_F))]^{-1}$ is the Fermi-Dirac distribution function. In solving for Eqn. (3.26), the following were assumed: At low temperature $kT << 1$, and $\frac{\partial f_0}{\partial \varepsilon} = \frac{-1}{k_\beta T} exp(-\frac{\varepsilon - \mu}{k_\beta T})$. The equation for $\vec{E}_{SAME}$ simplifies to

$$\vec{E}_{SAME} = \frac{E_g \vec{W} \hbar \omega_{\vec{q}} \eta}{2\rho V_s^3} \left\{ \Gamma(-1/2, \eta^2)\Gamma(-3/2, \eta^2) - \Gamma(0, \eta^2)\Gamma(-2, \eta^2) \right\} \times \left\{ \frac{3\sqrt{\pi}}{4} \Gamma(-1/2, \eta^2)^2 + \frac{9\pi}{16} \eta^2 \Gamma(0, \eta^2)^2 \right\}^{-2} \quad \textbf{(148)}$$

Amplification Of Hypersound In Graphene

We will proceed following the works of [269], here the acoustic wave will be consisdered as phonons of frequency (ω_q) in the short-wave region $ql >> 1$ (q is the acoustic wave number, l is the electron mean free path). The kinetic equation for the acoustic phonon population $N_{\vec{q}}(t)$ in the graphene sheet is given by

$$\frac{\partial N_{\vec{q}}}{\partial t} = \frac{2\pi}{\hbar} g_s g_v \sum_{k,k'} |C_{\vec{q}}|^2 \delta_{k,k'+\vec{q}} \{[N_{\vec{q}}(t)+1] f_{\vec{k}}(1-f_{\vec{k}'}) \delta(\varepsilon_{\vec{k}'} - \varepsilon_{\vec{k}} + \hbar\omega_{\vec{q}}) - N_{\vec{q}}(t) f_{\vec{k}'}(1-f_{\vec{k}}) \delta(\varepsilon_{\vec{k}'} - \varepsilon_{\vec{k}} - \hbar\omega_{\vec{q}})\} \quad \textbf{(149)}$$

where $g_s = g_v = 2$ accounts for the spin and valley degeneracies respectively, $N_{\vec{q}}(t)$ represent the number of phonons with a wave vector $\vec{q}$ at time t. The factor $N_{\vec{q}} + 1$ accounts for the presence of $N_{\vec{q}}$ phonons in the system when the additional phonon is emitted. The $f_{\vec{k}}(1-f_{\vec{k}})$ represents the probability that the initial $\vec{k}$ state is occupied and the final electron state $\vec{k}'$ is empty whilst the factor $N_{\vec{q}} f_{\vec{k}'}(1-f_{\vec{k}})$ is that of the boson and fermion statistics. The unperturbed electron distribution function is given by the shifted Fermi-Dirac function as

$$f_{\vec{p}} = [exp(-\beta(\varepsilon(\vec{p} - mv_D) - \chi))]^{-1} \quad \textbf{(150)}$$

where $f_{\vec{p}}$ is the Fermi-Dirac equilibrium function, with χ being the chemical potential, $\vec{p}$ is momentum of the electron, $\beta = 1/kT$, k is the Boltzmann constant and V_D is the net drift velocity relative to the ion lattice site. In Eqn. (149), the

summation over k and k' can be transformed into integrals by the prescription

$$\sum_{k,k'} \rightarrow \frac{A^2}{(2\pi)^4} \int d^2k d^2k'$$

where A is the area of the sample, and assuming that $N_q(t) >> 1$ yields

$$\frac{\partial N_{\vec{q}}}{\partial t} = \Gamma_{\vec{q}} N_{\vec{q}} \tag{151}$$

where

$$\Gamma_{\vec{q}} = \frac{A|\Lambda|^2 \hbar q}{(2\pi)^3 \hbar V_F \rho V_s} \int_0^\infty k dk \int_0^\infty k' dk' \int_0^{2\pi} d\phi \int_0^{2\pi} d\theta \{[f(k) - f(k')] \delta(k - k' - \frac{1}{\hbar V_F}(\hbar\omega_q - V_D \cdot \hbar\vec{q}))\} \tag{152}$$

with $k' = k - \frac{1}{\hbar V_F}(\hbar\omega_q - V_D \cdot \hbar\vec{q})$. Λ is the deformation potential constant, and ρ is the density of the graphene sheet. At low temperature $k_B T << 1$, the distribution function become $f(k) = exp(-\beta(\varepsilon(k)))$. Eqn. (152) can be expressed as

$$\Gamma_{\vec{q}} = \frac{A|\Lambda|^2 \hbar q}{(2\pi)^3 \hbar V_F \rho V_s} \int_0^\infty k dk (k - \frac{1}{\hbar V_F}(\hbar\omega_q - V_D \cdot \hbar\vec{q}))[exp(-\beta\hbar V_F k) - exp(-\beta\hbar V_F (k - \frac{1}{\hbar V_F}(\hbar\omega_q - V_D \cdot \hbar\vec{q})))] \tag{153}$$

Using standard intergrals, Eqn. (152) can be expressed finally as

$$\Gamma = \Gamma_0 \{2 - \beta\hbar\omega_q (1 - \frac{V_D}{V_s})\}[1 - exp(-\beta\hbar\omega_q (1 - \frac{V_D}{V_s}))] \tag{154}$$

where

$$\Gamma_0 = \frac{A|\Lambda|^2 kT \hbar q}{(2\pi)^3 \beta^3 \hbar^4 {V_F}^4 \rho V_s} \tag{155}$$

Acoustoelectric effect in Graphene

The appearance of a direct current when an acoustic wave is passing through a conducting medium is referred to as ”acoustoelectric effect” which was named and first discussed by Parmenter [314]. Recently, much work, both theoretical and experimental has been done on the absorption of ultrasonic waves via an interaction with the conduction electrons in metals, semimetals, and semiconductors. Hutson, et al., [315] discovered the amplification of ultrasonic waves in CdS via the same interaction in the presence of a d.c field. Using a phenomenological treatment, Weinreich [316] showed that when the conduction electrons drift with a velocity greater than sound in the presence of a d.c field, the wave is amplified instead of absorption. But this is valid only when the sound wavelength is longer than the mean free path, i.e., $ql << 1$ (where q is the acoustic wave lenght and l is the mean free path). Acoustoelectric effect (AE) in Bulk and Low-dimensional semiconducting materials has been extensively studied both experimentally [317–322] and theoretically [322, 323]. Recently, AE studies in nano-materials such as graphene [325] and CNT [326, 327] has attracted special attention. This is due to the remarkable electrical and mechanical properties of these materials especially the extreme electron mobility which persist at room temperatures. This makes graphene and CNT suitable for applications in electronic systems such as light storage in quantum wells [328], generating single electrons [329] and photons, particularly for quantum information processing [330–332] and for inducing charge pumping in nanotube quantum dots. Experimentally, AE studies have been reported in graphene [333, 334]. We will proceed following

the works of [269,271], the acoustoelectric current in graphene is given as

$$j_{\vec{ac}} = -\frac{e\tau A|C_q|^2}{(2\pi)^2 V_s}\int_0^\infty kdk\int_0^\infty k'dk'\int_0^{2\pi} d\phi\int_0^{2\pi} d\theta\{[f(k)-f(k')]\times V_i\delta(k-k'-\frac{1}{\hbar V_F}(\hbar\omega_q))\} \quad \textbf{(156)}$$

with $k' = k - \frac{1}{\hbar V_F}(\hbar\omega_q)$. For accoustic phonons, $C_q = \sqrt{|\Lambda|^2\hbar q/2\rho\hbar\omega_q}$, Λ is the constant of deformation potential, ρ is the density of the graphene sheet. τ is the relaxation constant, V_s is the velocity of sound, and A is the area of the graphene sheet. Here the acoustic wave will be considered as phonons of frequency (ω_q) in the short-wave region $ql >> 1$ (q is the acoustic wave number, l is the electron mean free path). The linear energy dispersion $E(k) = \pm\hbar V_F|k|$ (the Fermi velocity $V_F \approx 10^8$ ms^{-1}) at the Fermi level with low-energy excitation. From Eqn. (156), the velocity $V_i = V(k') - V(k)$. Differentiating the energy dispersion yields

$$V_i = \frac{2\hbar\omega_q}{\hbar V_F} \quad \textbf{(157)}$$

At low temperature $k_BT << 1$, the Fermi-Dirac distribution function becomes

$$f(k) = exp(-\beta(\varepsilon(k))) \quad \textbf{(158)}$$

Inserting Eqn. (157) and Eqn. (158) into Eqn. (156) gives

$$j_{\vec{ac}} = -\frac{2A|C_q|^2\tau\hbar\omega_q}{(2\pi)^3\hbar V_F V_s}\int_0^\infty kdk(k-\frac{1}{\hbar V_F}(\hbar\omega_q))[exp(-\beta\hbar V_F k) - exp(-\beta\hbar V_F(k-\frac{1}{\hbar V_F}(\hbar\omega_q)))] \quad \textbf{(159)}$$

Using standard integrals and after a cumbersome manipulations of Eqn. (159) yields the Acoustoelectric Current (j_{ac}) as

$$j_{ac} = j_0\{2 - \beta\hbar\omega_q\}[1 - exp(-\beta\hbar\omega_q)] \quad \textbf{(160)}$$

where

$$j_0 = -\frac{2\tau A|\Lambda|^2 kT\hbar q}{(2\pi)^3\beta^3\hbar^4 V_F{}^4\rho V_s} \quad \textbf{(161)}$$

Hypersound Absorption in Carbon Nanotube

Carbon Nanotubes (CNT's) have recently attracted a lot of interest for use in many semiconductor devices due to their remarkable electrical [335], mechanical [336], and thermal [337–340] properties which are mainly attributed to their unusual band structures [341]. The π-bonding and anti-bonding (π^*) energy band of a CNT crosses at the Fermi level in a linear manner [341]. In the linear regime, electron-phonon interactions in CNT at low temperatures leads to the emission of large number of coherent acoustic phonons. Studies of the effect of phonons on thermal transport [339, 341], on Raman scattering [342] and on electrical transport [343] in CNT is an active area of research. Also, the speed of electrons in the linear region is extremely high. This makes CNT a good candidate for application of high frequency electronic systems such as field effect transistors (FET's) [344], single electron memories [345] and chemical sensors [346]. Another important investigation in the linear regime is interaction of acoustic phonons with drift charges in CNT. It is worthy to note that the mechanism of absorption (amplification) is due to Cerenkov effect. For practical use of the Cerenkov acoustic-phonon

emission, the material must have high drift velocities and large densities of electrons [17]. Carbon Nanotubes (CNT) has electron mobility of 10^5 cm^2/Vs at room temperature. At low temperatures (T = 10 K), CNT exhibit good AE effect, which indicates that Cerenkov emission can take place in them [52]. We will proceed following the works of [267, 304] where the kinetic equation for the phonon distribution is given as

$$\begin{aligned}\frac{\partial N_{\vec{q}}}{\partial t} &= \frac{2\pi}{\hbar}\sum_{p}|C_{\vec{q}}|^2\{[N_{\vec{q}}(t)+1]f_{\vec{p}}(1-f_{\vec{p}'})\delta(\varepsilon_{\vec{p}'}-\varepsilon_{\vec{p}}+\hbar\omega_{\vec{p}}) \\ &- N_{\vec{q}}(t)f_{\vec{p}'}(1-f_{\vec{p}})\delta(\varepsilon_{\vec{p}'}-\varepsilon_{\vec{p}}+\hbar\omega_{\vec{q}})\} \qquad \textbf{(162)}\end{aligned}$$

where $N_{\vec{q}}(t)$ represents the number of phonons with wave vector $\vec{q}$ at time t. The factor $N_{\vec{q}}+1$ accounts for the presence of $N_{\vec{q}}$ phonons in the system when the additional phonon is emitted. The $f_{\vec{p}}(1-f_{\vec{p}})$ represents the probability that the initial $\vec{p}$ state is occupied and the final electron state $\vec{p}'$ is empty whilst the factor $N_{\vec{q}}f_{\vec{p}'}(1-f_{\vec{p}})$ is that of the boson and fermion statistics. The unperturbed electron distribution function is given by the shifted Fermi-Dirac function as

$$f_{\vec{p}} = [exp(-\beta(\varepsilon(\vec{p}-mv_D)-\mu))]^{-1} \qquad \textbf{(163)}$$

where $f_{\vec{p}}$ is the Fermi-Dirac equilibrium function, with μ being the chemical potential, $\vec{p}$ is momentum of the electron, $\beta = 1/kT$, k is the Boltzmann constant and V_D is the net drift velocity relative to the ion lattice site. In a more convenient

form, Eqn. (162) can be written as

$$\frac{\partial N_{\vec{q}}(t)}{\partial t} = 2\pi|C_{\vec{q}}|^2[\frac{N_{\vec{q}}(t)+1}{1-exp(-\beta(\hbar\omega_{\vec{q}}-\hbar\vec{q}\cdot V_D))} + \frac{N_{\vec{q}}}{1-exp(-\beta(\hbar\omega_{\vec{q}}-\hbar\vec{q}\cdot V_D))}] \times \sum_{\vec{p}}(f_{\vec{p}} - f_{\vec{p}'})\delta(\varepsilon_{\vec{p}'} - \varepsilon_{\vec{p}} + \hbar\omega_{\vec{q}}) \quad \textbf{(164)}$$

To simplifiy Eqn. (164), the following were utilised

$$Q = \sum_{\vec{p}} \frac{f_{\vec{p}} - f_{\vec{p}'}}{\varepsilon_{\vec{p}} - \varepsilon_{p'} - \hbar\omega_q - i\delta} \quad \textbf{(165)}$$

$$f_{\vec{p}} = [exp(-\beta(\varepsilon_{\vec{p}} - \mu)) + 1]^{-1} \quad \textbf{(166)}$$

Given that

$$\Gamma_{\vec{q}} = -2|C_{\vec{q}}|^2 ImQ(\hbar\vec{q}, \hbar\omega_{\vec{q}} - \hbar\vec{q}\cdot V_D) \quad \textbf{(167)}$$

the phonon generation rate simplifies to

$$\Gamma_{\vec{q}} = 2\pi|C_{\vec{q}}|^2 \sum_{\vec{p}} (f_{\vec{p}} - f_{\vec{p}'})\delta(\varepsilon_{\vec{p}} - \varepsilon_{\vec{p}'} - (\hbar\omega_{\vec{q}} - \hbar\vec{q}\cdot V_D)) \quad \textbf{(168)}$$

In Eqn. (168), $f_{\vec{p}} > f_{\vec{p}\prime}$ if $\varepsilon_{\vec{p}} < \varepsilon_{\vec{p}'}$. When $\hbar\omega_{\vec{q}} - \hbar\vec{q}\cdot V_D > 0$, the system would return to its equilibrium configuration when perturbed where

$$N^0_{\vec{q}} = [exp(-\beta(\hbar\omega_{\vec{q}} - \hbar\vec{q}\cdot V_D) - 1)]^{-1}$$

But $\hbar\omega_{\vec{q}} - \hbar\vec{q}\cdot V_D < 0$ leads to the Cerenkov condition of phonon instability (amplification). The linear energy dispersion $\varepsilon(\vec{p})$ relation for the CNT is given as [347]

$$\varepsilon(\vec{p}) = \varepsilon_0 \pm \frac{\sqrt{3}}{2\hbar}\gamma_0 b(\vec{p} - \vec{p}_0) \quad \textbf{(169)}$$

The ε_0 is the electron energy in the Brillouin zone at momentum p_0, b is the lattice constant , γ_0 is the tight-binding overlap integral ($\gamma_0 = 2.54$ eV). The $\pm$ sign indicates that in the vicinity of the tangent point, the bands exhibit mirror symmetry with respect to each point. The phonon and the electric field are directed along the CNT axis. Therefore $\vec{p}' = (\vec{p} + \hbar\vec{q})\cos(\theta)$, where θ is the scattering angle. At low temperature, the $kT << 1$, Eqn. (166) reduces to

$$f_{\vec{p}} = exp(-\beta(\varepsilon(p) - \mu)) \tag{170}$$

Inserting Eqn. (169 and 170) into Eqn. (168), and after some cumbersome calculations yield

$$\Gamma = \frac{4\hbar\pi|C_{\vec{q}}|^2 \exp(-\beta(\varepsilon_0 - \chi\vec{p}_0))}{\gamma_0 b\sqrt{3}(1-\cos(\theta))}\{\exp(-\beta(\chi\eta + \hbar\vec{q})\cos(\theta)) - \exp(-\beta\chi\eta)\} \tag{171}$$

where $\chi = \sqrt{3}\gamma_0 b/2\hbar$, and

$$\eta = \frac{2\hbar^2\omega_{\vec{q}}(1 - \frac{V_D}{V_s}) + \gamma_0 b\sqrt{3}\hbar\vec{q}\cos(\theta)}{\gamma_0 b\sqrt{3}(1-\cos(\theta))}$$

Acoustoelectric effect in CNT

Acoustoelectric effect in CNT's is now receiving attention with few experimental work done on it. Ebbecke et al., [111] studied the AE current transport in a single walled CNT, whilst Reulet et al., [112] studied AE in CNT, but in all these research there is no theoretical studies of AE in CNT. It is worthy to note that the mechanism of absorption (amplification) is due to Cerenkov effect. For practical use of the Cerenkov acoustic-phonon emission,

the material must have high drift velocities and large densities of electrons [348]. Carbon Nanotubes (CNT) have electron mobility of 10^5 cm^2/Vs at room temperature. At low temperatures (T = 10 K), CNT exhibit good AE effect, which indicates that Cerenkov emission can take place in them. Proceeding from [260, 261], the Acoustoelectric current j^{ac} in the hypersound regime $ql >> 1$ is given as

$$j = -\frac{4\pi\tau e}{(2\pi)^3}|C_q|^2 \int_0^\infty v_i[f(p+q) - f(p)]\delta(\varepsilon(p+q) - \varepsilon(p) - \hbar\omega)d^3p \quad \textbf{(172)}$$

where the velocity $v_i = v(p+q) - v(p)$, $f(\varepsilon(p))$ is the distribution function, p is the momentum of electrons and τ is the relaxation constant. The linear energy dispersion $\varepsilon(\vec{p})$ relation for the CNT is given as [349]

$$\varepsilon(\vec{p}) = \varepsilon_0 \pm \frac{\sqrt{3}}{2\hbar}\gamma_0 b(\vec{p} - \vec{p}_0) \quad \textbf{(173)}$$

The ε_0 is the electron energy in the Brillouin zone at momentum p_0, b is the lattice constant. The $\pm$ sign indicates that in the vicinity of the tangent point, the bands exhibit mirror symmetry with respect to each point. After collision, $\vec{p'} = (\vec{p} + \hbar\vec{q})\cos(\theta)$ is the component directed along the CNT axis, where θ is the scattering angle. At low temperature ($kT << 1$), the Fermi-Dirac equilibrium function is given as

$$f_{\vec{p}} = \exp(-\beta(\varepsilon_{\vec{p}} - \mu)) \quad \textbf{(174)}$$

with μ being the chemical potential, $\beta = 1/kT$, k is the Boltzmann constant. Inserting Eqn. (174) and Eqn. (173) into Eqn. (172), and after some

cumbersome calculations yield

$$j^{ac} = \frac{2e\pi|C_{\vec{q}}|^2}{\hbar}\exp(-\beta(\varepsilon_0 - \chi\vec{p}_0))\{\exp(-\beta(\chi\eta + \hbar\vec{q})\cos(\theta)) - \exp(-\beta\chi\eta)\} \tag{175}$$

where $\chi = \sqrt{3}\gamma_0 b/2\hbar$, and

$$\eta = \frac{-2\hbar^2\omega_{\vec{q}} + \gamma_0 b\sqrt{3}\hbar\vec{q}\cos(\theta)}{\gamma_0 b\sqrt{3}(cos(\theta) - 1)}$$

For acoustic phonons, $|C_{\vec{q}}| = \sqrt{\Lambda^2\hbar\vec{q}/2\rho V_s}$, where Λ is the deformation potential constant and ρ is the density of the material. Taking $\varepsilon_0 = \vec{p}_0 = 0$, the Eqn. (175) finally reduces to

$$j^{ac} = \frac{2e|\Lambda|^2\tau\hbar q^2\exp(-\beta\chi\eta)}{2\pi\hbar\omega_q}\{\sum_{n=-\infty}^{\infty}\frac{\exp(-n(\theta + \beta\chi\eta))}{I_n(\beta(\chi\eta + \hbar\vec{q}))} - 1\} \tag{176}$$

where $I_n(x)$ is the modified Bessel function. Considering the finite electron concentration, the matrix element can be modified as

$$|C_{\vec{q}}|^2 \to \frac{|C_q|^2}{|\aleph^{(el)}(\vec{q})|^2} \tag{177}$$

where $\aleph^{(el)}(\vec{q})$ is the electron permitivity. However, for acoustic phonons, $|C_{\vec{q}}| = \sqrt{\Lambda^2\hbar\vec{q}/2\rho V_s}$, where Λ is the deformation potential constant and ρ is the density of the material. Taking $\varepsilon_0 = \vec{p}_0 = 0$, the Eqn. (176) finally reduces to

$$\Gamma = \frac{|\Lambda|^2\hbar^3 q^2\exp(-\beta\chi\eta)}{2\pi\hbar\omega_q\gamma_0 b\sqrt{3}(1 - \cos(\theta))}\{\sum_{n=-\infty}^{\infty}\frac{\exp(-n(\theta + \beta\chi\eta))}{I_n(\beta(\chi\eta + \hbar\vec{q}))} - 1\} \tag{178}$$

CHAPTER FOUR

RESULTS AND DISCUSSIONS

Amplification in Graphene Nanoribbon

The parameters used in the numerical calculations are as follows: $\tau = 10^{-10}$ s, $\omega_q = 10^{10}\ s^{-1}$, $V_s = 5*10^3\ ms^{-1}$, $H = 2*10^3\ Am^{-1}$, $q = 2.23*10^6\ cm^{-1}$. The Eqn. (141) is analyzed graphically for varying electric field E_x, acoustic wavenumber q, the energy gap E_g and $\Omega\tau$. The results are graphically displayed. Figure 11, shows the amplification of acoustic waves obtained for

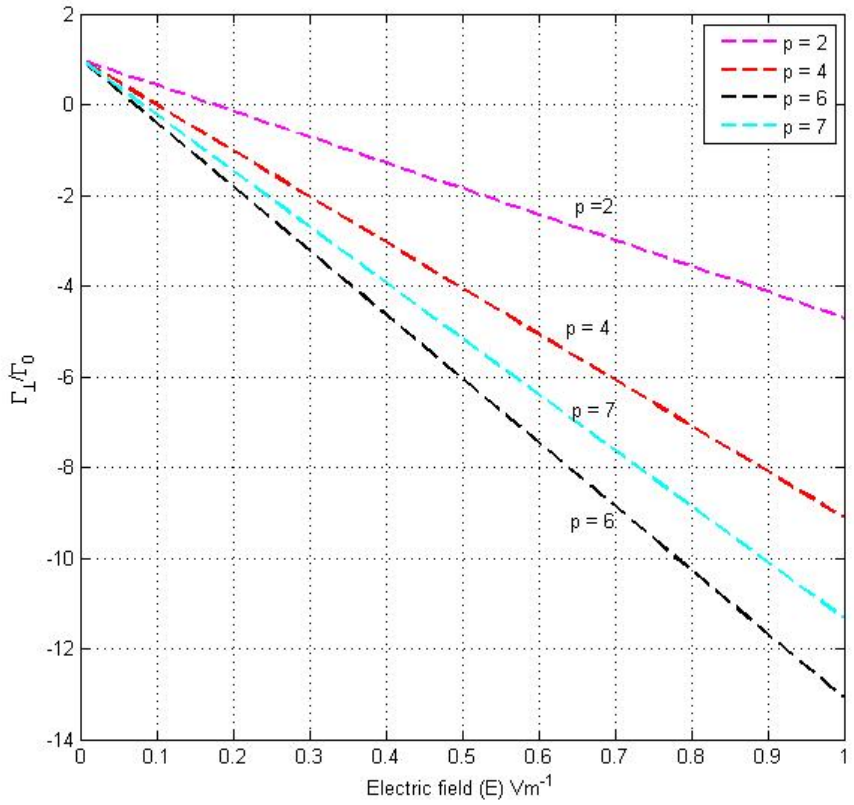

Figure 11: Dependence of Γ/Γ_0 on the electric field E_0 for 7-AGNR with the sub-band index $p_i = 2,4,6,7$

7-AGNR by varying the sub-band index $p_i = 2,4,6,7$ at specified electric fields. The maximum amplification was obtained at $p = 6$ but at $p = 7$, the amplification decreased. For a graph of Γ/Γ_0 against q, Figure 12, showed the

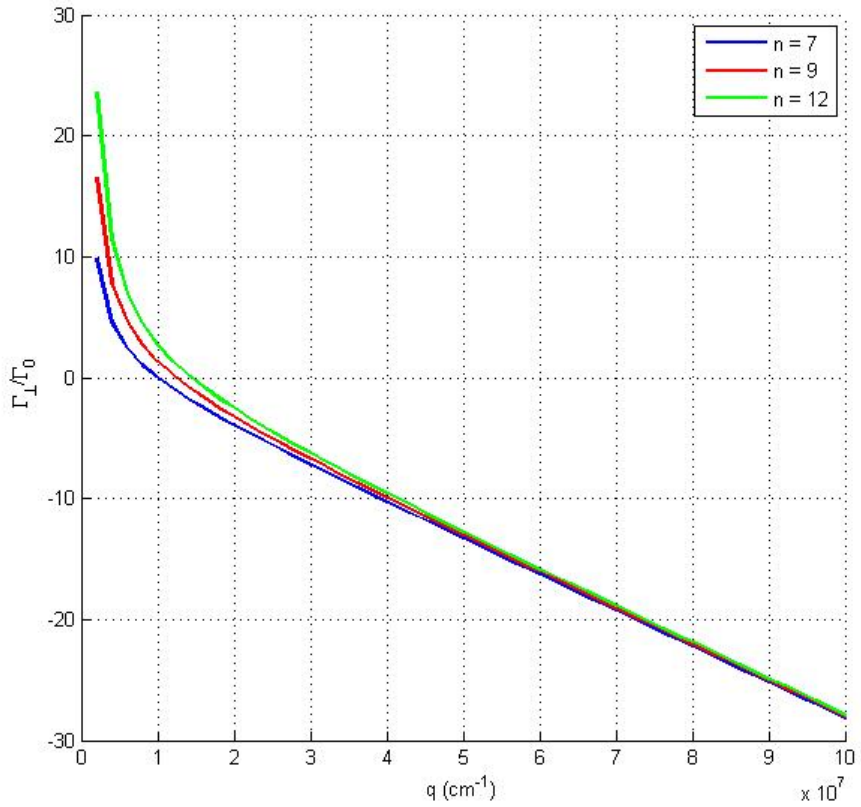

Figure 12: Dependence of Γ/Γ_0 on acoustic wave number q at widths of AGNR $n = 7,9,12$

non-linear graph for different widths of AGNR $(7,9,12)$. From the graph, at $q < 1.5 \times 10^7$ cm^{-1}, there was an absorption. Above this value ($q > 1.5 \times 10^7$ cm^{-1}), absorption switched over to amplification and converges at higher values of q.

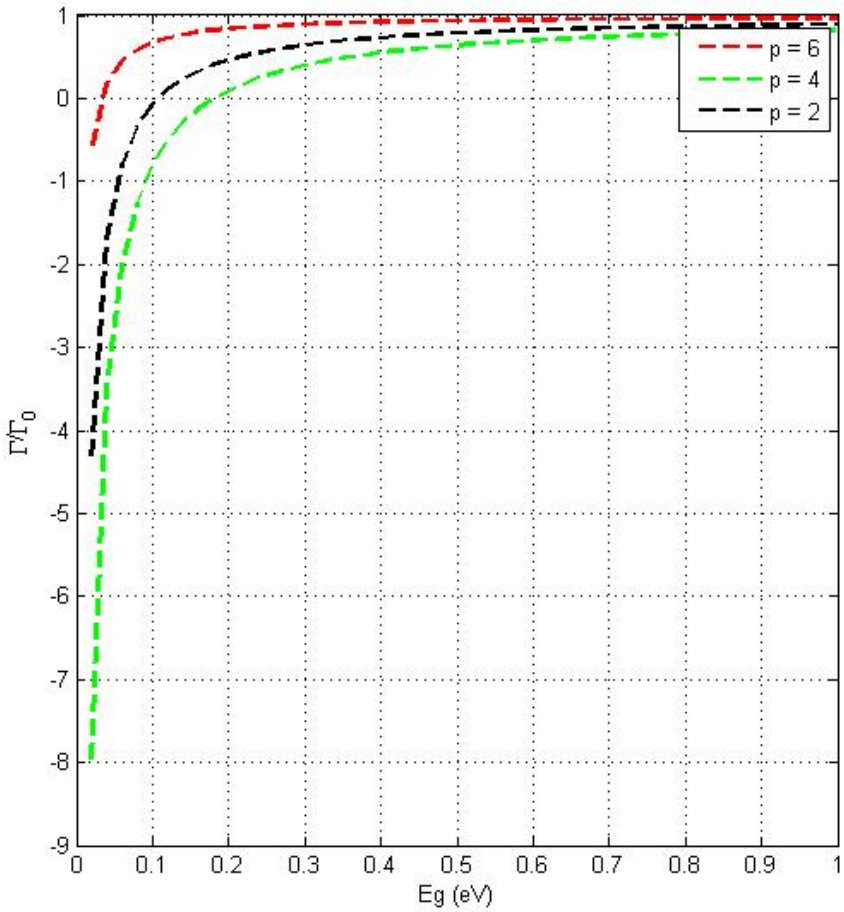

Figure 13: Dependence of Γ/Γ_0 on the energy gap (E_g) of 7-AGNR at sub-band index $p_i = 2,4,6$

For that of energy gap E_g against the amplification Γ/Γ_0 (see Figure 13), the Γ/Γ_0 varies for values of E_g between $0-0.5$ for 7-AGNR at $p_i = 1,2,3$. The graph of $(\Omega\tau)$ versus Γ/Γ_0 is presented in Figure 14. From the graph, $(\Omega\tau)$ increased steadily to a maximum at 0.92 then decreased again.

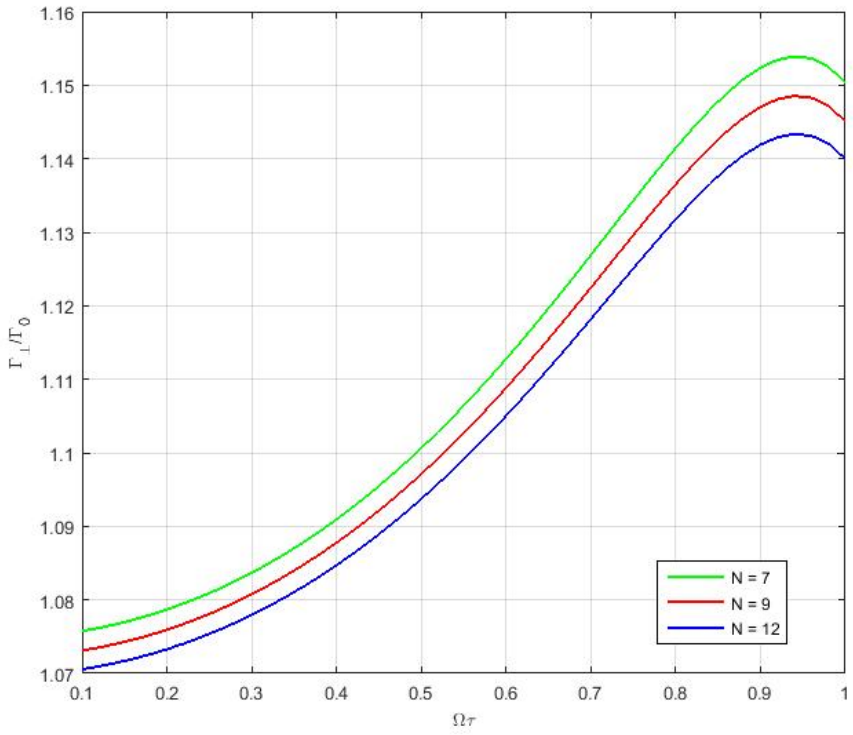

Figure 14: Dependence of Γ/Γ_0 on $\Omega\tau$ for the varying width of AGNR $n = 7, 9, 12$

In 3D representation, the dependence of Γ/Γ_0 on q and E are shown in Figures 15 and 16. There is amplification for 7-AGNR at $q = 2.0 * 10^6$ cm^{-1} but increasing $q = 2.5 * 10^6$ cm^{-1} modulates the graph.

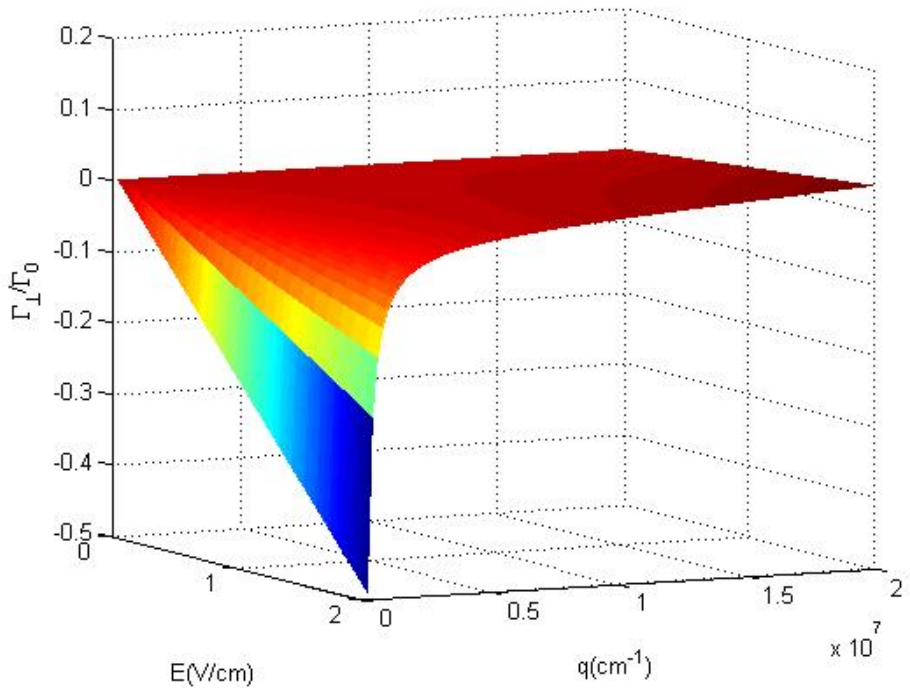

Figure 15: A 3D graph of Γ/Γ_0 on E_0 and q for $p = 1$ 7-AGNR at $\mathrm{q} = 2.0 * 10^6\ \mathrm{cm}^{-1}$

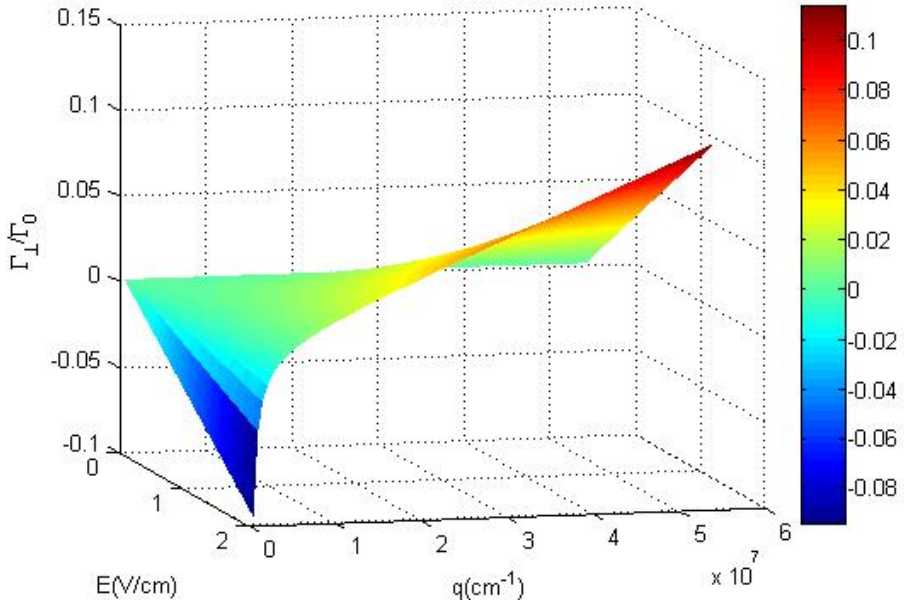

Figure 16: A 3D graph of Γ/Γ_0 on E_0 and q for $p = 1$ 7-AGNR, $\mathrm{q} = 2.5 * 10^6\ \mathrm{cm}^{-1}$

Studies of the transitions in sub-band in the AGNR by tight-binding energy dispersions agrees quantitatively to that of acoustic wave amplification using Boltzmann kinetic equation.

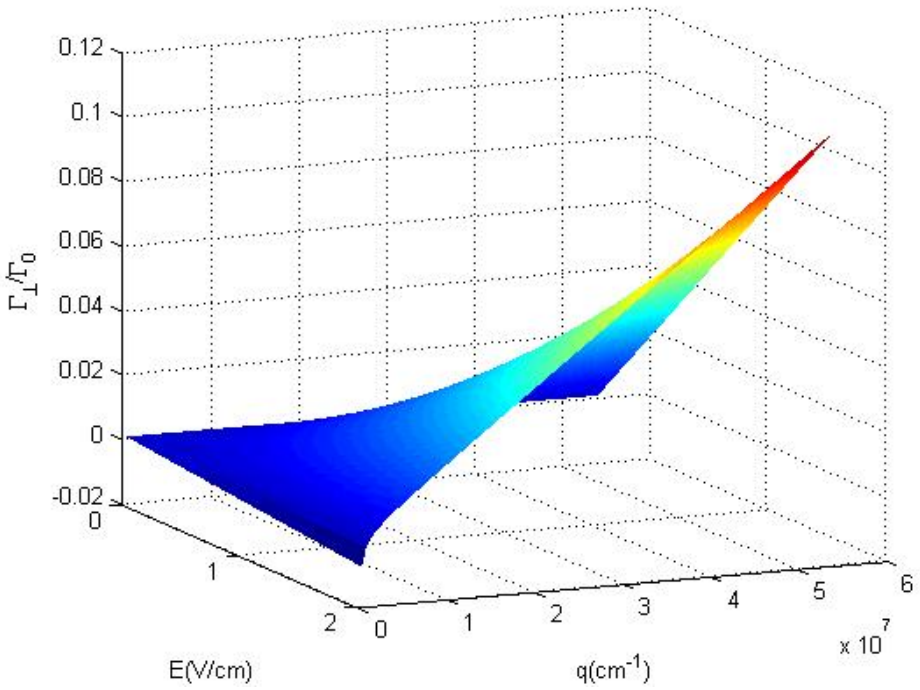

Figure 17: A 3D graph of Γ/Γ_0 on E_0 and q for 7-AGNR at $p = 6$

In tight-binding approximation, the electronic structure of AGNR strongly depends on its width [93]. This is verified by using 7-AGNR and 8-AGNR at $p = 6$ and an energy gap of 0.3 eV (see Figures 17 and 18). The 8-AGNR is purely absorbing but 7-AGNR is partially amplifying. The amplification of the acoustic wave in an external electric and magnetic field is studied using Boltzmann kinetic equation for electron-phonon interactions in AGNR. Analytical expressions for the amplification under different conditions are numerically analysed. The dependence of Γ/Γ_0 on E_0 and q are determined at different values of $\Omega\tau$, p_i and the width where the maximum value of the magnetic strength occurs at 0.93. That of Γ/Γ_0 against q is also analysed. In

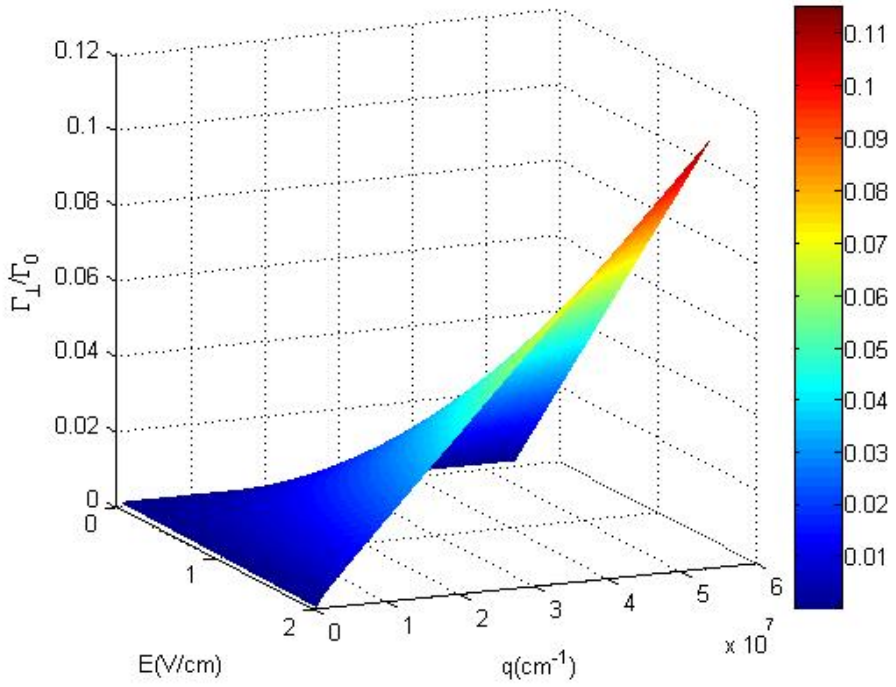

Figure 18: A 3D graph of Γ/Γ_0 on E_0 and q for 8-AGNR, at $p = 6$

particular, when q is increased from $2.0 * 10^6$ cm^{-1} to $2.5 * 10^6$ cm^{-1}, the amplification is modulated.

From Eqn. (148), the $\vec{E}_{SAME}$ is a function of the following parameters: magnetic field strength ($\eta = \Omega\tau$), α and the energy gap $E_g = 3ta_{c-c}\beta$. The E_g depends on the quantized wave vector β. The parameters used in the numerical calculations are $\tau = 10^{-10}\ s$, $\omega_q = 10^{10}\ s^{-1}$, $s = 5 * 10^3\ \text{ms}^{-1}$, $q = 2.23 * 10^6\ \text{cm}^{-1}$. In analysing the Eqn. (148), the condition $((1-\alpha^2) > 0)$ was considered. Figure 19 shows the dependence of $\vec{E}_{SAME}$ against the

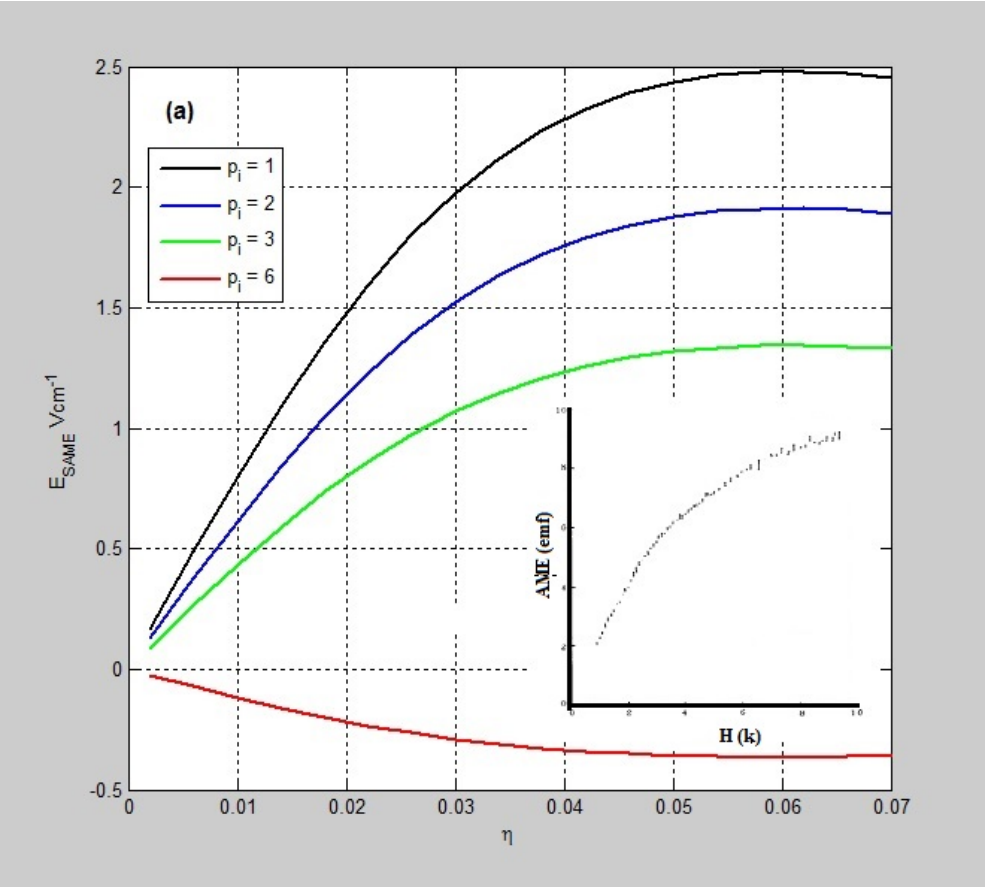

Figure 19: Dependence of $\vec{E}_{SAME}$ versus η for $N = 7$-GNR at different sub-bands. The insert shows the experimental observation of $\vec{E}_{AME}$ in graphite [312]

magnetic field strength η at various sub-bands for $\eta << 1$. Generally, $\vec{E}_{SAME}$ increased to a maximum value for three different values of p_i. The results obtained (see insert Figure 19) qualitatively agreed with an experimental graph

measured in graphite. Figure 20 is the general case when there is no limitation on η. It can be seen that, $\vec{E}_{SAME}$ decreased rapidly after the maximum point to a minimum value. For $p_i = 6$, there is an inversion of the graph. Figure 21, shows the dependence of $\vec{E}_{SAME}$ against N with different p_i.

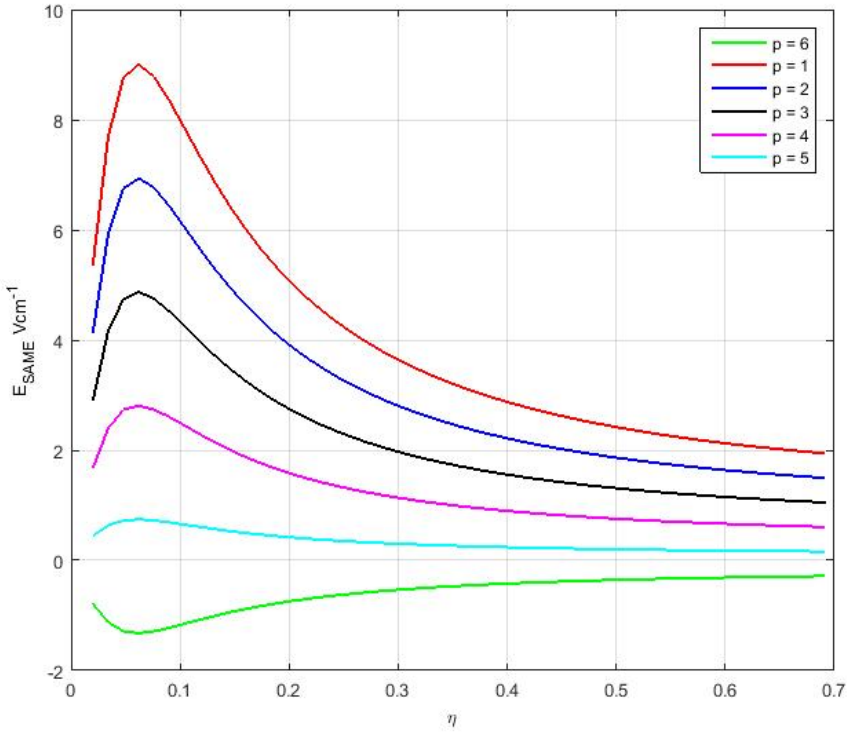

Figure 20: Dependence of $\vec{E}_{SAME}$ versus η for an extended graph of $\vec{E}_{SAME}$ against η

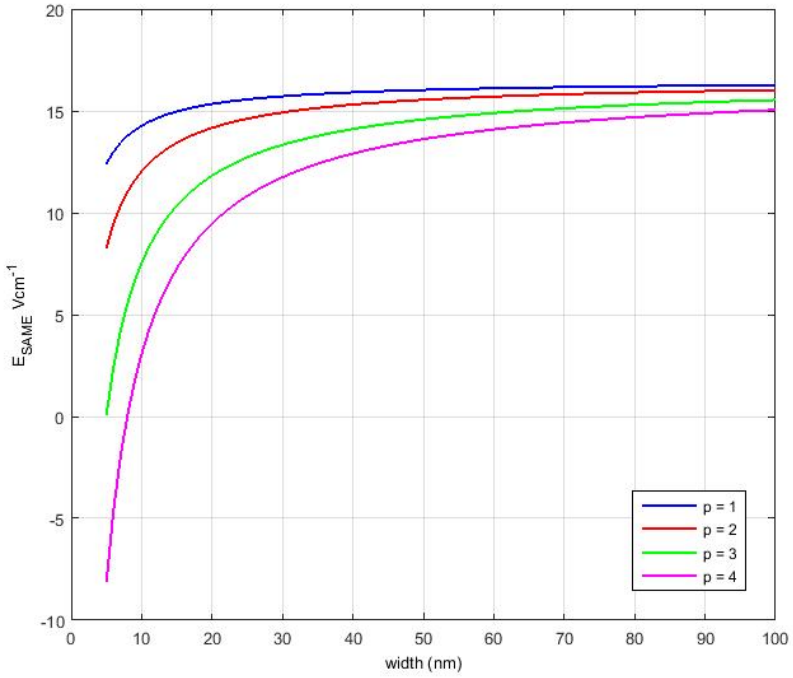

Figure 21: The $\vec{E}_{SAME}$ versus width for $p = 1, 2, 3, 4$

A 3D graph of $\vec{E}_{SAME}$ versus η at $p_i = 1$ and width at $p_i = 6$ are presented (see Figures 22 and 23) where Figure 22 shows an inversion of Figure 23.

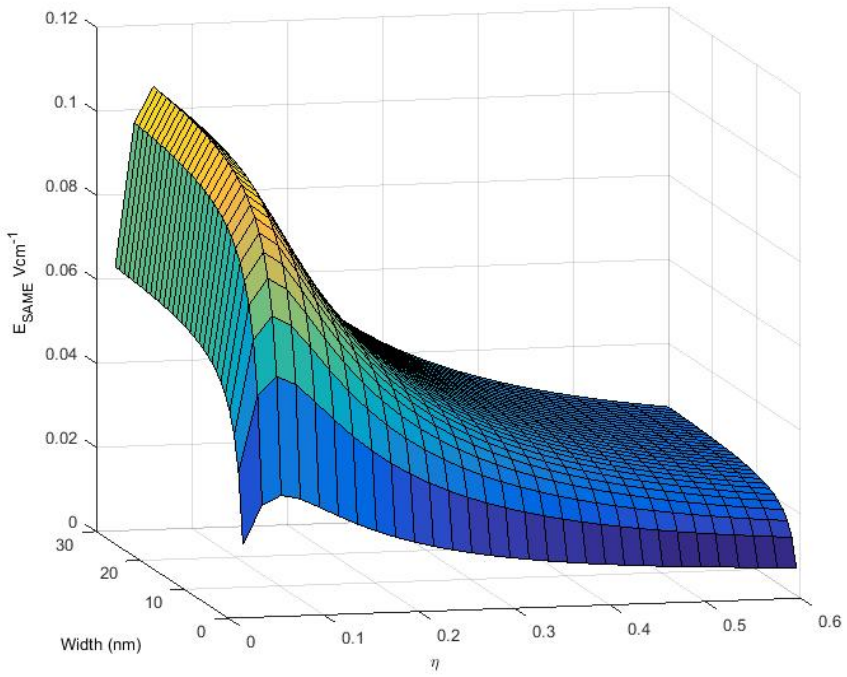

Figure 22: A 3D graph of $\vec{E}_{SAME}$ on width of GNR and η at p = 1

The acoustomagnetoelectric field E_{SAME} in GNR was studied. The dependence of E_{SAME} on the magnetic field strength η and the width N were numerically studied. The E_{SAME} obtained for low magnetic field strength in GNR

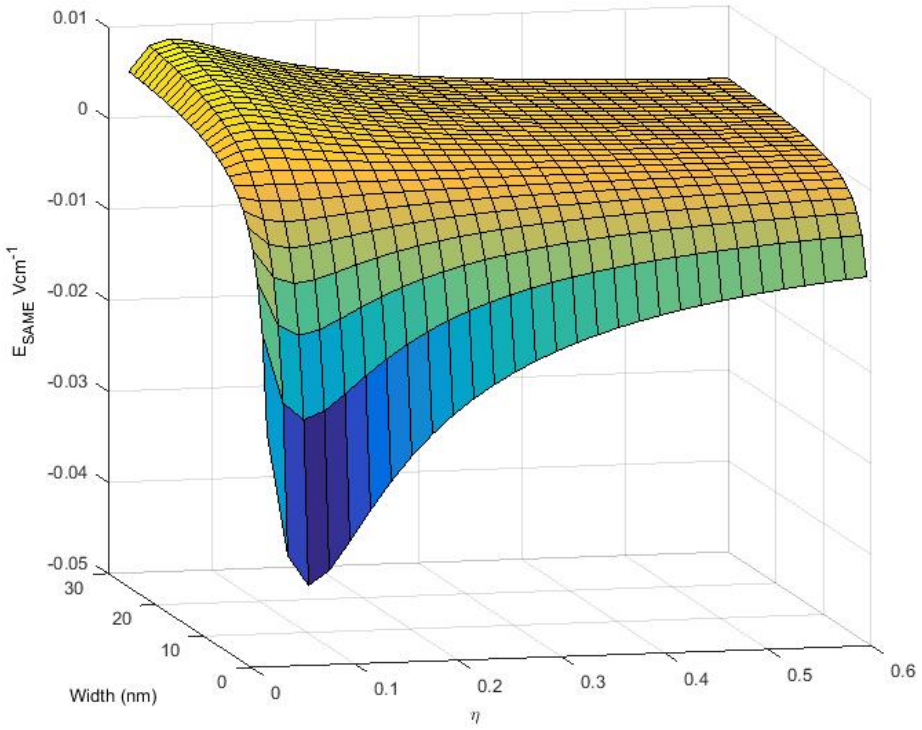

Figure 23: A 3D graph of $\vec{E}_{SAME}$ on width of GNR and η at p = 6

qualitatively agreed with experimentally observed graph in graphite but for strong magnetic fields, the E_{SAME} rapidly falls to a minimum. The graph is modulated by varying the sub-band index p_i with an inversion occuring at $p_i = 6$. At the maximum point, a magnetic field of $H = 3.2\ Am^{-1}$ was calculated which is far lower than that measured in graphite. The E_{SAME} also varies when plotted against the width of GNR at various sub-band indices p_i.

Hypersound Amplification of Graphene

The Eqn (125) is analysed numerically for a normalized graph of $\frac{\Gamma}{\Gamma_0}$ against $\frac{V_D}{V_s}$ and ω_q. The following parameters were used $\Lambda = 9$ eV, T $= 10$ K, $V_s = 2.1 \times 10^6$ cms^{-1} and $\vec{q} = 10^5$ cm^{-1}. In Figure 24, the graph for the dependence of $\frac{\Gamma}{\Gamma_0}$ on ω_q is plotted.

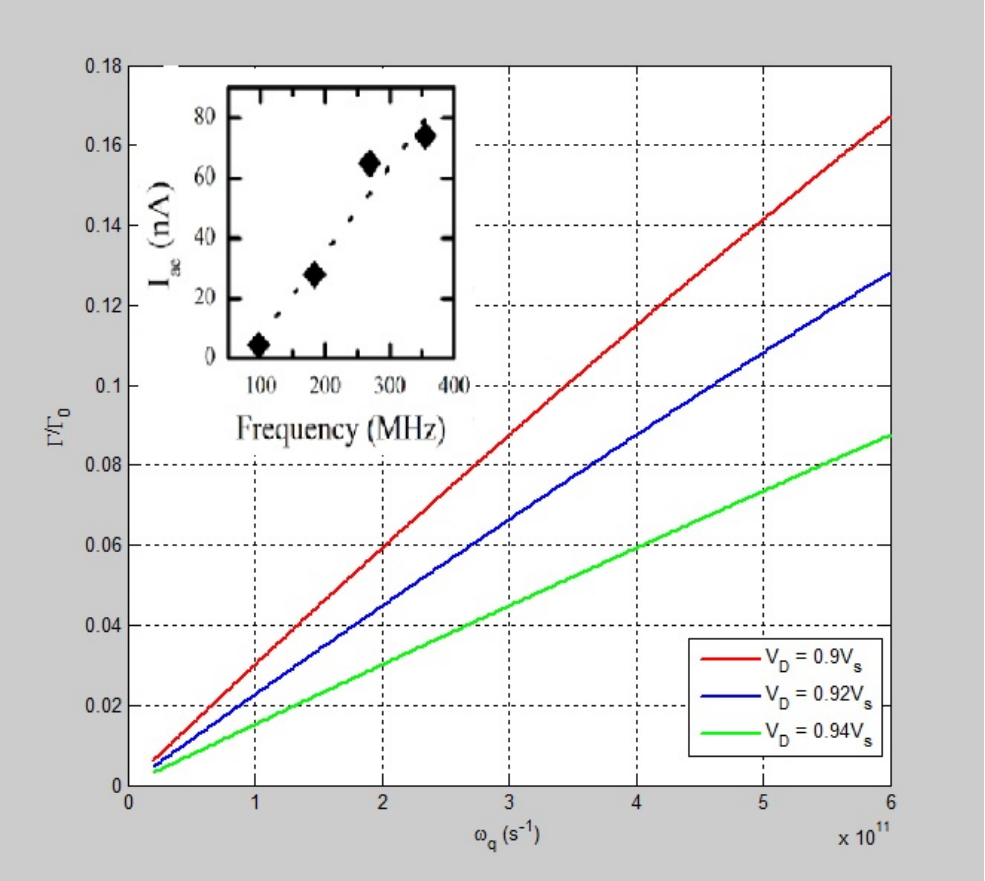

Figure 24: Dependence of Γ/Γ_0 on ω_q. Insert is the experimental verification of Acoustoelectric current versus acoustic phonon frequency [272]

In Figure 25, the dependence of $\frac{\Gamma}{\Gamma_0}$ on $\frac{V_D}{V_s}$ is analysed. From the graph, when $\frac{V_D}{V_s} < 1$, an absorption graph was observed, but when $\frac{V_D}{V_s} > 1$, gave an amplification of hypersound as is indicated in the work of Nunes and Fonseca [269]. The graph

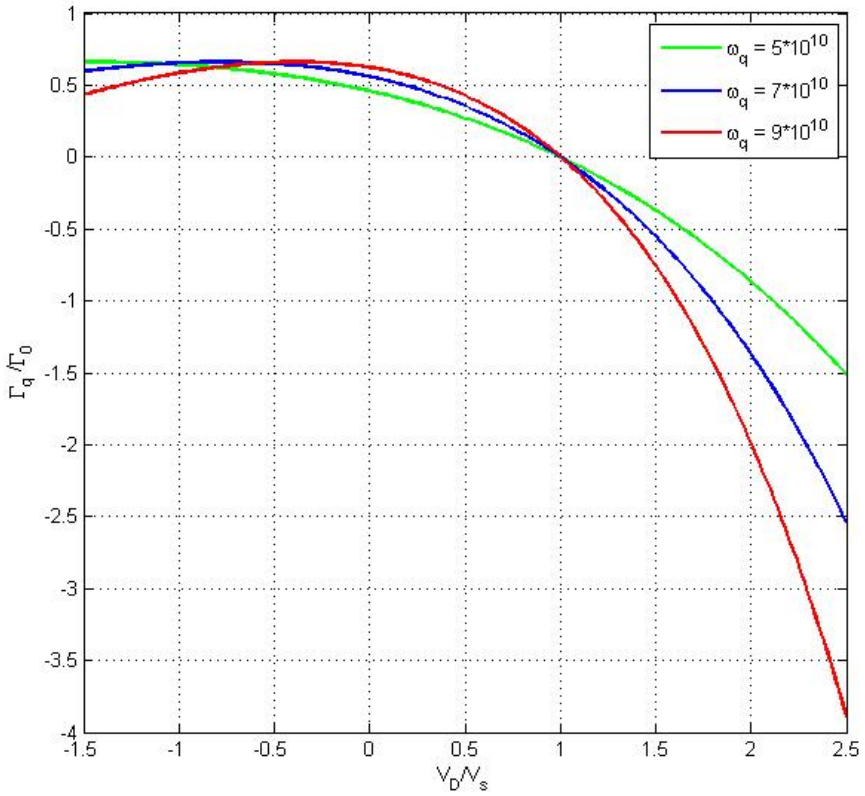

Figure 25: Dependence of Γ/Γ_0 on $\frac{V_D}{V_s}$ for varying ω_q

was obtained at $\frac{V_D}{V_s} < 1$. The insert shows an experimentally obtained graph of an acoustoelectric current for gate-controlled Graphene [272]. The hypersound absorption graph qualitively agreed with the experimentally obtained graph via the Weinriech relation [350].

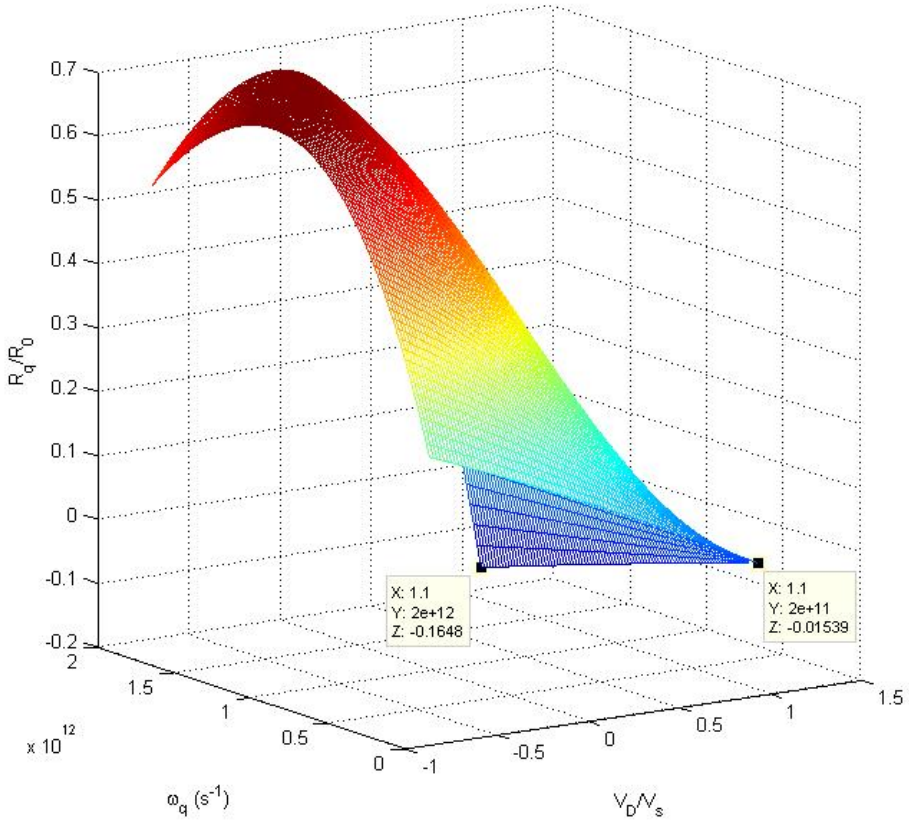

Figure 26: $3D$ representation of Γ/Γ_0 on $\frac{V_D}{V_s}$ and ω_q at 0.2 THz

To enhance the observed Amplification (Absorption), a $3D$ graph was plotted for frequencies $\omega_q = 0.2$, 0.4, and 1 THz (see Figures 26, 27 and 28). In Figure 26, the maximum amplification was obtained at $\frac{\Gamma}{\Gamma_0} = -0.16$ at $\omega_q = 2$ THz for $V_D = 1.1V_s$.

For Figure 27, at $V_D = 1.1V_s$, $\frac{\Gamma}{\Gamma_0} = -0.34$ whislt in Figure 28, for $V_D = 1.1V_s$, $\frac{\Gamma}{\Gamma_0} = -0.08$ was obtained.

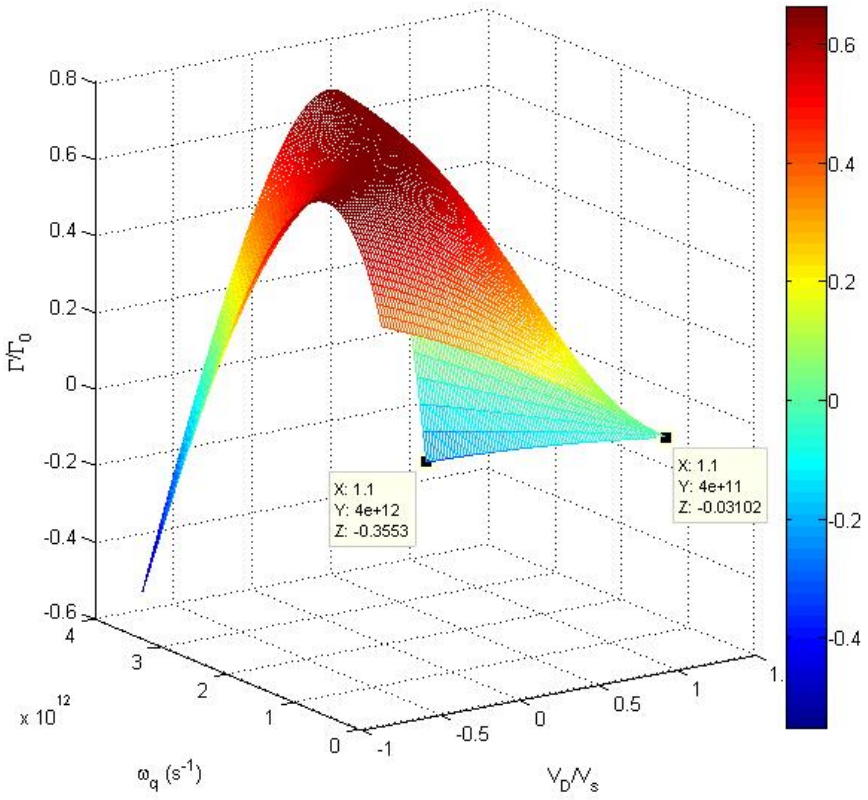

Figure 27: $3D$ representation of Γ/Γ_0 on $\frac{V_D}{V_s}$ and ω_q at 0.4 THz

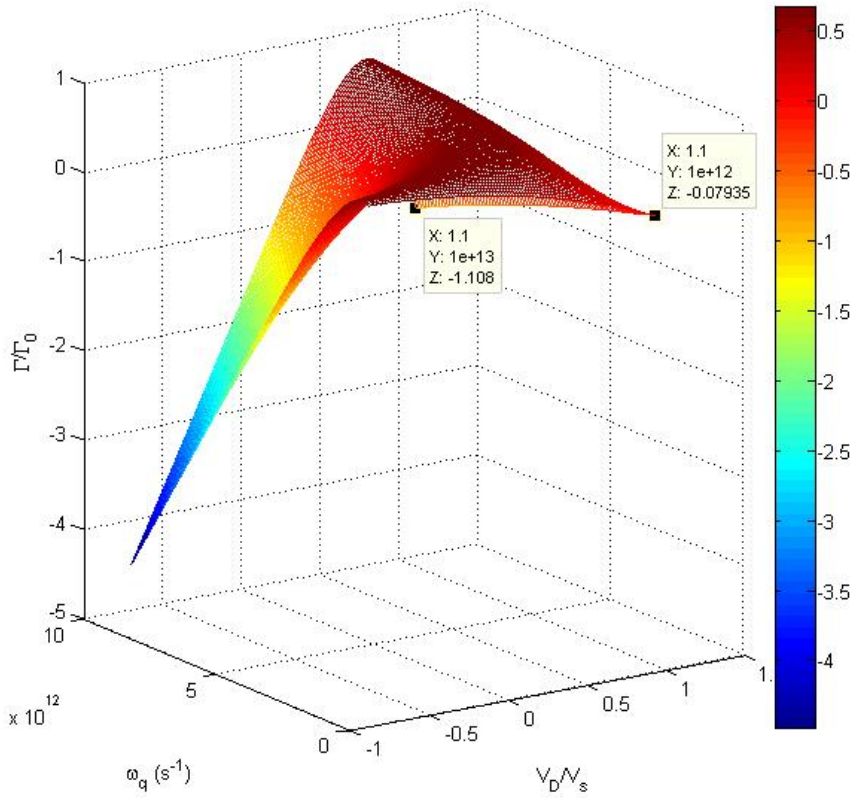

Figure 28: $3D$ representation of Γ/Γ_0 on $\frac{V_D}{V_s}$ and ω_q at 1 THz

It is interesting to note that, acoustic phonon frequencies above 10 THz can be attained. In Figure 29, at $V_D = 1.1V_s$, gave $\frac{\Gamma}{\Gamma_0} = -3.17$ which was obtained at $\omega_q = 20$ THz. For a gate controlled graphene, with $V_D = 1.1V_s$, the field E can be calculated since $E = V_D/\mu$. The electron mobility μ in graphene given as 2.0×10^4 cm^2/Vs, $V_s = 2.1 \times 10^5$cm/s gives $E = 11.5$ V/cm. For the source-to-drain voltage, $V_{sd} = V_D L/\mu$, (L being the length from the source to drain electrode in graphene), the in-plane current $I = enV_D L$ (n being the electron density) can be calculated. The generation of hypersound amplification (absorption) of acoustic - phonons in a gated controlled graphene is studied. The absorption obtained qualitatively agreed with an experimentally obtained acoustoelectric current in a gate-controlled graphene via the Weinrich relation.

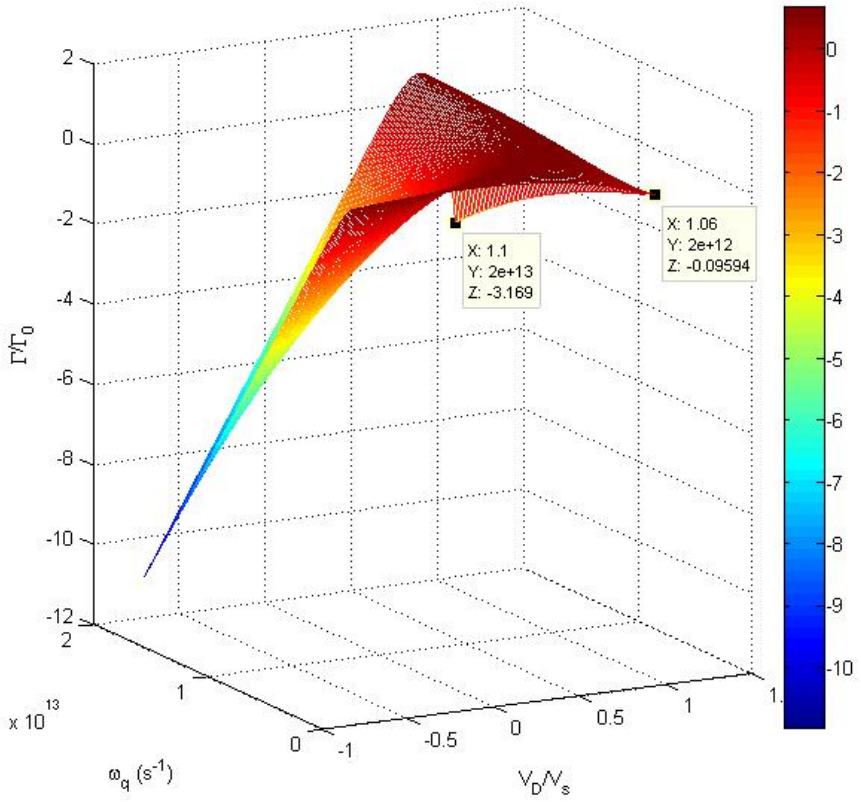

Figure 29: A graph of Γ/Γ_0 on $\frac{V_D}{V_s}$ and ω_q at 2 THz

For $\frac{V_D}{V_s} > 1$, the hypersound amplification obtained is similar to that of Nunes and Fonseca. For a drift velocity of $V_D = 1.1V_s$, a field of $E = 11.5\text{V/cm}$ was calculated. At frequency of 0.2THz, an amplification of $\Gamma/\Gamma_0 = -3.17$ is attained. From this work, the hypersound studies in graphene offers a much better source of higher phonon frequencies than the homogenous semiconductors which permit the use of graphene as hypersound phonon laser (SASER).

The Eqn. (160) is analysed numerically for a normalized graph of j/j_0 against ω_q and T. The following parameters were used $\Lambda = 9$ eV, $V_s = 2.1 \times 10^6$ cms^{-1} and $\vec{q} = 10^5$ cm^{-1}. In Figure 30, the graph for the dependence of j/j_0 on ω_q for varying T is plotted. From the Figure 30, the

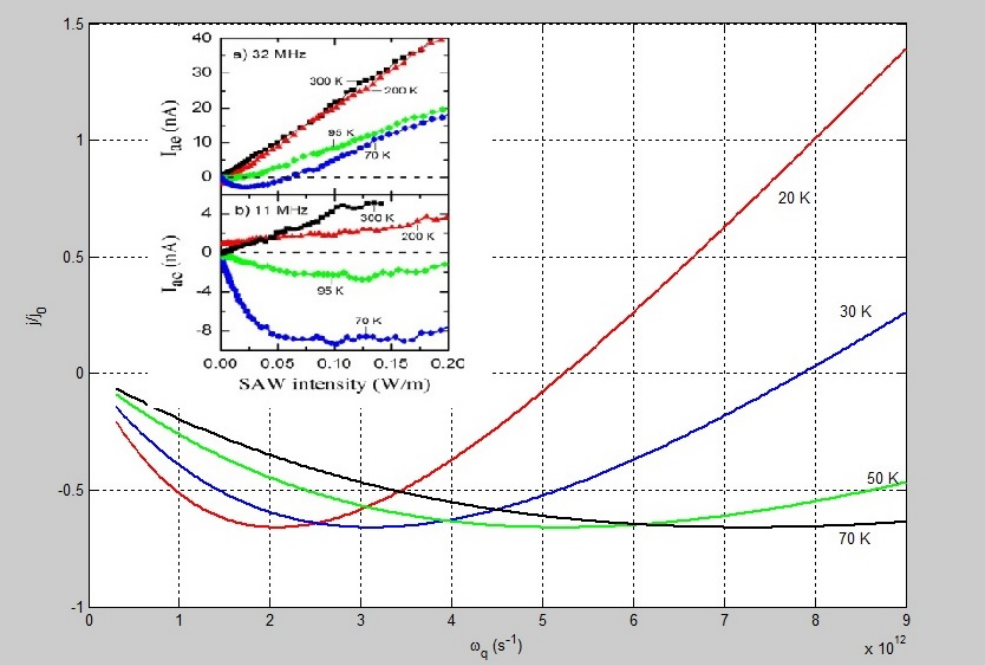

Figure 30: (a) Dependence of j/j_0 on ω_q for varying T. Insert: Dependence of Acoutoelectric Current (I_{ae}) on SAW intensity for varying T [272]

non-linear graph of Acoustoelectric current j/j_0 decreases with an increase in temperature. The insert is an experimentally obtained results of acoustoelectric current versus Surface Acoustic Wave (SAW) intensity. For acoustic phonons, the intensity is proportional to the frequency of the acoustic phonon $i.e. I = \hbar\omega_q flux$. Therefore, the theoretically obtained graph (see Figure 30) qualitatively agrees with that obtained experimentally by Bandhu and Nash [272].

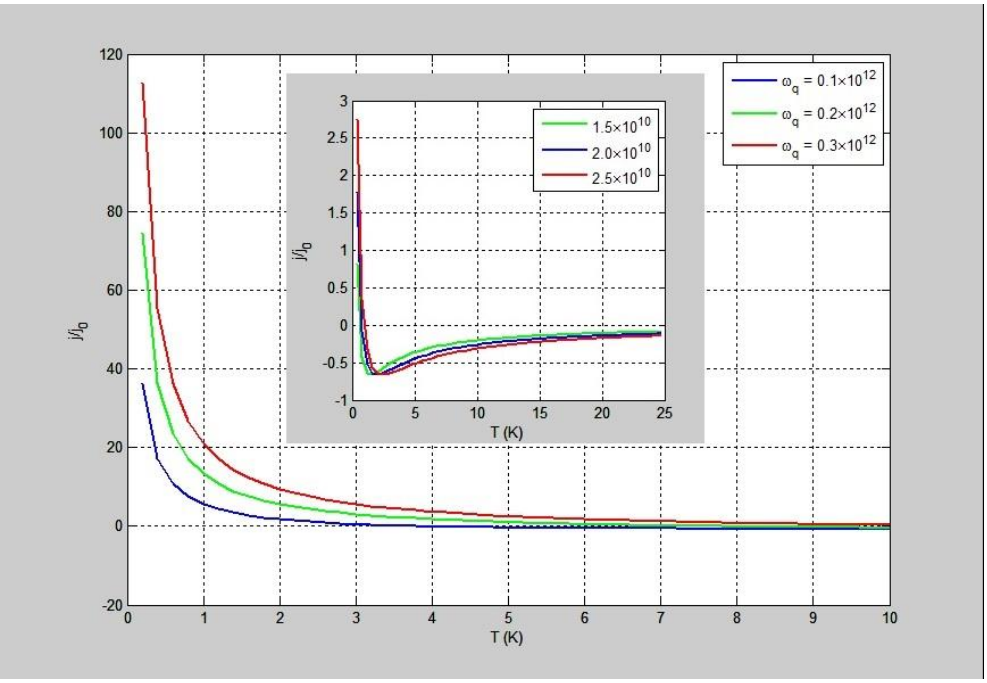

Figure 31: Dependence of j/j_0 on temperature T on varying $\omega_q(10^{10})$ s^{-1}, insert was plotted with $\omega_q(10^{12})$ s^{-1}

The acoustoelectric current j_{ac} relates the hypersound absorption as

$$j^{ac} = \frac{-2e\tau}{\hbar V_F}\Gamma \tag{179}$$

which is the Weinreich relation [350]. In Figure 31, the dependence of acoustoelectric current j/j_0 on temperature T is plotted with varying ω_q. At $\omega_q = 10^{12}$ s^{-1}, the acoustoelectric current decreases sharply to a minimum point and remain constant but at $\omega_q = 10^{10}$ s^{-1} (see insert graph), the graph decreased pass the $j/j_0 = 0$ point to a minimum then raises to a constant values. For better understanding of the relation between j/j_0, ω_q and T, a 3-D graph was plotted (See Figure 32). From the Figure 32, the maximum point was obtained at $T = 1.5$ K, $\omega_q = 6 \times 10^{11} s^{-1}$ and $j/j_0 = 1.006$ whilst the minimum point, $T = 1.5$ K, $\omega_q = 1.2 \times 10^{11} s^{-1}$ and $j/j_0 = -0.635$. The acoustoelectric effect in graphene is studied in the hypersound regime $ql >> 1$.

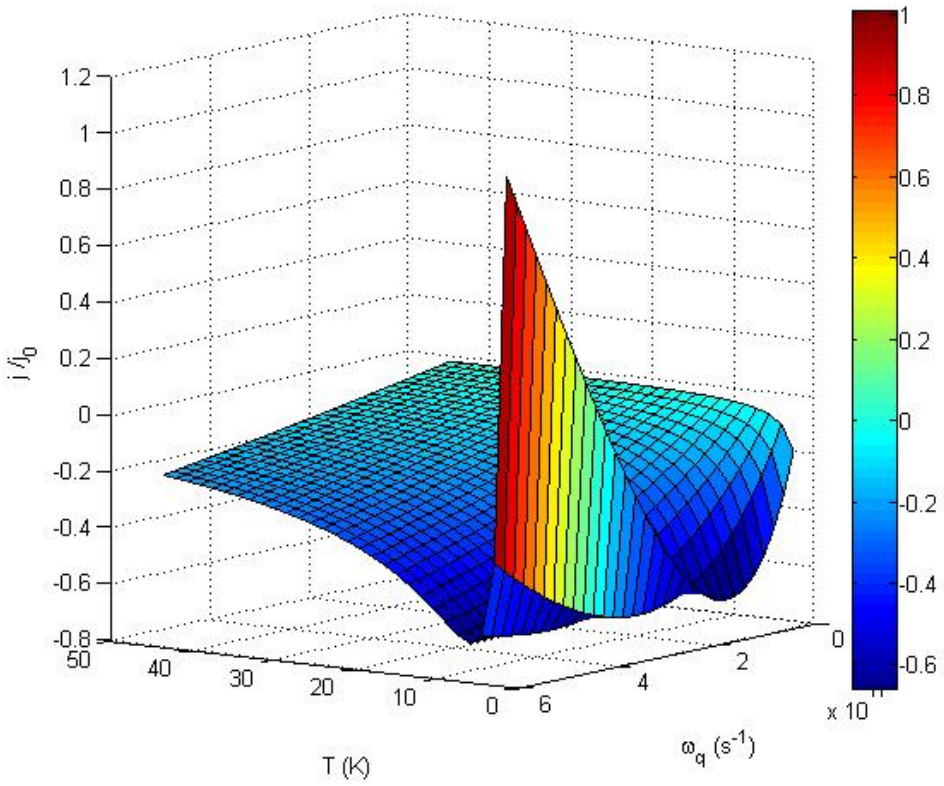

Figure 32: A 3D graph of the dependence of j/j_0 on ω_q and T

At low temperatures, the theoretically obtained acoustoelectric current j/j_0 qualitatively agreed with an experimentally obtained results.

Hypersound Absorption In Carbon Nanotube

The parameters used in the numerical evaluation of Eqn(171) are: $|\Lambda| = 9$ eV, b $= 1.42$ nm, q $= 10^7$ cm^{-1}, $\omega_q = 10^{12}$ s^{-1}, $V_s = 4.7 \times 10^5$ cms^{-1}, T $= 10$ K, and $\theta > 0$. The dependence of the absorption coefficient (Γ) on the acoustic wave number ($\vec{q}$), the frequency (ω_q) and (γ) at various harmonics ($n = 0, \pm 1, \pm 2$) are presented below. For $n = 0$, the graph of Γ versus $\vec{q}$ at

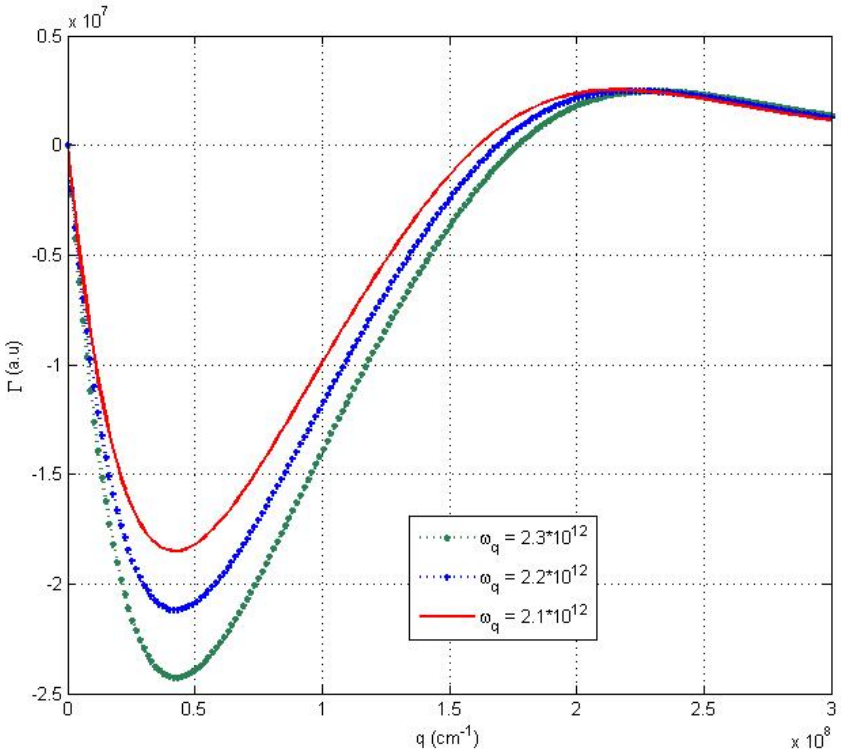

Figure 33: Dependence of Γ on q for varying ω_q at $V_D = 1.2V_s$

varying frequencies and that of Γ versus ω_q for various acoustic wave numbers are shown in Figures 33 and 34. In Figure 33, an amplification curve was observed, where the minimum value increases by increasing ω_q but above $\omega_q = 1.6 \times 10^{12}\ s^{-1}$, an absorption was obtained. In Figure 34, it was observed that absorption switched over to amplification when the $\vec{q}$ values were increased.

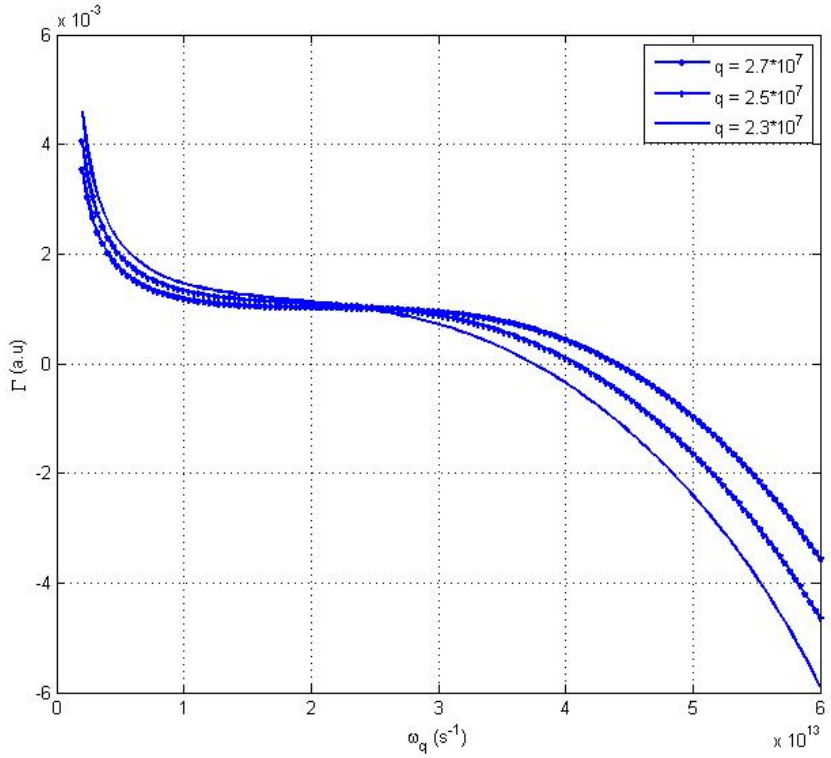

Figure 34: Γ on ω_q for varying $\vec{q}$ at $V_D = 1.2V_s$

For $n = \pm 1$ (first harmonics), in Figure 35, it was observed that absorption exceeds amplification and the peaks shift to the right. A further increase in ω_q values caused an inversion of the graph where amplification exceeds absorption (see Figure 36).

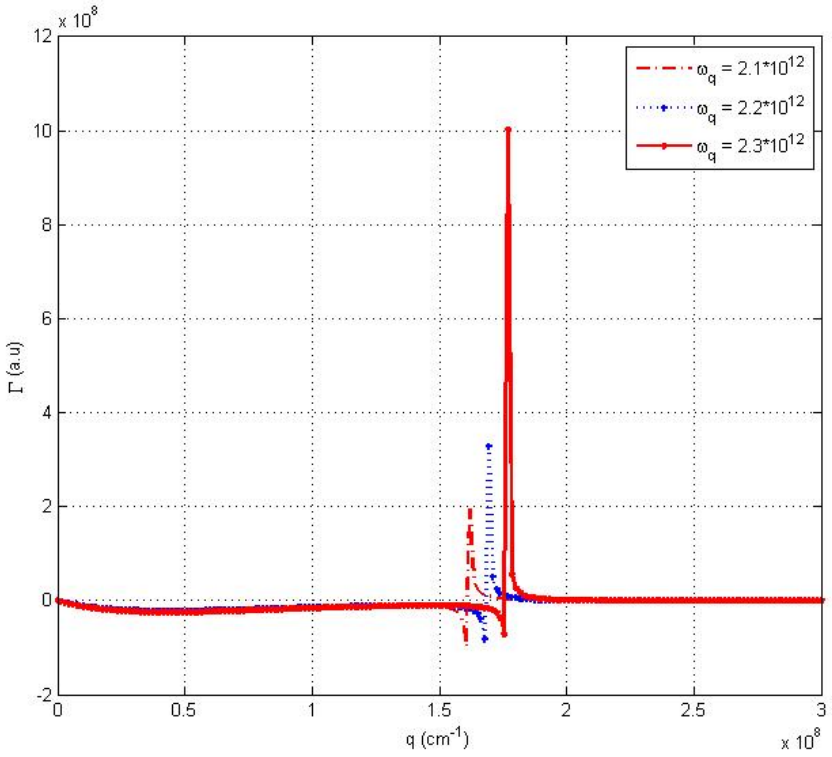

Figure 35: Dependence of Γ on $\vec{q}$ at $V_D = 1.2V_s$ showing Absorption exceeds Amplification

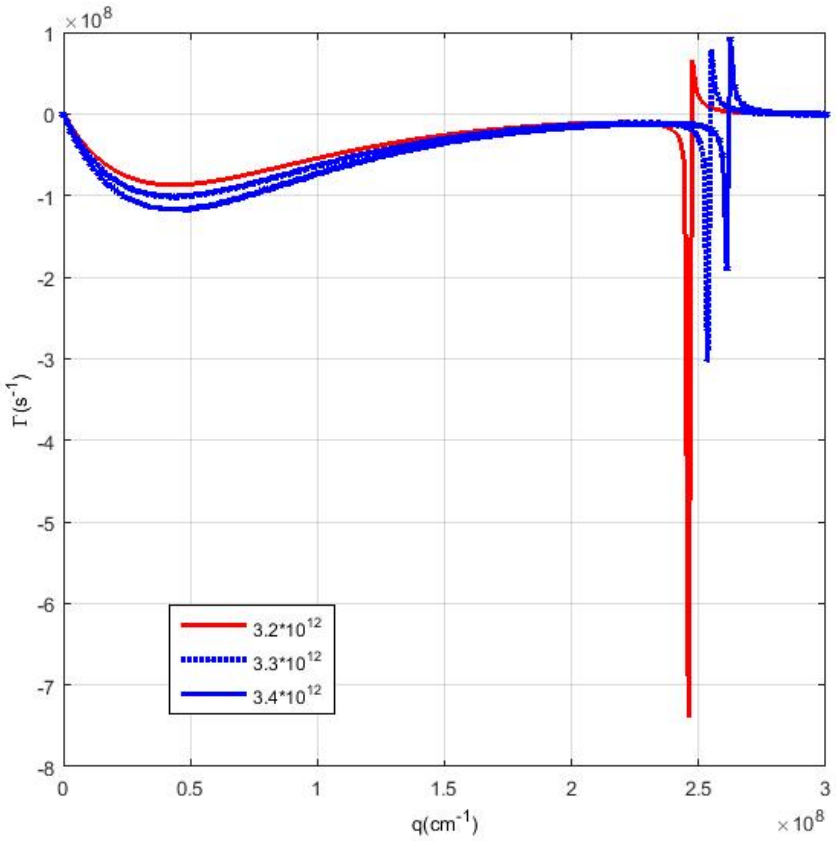

Figure 36: Dependence of Γ on $\vec{q}$ at $V_D = 1.2V_s$ showing amplification exceeds absorption

A similar observation was seen in Figure 37 and 38, where, the peak values shift to the right and decreases with increasing $\vec{q}$ values (see Figure 37) but in Figure 38, an inversion of the graph occurred for increasing values of $\vec{q}$.

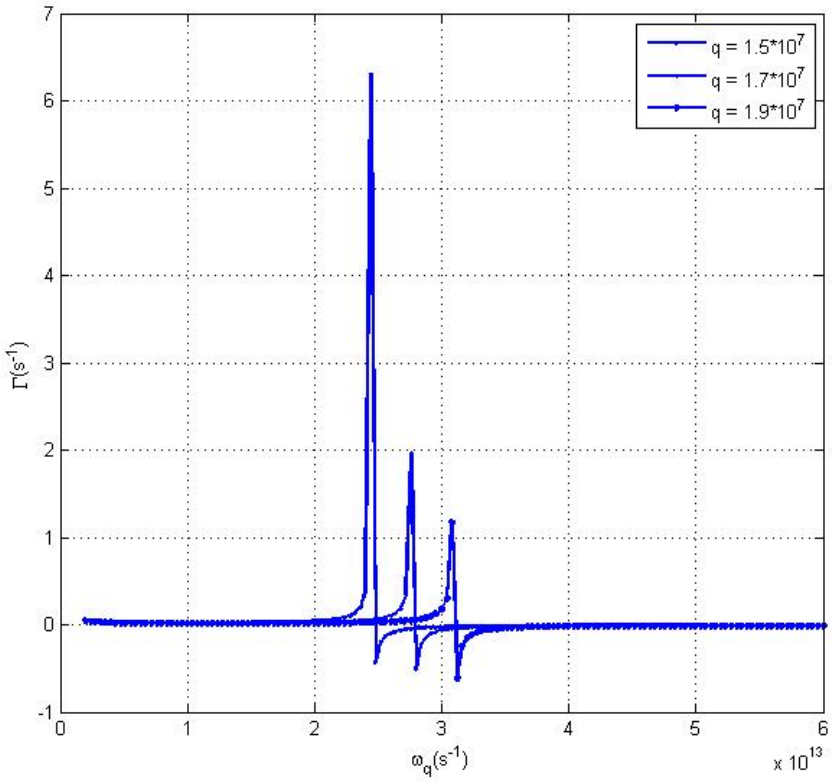

Figure 37: Dependence of Γ on ω_q where absorption exceeds amplification

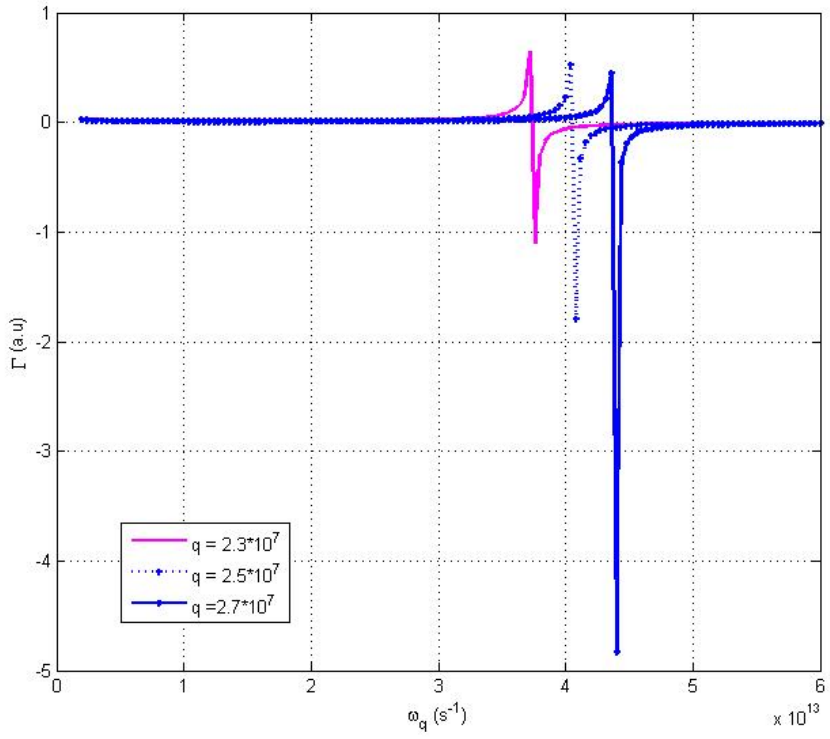

Figure 38: Dependence of Γ on ω_q where amplification exceeds absorption

Figures 39 and 40, shows the dependence of Γ on γ by varying either ω_q or $\vec{q}$. In both graphs, when $\gamma = -0.10$, a maximum amplification was obtained. In both graphs, when $\gamma < 0$, produce non-linear graphs which satisfy the Cerenkov condition, but at $\gamma > 0$, the graph returns to zero.

The observed peaks in Figure 39, shift to the left by increasing ω_q whilst in Figure 40, they shift to the right for increasing $\vec{q}$.

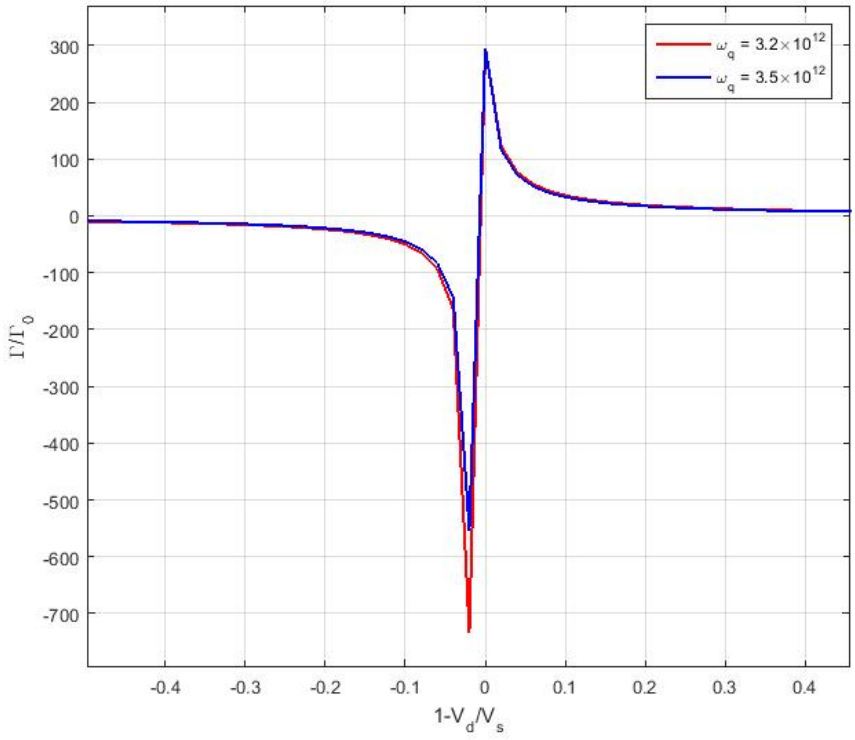

Figure 39: Dependence of Γ on γ at $\theta = 80^0\ C$ by increasing ω_q

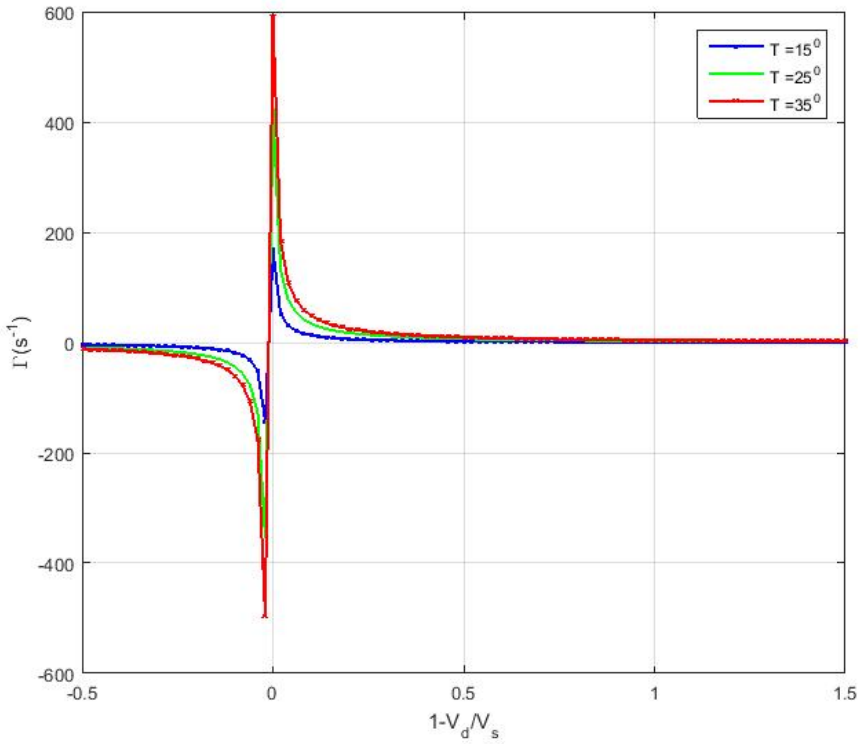

Figure 40: Dependence of Γ on γ at $\theta = 80^0$ C by increasing $T = 15, 25, 35$ K

For further elucidation, a 3D graph of Γ versus ω_q and γ or Γ versus $\vec{q}$ and γ are presented in Figures 41 and 42.

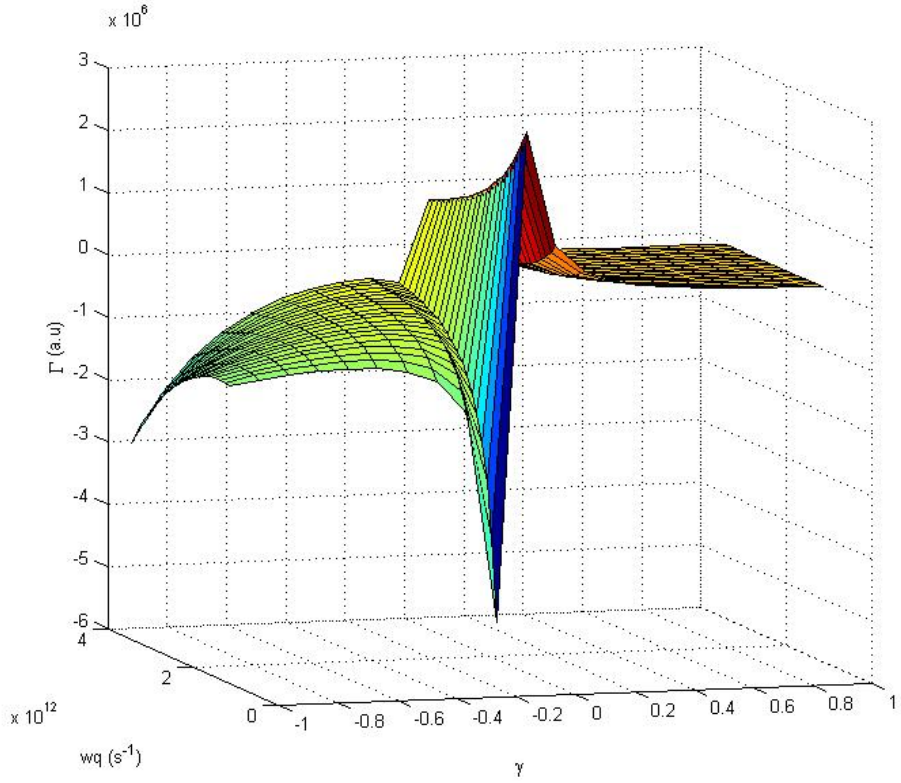

Figure 41: Dependence of Γ on ω_q and γ

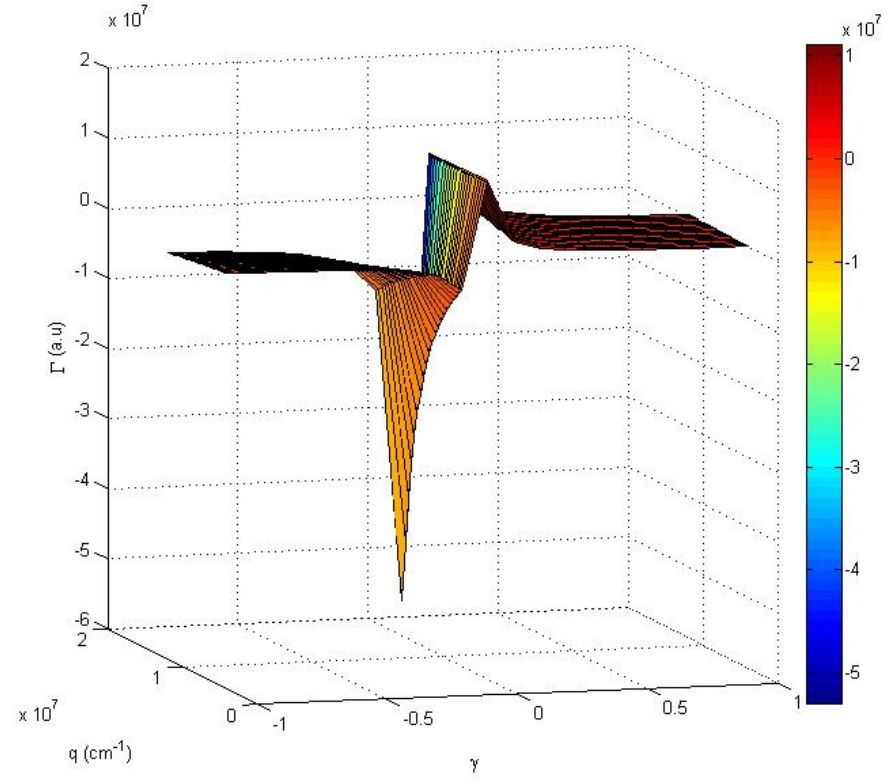

Figure 42: Dependence of Γ on $\vec{q}$ and γ

For $n = \pm 2$ (second harmonics), the dependence of the absorption coefficient Γ on ω_q is presented in 2D and 3D forms as shown in Figures 43 and 44. In Figure 43, an absorption graph was obtained. The insert shown is an experimental results obtained for the acoustoelectric current in SWCNT [111].

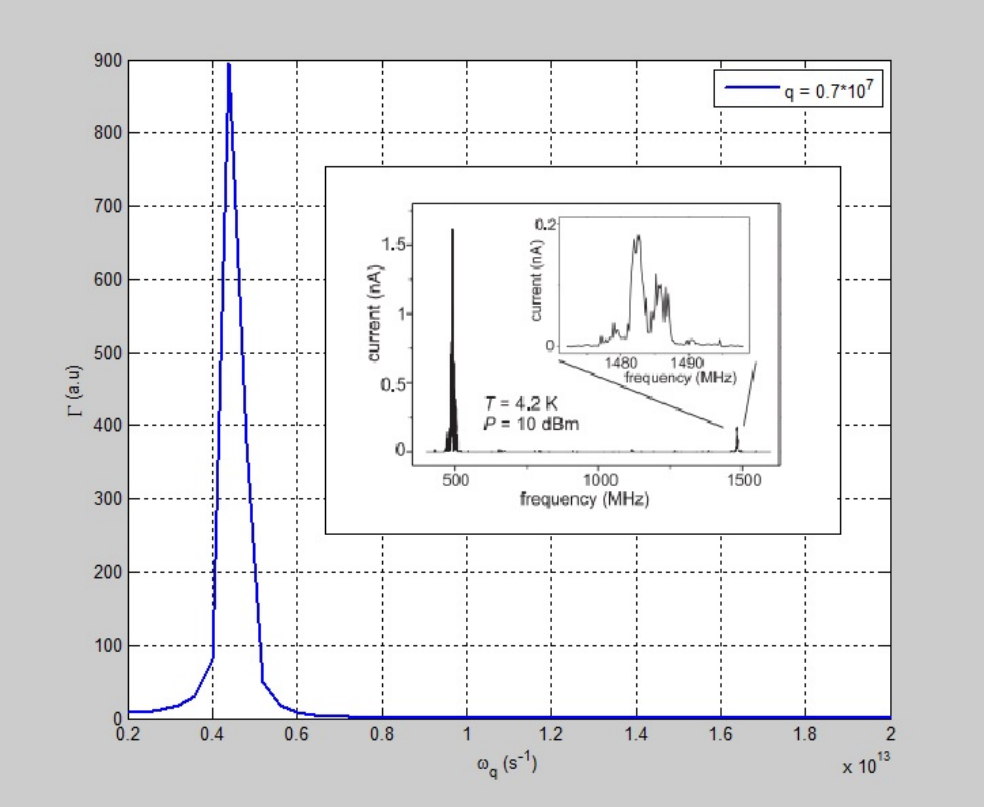

Figure 43: Second harmonic graph of the dependence of Γ on ω_q. Insert shows the experimental graph for acoustoelectric current versus frequency [111]

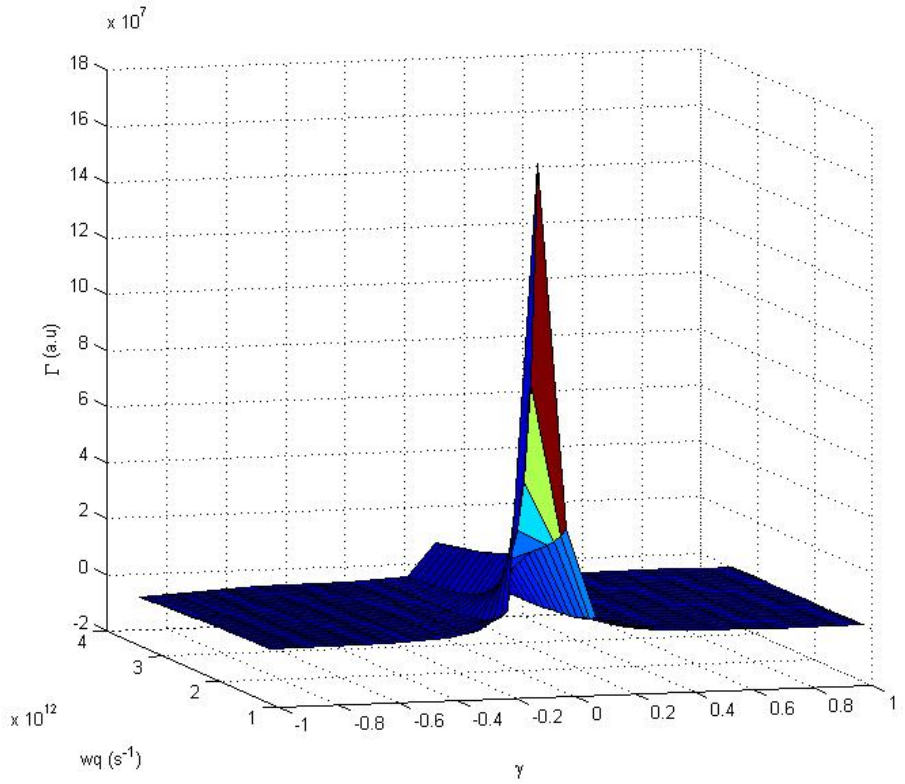

Figure 44: Dependence of Γ on $\vec{q}$ and γ

Figure 44 is the 3D representation of the absorption in second harmonics. From Weinreich relation [350], the absorption coefficient is directly related to the acoustoelectric current, therefore from Figure 46, the results obtained for the absorption coefficient qualitatively agree with the experimental results presented (see insert). In the 3D graphs,the maximum amplification and absorption occurred at $\gamma = -0.1$ which is equivalent to $V_D = 1.1V_s$. With the electric field $E = \frac{V_D}{\mu}$ gives $E = 51.7$ V/cm. The expression for Hypersound Absorption of acoustic phonons in a degenerate Carbon Nanotube (CNT) was deduced theoretically and graphically presented. In this work, the acoustic waves were considered to be a flow of monochromatic phonons in the short wave region ($ql >> 1$). The general expression obtained was analysed numerically for $n = 0, \pm 1, \pm 2$ (where n is an integer). From the graphs, at

certain values of ω_q and $\vec{q}$, an Amplification was observed to exceed Absorption or vice-versa . For $\gamma < 0$, the maximum Amplification was observed at $V_D = 1.1V_s$ which gave us a field of $E = 51.7$ Vcm^{-1}. This field is far lower than that observed in superlattice and homogeneous semiconductors permitting the CNT to be a suitable material for hypersound generator (SASER). A similar expression can be seen in the works of Nunes and Fonseca [54]. Very interesting to this work is the qualitative agreement of the absorption graph to an experimental graph resulting from an acoustoelectric current via the Weinriech relation.

Acoustoelectric in Carbon Nanotube

The analytical solution of Eqn(178) is obtained numerically and the results presented graphically. The parameters used in the numerical evaluation are: $|\Lambda| = 9$ eV, $b = 1.42$ nm, $q = 10^7$ cm^{-1}, $\omega_q = 10^{12}$ s^{-1},$V_s = 4.7 \times 10^5$ cms^{-1}, T = 10 K, and $\theta > 0$. The dependence of j^{ac} on the acoustic wave number ($\vec{q}$) and the frequency (ω_q) at various harmonics ($n = \pm 1, \pm 2$) are presented. For $n = \pm 1$, the non-linear graph (with an initial curve) increases sharply to a maximum then decreases to a constant minimum value (see Figure 45). By

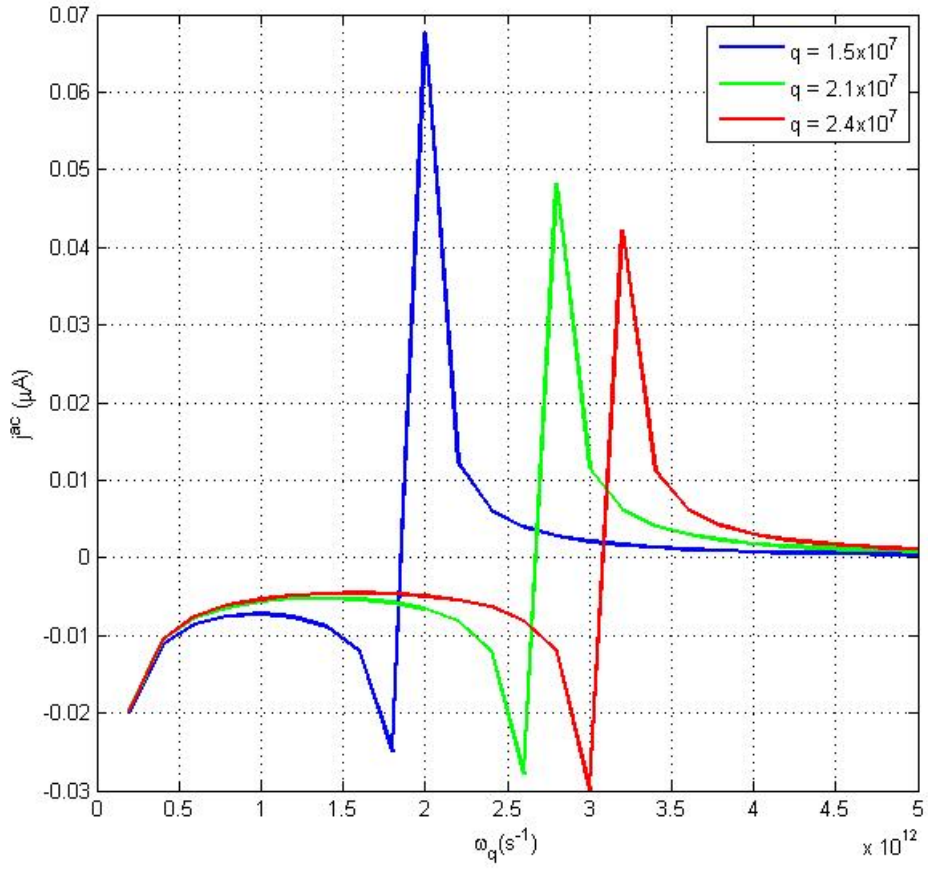

Figure 45: Dependence of j^{ac} on ω_q at varying $\vec{q}$

increasing the values of $\vec{q}$, the graph shifts to the right with decreasing amplitude. In Figure 46, it was observed that at $\omega_q = 0.6 \times 10^{12}$ s, the j^{ac} increases to a maximum point and then falls to a minimum value. Increasing

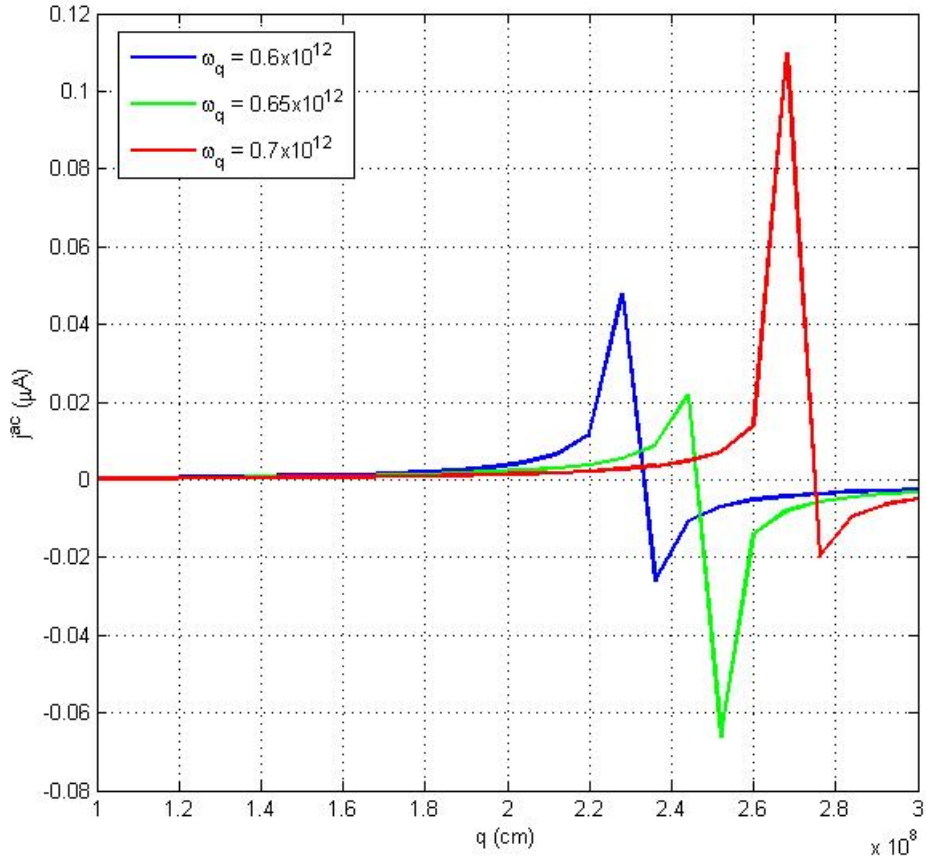

Figure 46: Dependence of j^{ac} on $\vec{q}$ for varying ω_q

the values of ω_q, shift the graph to the right. More interesting is the nature of the acoustoelectric current j^{ac}. At $\omega_q = 0.6 \times 10^{12}$ s, the ratio of the peaks balances on both side of the j^{ac} axis. At $\omega_q = 0.65 \times 10^{12}$ s, the ratio of the j^{ac} peaks is more towards the negative side but a reverse occurs when $\omega_q = 0.7 \times 10^{12}$ s.

For $n = \pm 2$ (see Figures 47 and 48), the graph obtained for j^{ac} versus ω_q qualitatively agreed with an experimentally obtained results. In Figure 47, it is also observed that the dependence of j^{ac} on q is strongly non-linear.

$$\frac{j^{ac}}{\Gamma} = \frac{2e\tau\gamma_0 b\sqrt{3}}{\hbar}(cos(\theta) - 1) \qquad \textbf{(180)}$$

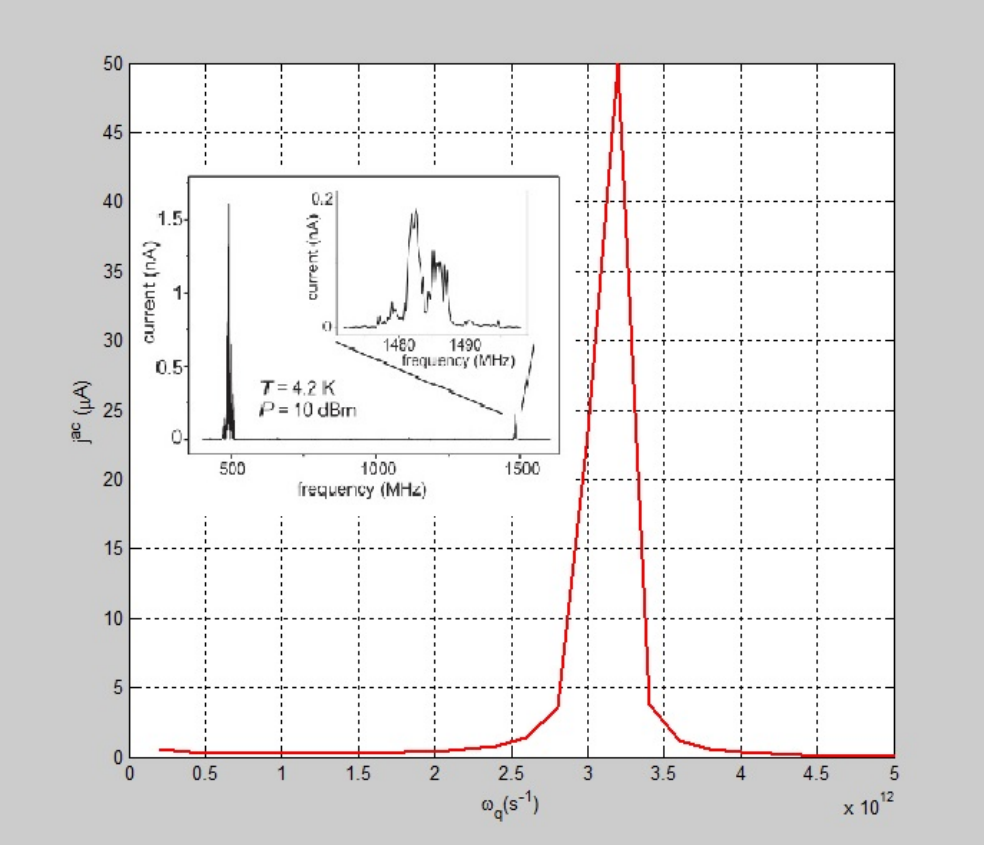

Figure 47: Dependence of j^{ac} on ω_q at various $\vec{q}$ insert shows the experimentally obtained acoustoelectric current [111]

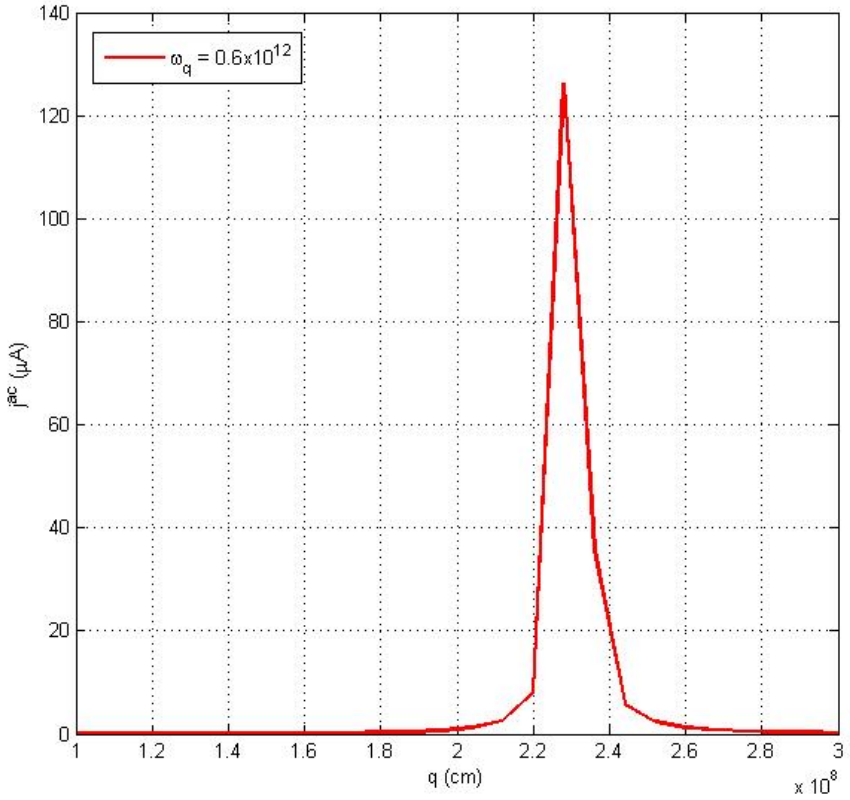

Figure 48: Dependence of j^{ac} on $\vec{q}$ for a given ω_q

The ratio of $\frac{j^{ac}}{\Gamma}$ (where Γ is the hypersound absorption) in the absence of a drift velocity V_D [43] is given as

$$\frac{j^{ac}}{\Gamma} = \frac{2e\tau\gamma_0 b\sqrt{3}}{\hbar}(cos(\theta) - 1) \qquad \textbf{(181)}$$

which is the Weinreich relation [350] and is dependent on the scattering angel θ. For $n = \pm 1$, the ratio of the height of the peaks in the positive side of j^{ac} far exceeded that in the negative side (see Figure 48).

For better understanding of the obtained graphs, a 3D graph of j^{ac} versus ω_q and $\vec{q}$ are presented in Figure (49 and 50).

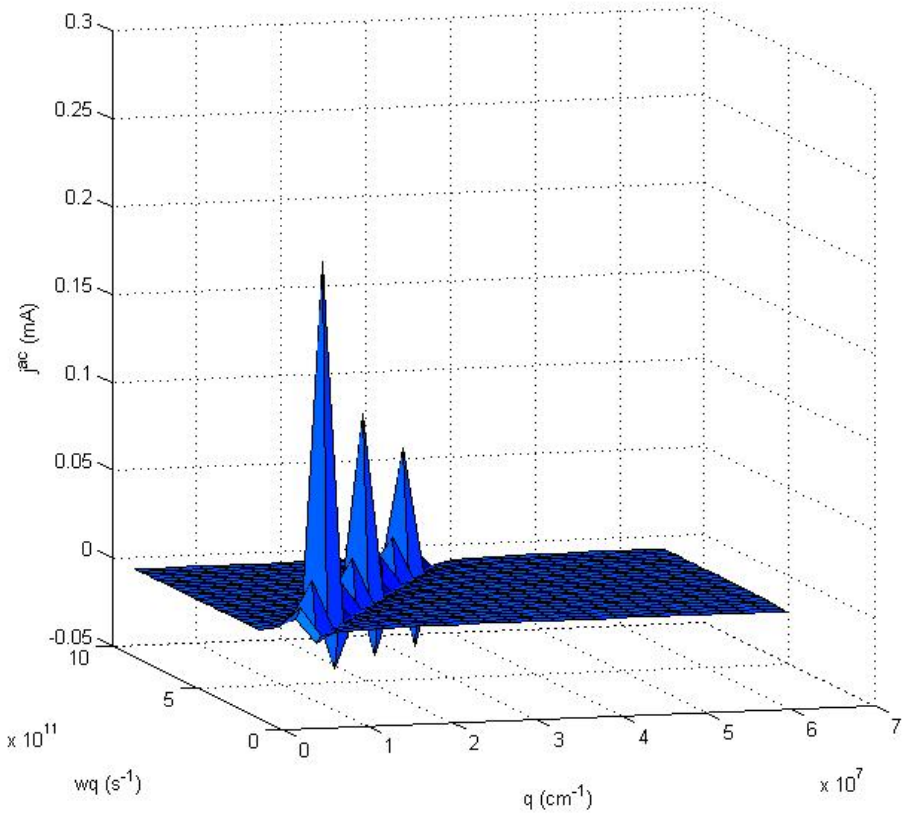

Figure 49: Dependence of j^{ac} on γ and $\vec{q}$ at the first harmonics $n = \pm 1$

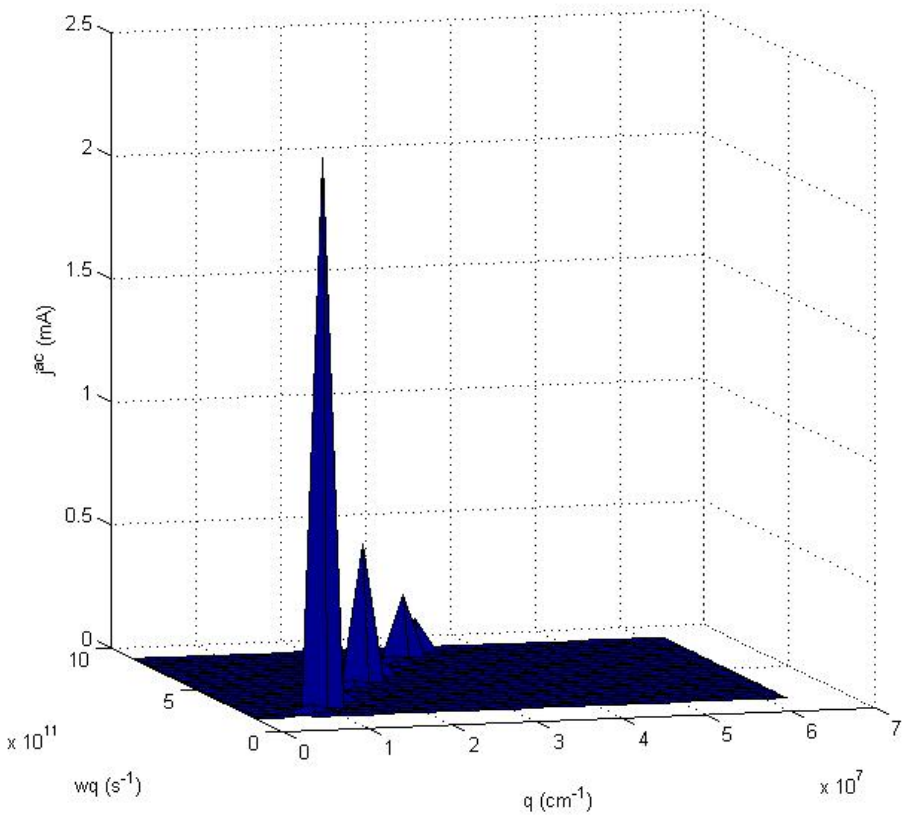

Figure 50: Dependence of j^{ac} on γ and $\vec{q}$ at the second harmonics $n = \pm 2$

In Figure 50, for $n = \pm 2$, the graph showed peaks at certain intervals. The *AE* in a degenerate *CNT* is studied for hypersound in the regime $ql >> 1$. A strong nonlinear dependence of j^{ac} on the acoustic wavenumber $\vec{q}$ and the frequency ω_q are observed. The dominant mechanism for such non-linear behaviour is the *AE* which give rise to the acoustoelectric current j^{ac}. The analytically obtained acoustoelectric current j^{ac} qualitatively agrees with an experimentally obtained result.

CHAPTER FIVE

SUMMARY, CONCLUSIONS AND RECOMMENDATIONS

Summary

Studies of acoustic effects in Carbon Allotropes such as Graphene, Carbon Nanotube, and Graphene Nanoribbon were done in the hypersound regime having $ql > 1$. Topics treated include hypersound amplification/absorption, Acoustoelectric Effect (AE), and Acoustomagnetoelectric Effect (AME) in the said materials of Carbon Allotropes. From the Boltzmann kinetic equation, the general formula for Amplification and Acoustomagnetoeletric field (E_{SAME}) in Graphene Nanoribbon (GNR) was derived using the energy dispersion $\varepsilon(p)$ near the Fermi point.

Conclusions

The amplification of the acoustic wave in an external electric and magnetic fields was studied using the kinetic equation for electron-phonon interactions in AGNR. Analytical expressions for the Amplification under different conditions were numerically analysed. The dependence of Γ/Γ_0 on E_0 and q are determined at different values of ϕ, p_i and the width where the maximum value of the magnetic strength occurs at 0.93. That of Γ/Γ_0 against q was also analysed. In particular, when q is increased from $2.0 * 10^6$ cm^{-1} to $2.5 * 10^6$ cm^{-1}, the amplification obtained is modulated. This indicates

intraband transition of SASER in AGNR. The E_{SAME} is analysed numerically at various sub-bands for parameters including the width of the GNR, the magnetic strength η and α. The graphs of $\vec{E}_{SAME}$ against these parameters are presented and analysed. For $\vec{E}_{SAME}$ against the width of GNR and α, it was observed that $\vec{E}_{SAME}$ increases to a saturation value of 15Vcm^{-1} and remains constant but asymptotically increases at approximately $\alpha = 1$. For a graph of $\vec{E}_{SAME}$ against η or α, the E_{SAME} varies for increases in the sub-band but invert at $p_i = 6$.

The generation of hypersound amplification (absorption) of acoustic phonons in graphene is studied. For $\frac{V_D}{V_s} > 1$, the hypersound amplification obtained is similar to that of Nunes and Fonseca but for $\frac{V_D}{V_s} < 1$, an absorption is obtained which could lead to acoustoelectric effect in graphene. The absorption obtained qualitatively agreed with an experimentally obtained acoustoelectric current in a graphene via the Weinrich relation. For a drift velocity of $V_D = 1.1V_s$, a field of $E = 11.5$ V/cm was calculated. At frequency of 0.2 THz, an amplification of $\Gamma/\Gamma_0 = -3.17$ is attained. From this work, the hypersound studies in graphene offers a much better source of higher phonon frequencies than the homogenous semiconductors which permit the use of graphene as hypersound phonon laser (SASER).

The acoustoelectric effect in graphene is studied in the hypersound regime $ql >> 1$. At low temperatures , the theoretically obtained Acoustoelectric current j/j_0 qualitatively agreed with an experimentally obtained results.

The expression for Hypersound Absorption of acoustic phonons in a degenerate CNT was deduced theoretically and graphically presented. In this

work, the acoustic waves were considered to be a flow of monochromatic phonons in the short wave region ($ql >> 1$). The general expression obtained was analysed numerically for $n = 0, \pm 1, \pm 2$ (where n is an integer). From the graphs, at certain values of ω_q and $\vec{q}$, an Amplification was observed to exceed absorption or vice-versa . For $\gamma < 0$, the maximum amplification was observed at $V_D = 1.1V_s$ which gave us a field of $E = 51.7$ Vcm^{-1}. This field is far lower than that observed in superlattice and homogeneous semiconductors permitting the CNT to be a suitable material for hypersound generator (SASER). A similar expression can be seen in the works of Nunes and Fonseca [269]. Very interesting to our work is the qualitative agreement of the absorption graph to an experimental graph resulting from an acoustoelectric current via the Weinriech relation.

The AE in a degenerate CNT is studied for hypersound in the regime $ql >> 1$. A strong nonlinear dependence of j^{ac} on the acoustic wavenumber $\vec{q}$ and the frequency ω_q are observed. The dominant mechanism for such non-linear behaviour is the acoustoelectric effect which gives rise to the acoustoelectric current j^{ac}. The analytically obtained acoustoelectric current j^{ac} qualitatively agrees with an experimentally obtained result.

Recommendations

Research conducted in this thesis on the study of acoustic effects in Carbon allotropes opens up a range of possibilities for further studies in this area. These are

- This work could be done using Silicon, and Germanium since they are in the same period as that of Carbon.
- Further, the extension of this work probably to Black phosphorus is possible since it also have a band gap just like Silicon.
- Acousto-concentration and Acousto-thermal effects could be studied in all the Allotropes of Carbon.

REFERENCES

[1] Hirsch, A. *The era of carbon allotropes*. Nature materials, 9 (11), (2010), 868-871.

[2] Greenwood, N. N., Earnshaw, A. *Chemistry of the Elements. 2nd ed.*; Reed Educational and Professional Publishing Ltd: Oxford, (1997), pp. 268-327.

[3] Sladkov, A. M. *Carbyne: the third allotropic form of carbon*. M: Nauka, (2003), 28-55.

[4] Kroto H.W., Heath JR, O'Brien S.C., Curl R.F., Smalley R.E. *C60: Buckminsterfullerene*. Nature 318 (6042):(1985), 162-163.

[5] Iijima S., Ichihashi T. *Single-shell carbon nanotubes of 1-nm diameter*. Nature 363 (6430): (1993), 603-605.

[6] Novoselov, K. S. A., Geim, A. K., Morozov, S., Jiang, D., Katsnelson, M., Grigorieva, I., and Firsov, A. *Two-dimensional gas of massless Dirac fermions in graphene*. nature, 438 (7065), (2005), 197-200.

[7] Charlier J. C., Rignanese G.M. *Electronic structure of carbon nanocones*. Phys Rev Lett 86 (26): (2001), 5970-5973.

[8] Jin C., Lan H., Peng L., Suenaga K., Iijima S. *Deriving carbon atomic chains from graphene*. Phys Rev Lett 102 (20): (2009), 205501.

[9] Li Y, Xu L, Liu H, Li Y, *Graphdiyne and graphyne: From theoretical*

predictions to practical construction. Chem Soc Rev 43 (8): (2014), 2572-2586.

[10] Balandin, A. A. *Thermal properties of graphene and nanostructured carbon materials*. Nature materials, 10 (8), (2011), 569-581.

[11] Pierson, Hugh O. *Handbook of carbon, graphite, diamonds and fullerenes: processing, properties and applications*, William Andrew, 2012.

[12] Howe, J. P. *Properties of Graphite*. Journal of the American Ceramic Society, 35 (11), (1952), 275-283.

[13] Chambers, C., and Holliday, A. K. *Modern inorganic chemistry*. Group, 4, (1975), 160.

[14] Zacharia, R., Ulbricht, H., and Hertel, T. *Interlayer cohesive energy of graphite from thermal desorption of polyaromatic hydrocarbons*. Physical Review B, 69 (15), (2004), 155406.

[15] Barone, V., and Fliszar, S. *Theoretical energies of representative carbon-carbon bonds*. International Journal of Quantum Chemistry, 55 (6), (1995), 469-476.

[16] Gillespie, R. J. *Teaching molecular geometry with the VSEPR model*, Journal of Chemical Education 81 (3): (2004), 298-304

[17] Lide, D. R. *A survey of carbon-carbon bond lengths*. Tetrahedron, 17(3), (1962), 125-134.

[18] Robertson, J. *Diamond-like amorphous carbon*. Materials Science and Engineering: R: Reports, 37(4), (2002), 129-281.

[19] Tersoff, J. *Empirical interatomic potential for carbon, with applications to amorphous carbon*. Physical Review Letters, 61(25), (1988), 2879.

[20] Blase, X., Benedict, L. X., Shirley, E. L., and Louie, S. G. *Hybridization effects and metallicity in small radius carbon nanotubes*. Physical review letters, 72 (12), (1994), 1878.

[21] Dral, P. O. *Theoretical Study of Electronic Properties of Carbon Allotropes*, Theoretische Studien der elektronischen Eigenschaften von Kohlenstoff-Allotropen, (2013), 3763.

[22] Novoselov K. S., Geim A. K., Morozov S. V., Jiang D., Zhang Y., Dubonos S. V., Grigorieva IV, Firsov A. A. *Electric field effect in atomically thin carbon films*. Sci, 306: (2004), 666.

[23] Castro Neto A. H., Guinea F., Peres N. M., Novoselov K. S., Geim A. K. *The electronic properties of graphene*. Phys, 81: (2009), 109.

[24] Chico, L., Crespi, V. H., Benedict, L. X., Louie, S. G., and Cohen, M. L. *Pure carbon nanoscale devices: nanotube heterojunctions*. Physical Review Letters, 76(6), (1996), 971.

[25] McEuen, P. L., Fuhrer, M. S., Park, H. *Single-walled carbon nanotube electronics* IEEE Trans. Nanotechnol. 1, (2002), 78.

[26] Booth, T. J., Blake, P., Nair, R. R., Jiang, D., Hill, E. W., Bangert, U., Bloch, A., Gass, M., Novoselov, K. S., Katsnelson, M. I., and Geim, A. K. *Graphene-based materials in electrochemistry*,Nano Lett. 8, (2008), 2442.

[27] Willett, R. L., K. W. West, and L. N. Pfeiffer. *Transition in the correlated 2D electron system induced by a periodic density modulation*. Physical review letters 78, no. 23 (1997): 4478.

[28] Shapere, A., and Wilczek, F., (eds.) *Geometrical Phases in Physics*, World Scientific, Singapore, Vol. 5, (1989).

[29] Novoselov, K. S., Geim, A. K., Morozov, S. V., Jiang, D., Katsnelson, M. I., Grigorieva, I. V., Dubonos, S. V., and Firsov, A. A. *Two-dimensional gas of massless Dirac fermions in graphene*, Nature 438, (2005), 197.

[30] Geim, A.K. and Novoselov, K.S. *The rise of graphene*, Nature Materials 6, (2007), 183-191.

[31] Lin, Y. M., Dimitrakopoulos, C., Jenkins, K. A., Farmer, D. B., Chiu, H. Y., Grill, A., Avouris, P. *100-GHz transistors from wafer-scale epitaxial graphene*, Science 327, (2010), 662.

[32] Zheng, Q., Hao W., Nan W., Rui Y., Yuehui Ma, Weijun G., Junzhong W., and Kejian D. *Graphene-based biosensors for biomolecules detection*. Current Nanoscience 10, no. 5 (2014): 627-637.

[33] Ryzhii, V., Satou, A., and Otsuji, T. *Plasma waves in two-dimensional electron-hole system in gated graphene heterostructures*. Journal of applied physics 101, no. 2 (2007): 024509.

[34] Wallace, P. R. *The band theory of graphite*. Physical Review, 71 (9), (1947), 622.

[35] Zhou, S. Y., Gweon, G. H., Fedorov, A. V., First, P. N., De Heer, W. A., Lee, D. H., and Lanzara, A. *Substrate-induced bandgap opening in epitaxial graphene*. Nature materials, 6(10), (2007), 770-775.

[36] Gunlycke, D., and White, C. T. *Tight-binding energy dispersions of armchair-edge graphene nanostrips*. Physical Review B, 77 (11), (2008), 115116.

[37] Ahmadi, M. T, Michael L. P. Tan, Razali I., and Vijay K. A. *The high-field drift velocity in degenerately-doped silicon nanowires*. International Journal of Nanotechnology 6, no. 7-8 (2009): 601-617.

[38] Novoselov, K. S., Geim, A. K., Morozov, S. V., Jiang, D., Zhang, Y., Dubonos, S. A., and Firsov, A. A. *Electric field effect in atomically thin carbon films*. science, 306, (2004), 666-669.

[39] Novoselov, K. S., Jiang, D., Schedin, F., Booth, T. J., Khotkevich, V. V., Morozov, S. V., and Geim, A. K. *Two-dimensional atomic crystals*. Proceedings of the National Academy of Sciences of the United States of America, 102, (2005), 10451-10453.

[40] Katsnelson, M. I., Novoselov, K. S., and Geim, A. K. *Chiral tunnelling and the Klein paradox in graphene*. Nature physics, 2, (2006), 620-625.

[41] Geim, A. K. *Graphene: status and prospects*. science, 324, (2009), 1530-1534.

[42] Kim, K. S., Zhao, Y., Jang, H., Lee, S. Y., Kim, J. M., Kim, K. S.,and

Hong, B. H. *Large-scale pattern growth of graphene films for stretchable transparent electrodes*. Nature, 457, (2009), 706-710.

[43] Riedl, C. *Epitaxial Graphene on Silicon Carbide Surfaces: Growth, Characterization, Doping and Hydrogen Intercalation*, (2010).

[44] Reina, A., Jia, X., Ho, J., Nezich, D., Son, H., Bulovic, V., and Kong, J. *Large area, few-layer graphene films on arbitrary substrates by chemical vapor deposition*. Nano letters, 9 (1), (2008), 30-35.

[45] Aristov, V. Y., Urbanik, G., Kummer, K., Vyalikh, D. V., Molodtsova, O. V., Preobrajenski, A. B., and Knupfer, M. *Graphene synthesis on cubic SiC/Si wafers. Perspectives for mass production of graphene-based electronic devices*. Nano letters, 10 (3), (2010), 992-995.

[46] Stankovich, S., Dikin, D. A., Piner, R. D., Kohlhaas, K. A., Kleinhammes, A., Jia, Y., and Ruoff, R. S. *Synthesis of graphene-based nanosheets via chemical reduction of exfoliated graphite oxide*. Carbon, 45 (7), (2007), 1558-1565.

[47] Hummers Jr, W. S., and Offeman, R. E. *Preparation of graphitic oxide*. Journal of the American Chemical Society, 80 (6), (1958), 1339-1339.

[48] McAllister, M. J., Li, J. L., Adamson, D. H., Schniepp, H. C., Abdala, A. A., Liu, J., and Aksay, I. A. *Single sheet functionalized graphene by oxidation and thermal expansion of graphite*. Chemistry of Materials, 19 (18), (2007), 4396-4404.

[49] Chattopadhyay, J., Mukherjee, A., Hamilton, C. E., Kang, J., Chakraborty,

S., Guo, W., and Billups, W. E. *Graphite epoxide*. Journal of the American Chemical Society, 130 (16), (2008), 5414-5415.

[50] Chandra, S., Sahu, S., and Pramanik, P. *A novel synthesis of graphene by dichromate oxidation*. Materials Science and Engineering: B, 167 (3), (2010), 133-136.

[51] Stankovich, S., and Dikin, D. A. *High-yield production of graphene by liquid-phase*. Carbon, 45, (2007), 1558-1565.

[52] Wang, G., Shen, X., Yao, J., and Park, J. *Graphene nanosheets for enhanced lithium storage in lithium ion batteries*. Carbon, 47 (8), (2009), 2049-2053.

[53] Wang, G., Yang, J., Park, J., Gou, X., Wang, B., Liu, H., and Yao, J. *Facile synthesis and characterization of graphene nanosheets*. The Journal of Physical Chemistry C, 112 (22), (2008), 8192-8195.

[54] Si, Y., and Samulski, E. T. *Synthesis of water soluble graphene*. Nano letters, 8 (6), (2008), 1679-1682.

[55] Fan, X., Peng, W., Li, Y., Li, X., Wang, S., Zhang, G., and Zhang, F. *Deoxygenation of exfoliated graphite oxide under alkaline conditions: a green route to graphene preparation*. Advanced Materials, 20 (23), (2008), 4490-4493.

[56] Wakeland, S., Martinez, R., Grey, J. K., and Luhrs, C. C. *Production of graphene from graphite oxide using urea as expansion-reduction agent*. Carbon, 48 (12), (2010), 3463-3470.

[57] Chen, W., Yan, L., and Bangal, P. R. *Preparation of graphene by the rapid and mild thermal reduction of graphene oxide induced by microwaves*. Carbon, 48 (4), (2010), 1146-1152.

[58] Leininger, S., Olenyuk, B., and Stang, P. J. *Self-assembly of discrete cyclic nanostructures mediated by transition metals*. Chemical Reviews, 100 (3), (2000), 853-908.

[59] Kroto, H. W. *The stability of the fullerenes Cn, with n = 24, 28, 32, 36, 50, 60 and 70*. Nature, 329 (6139), (1987), 529-531.

[60] Kretschmer, W., Fostiropoulos, K., and Huffman, D. R. *The infrared and ultraviolet absorption spectra of laboratory-produced carbon dust: evidence for the presence of the C60 molecule*. Chemical Physics Letters, 170 (2), (1990), 167-170.

[61] Alekseyev, N. I., and Dyuzhev, G. A. *Fullerene formation in an arc discharge*. Carbon, 41 (7), (2003), 1343-1348.

[62] Howard, J. B., McKinnon, J. T., Makarovsky, Y., Lafleur, A. L., and Johnson, M. E. *Fullerenes C60 and C70 in flames*. Nature, 352 (6331), (1991), 139-141.

[63] Howard, J. B., Lafleur, A. L., Makarovsky, Y., Mitra, S., Pope, C. J., and Yadav, T. K. *Fullerenes synthesis in combustion*. Carbon, 30 (8), (1992), 1183-1201.

[64] Xie, S. Y., Huang, R. B., Yu, L. J., Ding, J., and Zheng, L. S. *Microwave*

synthesis of fullerenes from chloroform. Applied physics letters, 75, (1999), 2764.

[65] Koshio, A., Yudasaka, M., Ozawa, M., and Iijima, S. *Fullerene formation via pyrolysis of ragged single-wall carbon nanotubes*. Nano Letters, 2(9), (2002), 995-997.

[66] Taylor, R., Langley, G. J., Kroto, H. W., and Walton, D. R. *Formation of C60 by pyrolysis of naphthalene*,. Nature, 366 (6457), (1993), 728-731.

[67] Chen, C., and Lou, Z. *Formation of C60 by reduction of CO2*. The Journal of Supercritical Fluids, 50 (1), (2009), 42-45.

[68] Koprinarov, N., Marinov, M., Konstantinova, M., and Ranguelov, B. *Fullerene structure synthesis by DC arc discharge in ferrocene vapours*. Vacuum, 58 (2), (2000), 208-214.

[69] Richter, H., De Hoffmann, E., Doome, R., Fonseca, A., Gilles, J. M., Nagy, J. B., and Van Tiggelen, P. J. *Fullerene formation in acetylene/oxygen/argon/chlorine flames*. Carbon, 34 (6), (1996), 797-803.

[70] Scott, L. T. *Methods for the chemical synthesis of fullerenes*. Angewandte Chemie International Edition, 43 (38), (2004), 4994-5007.

[71] Ugarte, D. *Curling and closure of graphitic networks under electron-beam irradiation*. Nature, 359 (6397), (1992), 707-709.

[72] Nakada, K., Fujita, M., Dresselhaus, G., and Dresselhaus, M. S. *Edge state in graphene ribbons: Nanometer size effect and edge shape dependence*. Physical Review B, 54 (24), (1996), 17954.

[73] Wakabayashi, K., Fujita, M., Ajiki, H., and Sigrist, M. *Electronic and magnetic properties of nanographite ribbons*. Physical Review B, 59 (12), (1999), 8271.

[74] Miyamoto, Y., Nakada, K., and Fujita, M. *First-principles study of edge states of H-terminated graphitic ribbons*. Physical Review B, 59 (15), (1999), 9858.

[75] Kawai, T., Miyamoto, Y., Sugino, O., and Koga, Y. *Graphitic ribbons without hydrogen-termination: Electronic structures and stabilities*. Physical Review B, 62 (24), (2000), R16349.

[76] Okada, S., and Oshiyama, A. *Magnetic ordering in hexagonally bonded sheets with first-row elements*. Physical review letters, 87 (14), (2001), 146803.

[77] Lee, H., Son, Y. W., Park, N., Han, S., and Yu, J. *Magnetic ordering at the edges of graphitic fragments: Magnetic tail interactions between the edge-localized states*. Physical Review B, 72 (17), (2005), 174431.

[78] Ezawa, M. *Peculiar width dependence of the electronic properties of carbon nanoribbons*. Physical Review B, 73 (4), (2006), 045432.

[79] Brey, L., and Fertig, H. A. *Electronic states of graphene nanoribbons studied with the Dirac equation*. Physical Review B, 73 (23), (2006), 235411.

[80] Charlier, J. C., Eklund, P. C., Zhu, J., and Ferrari, A. C. *Electron and*

phonon properties of graphene: their relationship with carbon nanotubes. Carbon, (2008), pp. 673-709.

[81] Abanin, D. A., Lee, P. A., and Levitov, L. S. *Spin-filtered edge states and quantum Hall effect in graphene*. Physical review letters, 96 (17), (2006),176803.

[82] Son, Y. W., Cohen, M. L., and Louie, S. G. *Energy gaps in graphene nanoribbons*. Physical review letters, 97 (21), (2006), 216803.

[83] Charlier, J.C., Eklund, P.C., Zhu, J. and Ferrari, A.C. *Electron and phonon properties of graphene: their relationship with carbon nanotubes*. Carbon nanotubes, (2007), pp. 673-709.

[84] Son, Y. W., Cohen, M. L., and Louie, S. G. *Half-metallic graphene nanoribbons*. Nature, 444 (7117), (2006), 347-349.

[85] Son, Y. W., Cohen, M. L., and Louie, S. G. *Energy gaps in graphene nanoribbons*. Physical review letters, 97 (21), (2006), 216803.

[86] Shemella, P., Zhang, Y., Mailman, M., Ajayan, P. M., and Nayak, S. K. *Energy gaps in zero-dimensional graphene nanoribbons*. Applied Physics Letters, 91 (4), (2007), 042101.

[87] Ren, W., Saito, R., Gao, L., Zheng, F., Wu, Z., Liu, B., and Cheng, H. M. *Edge phonon state of mono-and few-layer graphene nanoribbons observed by surface and interference co-enhanced Raman spectroscopy*. Physical Review B, 81 (3), (2010), 035412.

[88] Huang, B., Yan, Q. M., Li, Z. Y., and Duan, W. H. *Towards graphene nanoribbon-based electronics*. Frontiers of Physics in China, 4, (2009) 269-279.

[89] Wang, Z. F., Li, Q., Zheng, H., Ren, H., Su, H., Shi, Q. W., and Chen, J. *Tuning the electronic structure of graphene nanoribbons through chemical edge modification: A theoretical study*. Physical Review B, 75 (11), (2007), 113406.

[90] Huaixiu Z., Zhengfei W., Tao L., Qinwei S., and Jie C. *Analytical study of electronic structure in Armchair Graphene Nanoribbons*, arXiv.cond-mat.0612378v2, (2006).

[91] Mahdi M., Hamed N., Mahdi P., Morteza F., and Hans K. *Analytical models of approximate for wave functions and energy dispersion in zigzag graphene nanoribbons*, J. Applied Physics 111, 074318, (2012).

[92] Brey, L., and Fertig, H. A. *Emerging zero modes for graphene in a periodic potential*. Physical review letters, 103 (4),(2009), 046809.

[93] Wagner, P., Ewels, C., Adjizian J.,Magaud, L., Pochet, P., Roche S., Lopez-Bezanilla, A., Ivanovskaya, V., Abu Yaya, Rayson, M., Briddon, P., and Humbert, B. *Band gap Engineering via Edge-Functionalization of Graphene Nanoribbons*, J. Physical Chemistry C, (2013), 26790, .

[94] Charlier, J. C., Eklund, P. C., Zhu, J., and Ferrari, A. C. *Electron and phonon properties of graphene: their relationship with carbon nanotubes*. In Carbon nanotubes (2008), (pp. 673-709).

[95] Kan, E. J., Li, Z., Yang, J., and Hou, J. G. *Half-metallicity in edge-modified zigzag graphene nanoribbons*. Journal of the American Chemical Society, 130 (13), (2008), 4224-4225.

[96] Lee, G., and Cho, K. *Electronic structures of zigzag graphene nanoribbons with edge hydrogenation and oxidation*. Physical Review B, 79 (16), (2009), 165440.

[97] Yu, S. S., Zheng, W. T., and Jiang, Q. *Electronic properties of nitrogen-/boron-doped graphene nanoribbons with armchair edges*. Nanotechnology, IEEE Transactions on, 9 (1), (2010), 78-81.

[98] Jadaun, P., Sahu, B. R., Register, L. F., and Banerjee, S. K. *Density functional theory studies of interactions of graphene with its environment: Substrate, gate dielectric and edge effects*. Solid State Communications, 152 (15), (2012), 1497-1502.

[99] Iijima, S. *Helical microtubules of graphitic carbon*. nature, 354 (6348), (1991), 56-58.

[100] Ebbesen, T. W. *Carbon nanotubes*. Physics Today, 49 (6), (1996), 26-35.

[101] Rodriguez, N. M., , 7. Mater. B.es. 8 (1993), 3233 .

[102] Bandaru, Prabhakar R. *Electrical properties and applications of carbon nanotube structures*. Journal of nanoscience and nanotechnology 7, no. 4-5, (2007): 1239-1267.

[103] Ruoff, Rodney S., and Donald C. L. *Mechanical and thermal properties of carbon nanotubes*. Carbon 33, no. 7 : (1995), 925-930.

[104] Dresselhaus, M.S., Dresselhaus, G. and Jorio, A. *Unusual proterties and Structure of Carbon Nannotubes*. Annual Review of Materials Research, Vol. 34: (2004), 247-278, .

[105] Saito, R., Dresselhaus, G., Dresselhaus, M. *Physical Properties of Carbon Nanotubes*. Imperial College Press, London, (1998).

[106] Chen, P., Wu, X., Sun, X., Lin, J., Ji, W., and Tan, K. L. *Electronic structure and optical limiting behavior of carbon nanotubes*. Physical review letters, 82 (12), 2548,(1999).

[107] Charlier, J. C., Blase, X., and Roche, S. *Electronic and transport properties of nanotubes*. Reviews of modern physics, 79 (2), (2007), 677.

[108] Pedersen, T. G., Flindt, C., Pedersen, J., Mortensen, N. A., Jauho, A. P., and Pedersen, K. *Graphene antidot lattices: designed defects and spin qubits*. Physical review letters, 100 (13), (2008), 136804.

[109] Komirenko, S.V., Kim, K. W., Demidenko, A. A., Kochelap, V. A., Strocio, M. A. *Cerenkov generation of high-frequency confined acoustic phonons in quantum wells*. arXiv:cond-mat/9911381v1, (1999).

[110] Glavin, B. A., Kochelap, V. A., Linik, T. L., Kim, K. W. *Generation of high-frequency of cohenrent acoustic phonons in Superlattice under hopping transport in linear theory of phonon instability*. Physical review B, (2002).

[111] Ebbecke, J., Strobl, C. J., and Wixforth, A. *Acoustoelectric current*

transport through single-walled carbon nanotubes, Physical Review B, APS, (2004).

[112] Reulet, B., Kasumov, Yu. A. , Kociak, M., Deblock, R., Khodos, I. I., Gorbatov, Yu. B. , Volkov, V. T. , Journet, C., and Bouchiat, H. *Acoustoelectric Effect in Carbon Nanotubes*, physical Review letters, Vol. 85 Number 12, 25, (2000).

[113] Zhao, X. F., Zhang, J., Chen, S. M. and Xu, W. *Cerenkov acoustic-phonon emission generated electrically from a polar semiconductor*. Journal of Applied Physics 105, 104514 (2009).

[114] Mavrinskiy, A. V., and Baitinger, E. M. *Thermoelectric power in carbon nanotubes. Semiconductors*. 43, no. 4 (2009): 480-484.

[115] Jorio, A., Dresselhaus, G., and Dresselhaus, M. S. *Carbon nanotubes: advanced topics in the synthesis, structure, properties and applications*. (Vol. 111), (2007).

[116] O'connell, M. J. *Carbon nanotubes: properties and applications*. (2006). CRC press.

[117] Thostenson, E. T., Ren, Z., and Chou, T. W. *Advances in the science and technology of carbon nanotubes and their composites*. Composites science and technology, 61 (13), (2001), 1899-1912.

[118] Mallick, P. K. *PFiber-reinforced composites: materials, manufacturing, and design*. CRC press, (2007) .

[119] Mostofizadeh, A., Li, Y., Song, B., and Huang, Y. *Synthesis, properties, and applications of low-dimensional carbon-related nanomaterials*. Journal of nanomaterials, (2011), 16.

[120] Lukkassen, D., and Meidell, A. *Advanced materials and structures and their fabrication processes*. Narrik University College, Hin. (2003).

[121] Mukhopadhyay, S. *Nanoscale Multifunctional Materials: Science and Applications*. John Wiley and Sons, (2011).

[122] Luo, J., Jiang, S., and Liu, X. *PEfficient one-pot synthesis of mussel-inspired molecularly imprinted polymer coated graphene for protein-specific recognition and fast separation*. The Journal of Physical Chemistry C, 117 (36), (2013), 18448-18456.

[123] Windler, L., Lorenz, C., Von Goetz, N., Hungerbuhler, K., Amberg, M., Heuberger, M., and Nowack, B. *Release of titanium dioxide from textiles during washing*. Environmental science and technology, 46 (15), (2012), 8181-8188.

[124] Alli, S. M. A. *Nanoscience and Nanotechnology: Issues and Applications in Agri-Food, Biomedical, and Environmental Sciences*, (2012); 2 (1): 61-86

[125] Yu, M. F., Lourie, O., Dyer, M. J., Moloni, K., Kelly, T. F., and Ruoff, R. S. *Strength and breaking mechanism of multiwalled carbon nanotubes under tensile load*. Science, 287 (5453), (2000), 637-640.

[126] Tans, S. J., Devoret, M. H., Dai, H., Thess, A., Smalley, R. E., Georliga,

L. J., and Dekker, C. *Individual single-wall carbon nanotubes as quantum wires*. Nature, 386 (6624), (1997), 474-477.

[127] Zhang, Y., Franklin, N. W., Chen, R. J., and Dai, H. *Metal coating on suspended carbon nanotubes and its implication to metal-tube interaction*. Chemical Physics Letters, 331 (1), (2000), 35-41.

[128] Allaoui, A., Bai, S., Cheng, H. M., and Bai, J. B. *Mechanical and electrical properties of a MWNT/epoxy composite*. Composites Science and Technology, 62 (15), (2002), 1993-1998.

[129] Lu, X., and Chen, Z. *Curved pi-conjugation, aromaticity, and the related chemistry of small fullerenes*. Chemical Reviews, 105 (10), (2005), 3643-3696.

[130] Zhou, X., Park, J. Y., Huang, S., Liu, J., and McEuen, P. L. *Band structure, phonon scattering, and the performance limit of single-walled carbon nanotube transistors*. Physical Review Letters, 95 (14), (2005), 146805.

[131] Dai, H., Javey, A., Pop, E., Mann, D., Kim, W., and Lu, Y. *Electrical transport properties and field effect transistors of carbon nanotubes*. Nano, 1 (01), (2006), 1-13.

[132] Hong, S., and Myung, S. *Nanotube Electronics: A flexible approach to mobility*. Nature Nanotechnology, 2 (4), (2007), 207-208.

[133] Javey, A., Qi, P., Wang, Q., and Dai, H. *Ten-to 50-nm-long quasi-ballistic carbon nanotube devices obtained without complex lithography*.

Proceedings of the National Academy of Sciences of the United States of America, 101 (37), (2004), 13408-13410.

[134] Pierson, H. O. *Handbook of carbon, graphite, diamonds and fullerenes: processing, properties and applications*. William Andrew, (2012).

[135] Harris, P. J., and Tsang, S. C. *High-resolution electron microscopy studies of non-graphitizing carbons*. Philosophical Magazine A, 76 (3), (1997), 667-677.

[136] Zou, Q., Wang, M. Z., Gong, W., Yu, Q. H., Li, Y. G., and Zhao, Y. C. *Nanopolycrystalline Diamond Sintered from Onion-Like Carbon*. Journal of Nanomaterials, (2014).

[137] Pervolaraki, M., Komninou, P., Kioseoglou, J., Othonos, A., and Giapintzakis, J. *Ultrafast pulsed laser deposition of carbon nanostructures: Structural and optical characterization*. Applied Surface Science, 278, (2013), 101-105.

[138] Iancu, C., and Stancioiu, A. *Graphene: A new material, Fiability and Durability/Fiabilitate si Durabilitate*, (1), (2011).

[139] Tan, E. P. S., Goh, C. N., Sow, C. H., and Lim, C. T. *Tensile test of a single nanofiber using an atomic force microscope tip*. Applied Physics Letters, 86 (7), (2005), 073115.

[140] Tan, E. P. S., and Lim, C. T. *Mechanical characterization of nanofibers-a review*. Composites Science and Technology, 66 (9), (2006), 1102-1111.

[141] Tanaka, A., Yoon, S. H., and Mochida, I. *Preparation of highly crystalline nanofibers on Fe and Fe-Ni catalysts with a variety of graphene plane alignments*. Carbon, 42 (3), (2004), 591-597.

[142] Bezemer, G. L., Radstake, P. B., Falke, U., Oosterbeek, H., Kuipers, H. P. C. E., Van Dillen, A. J., and De Jong, K. P. *Investigation of promoter effects of manganese oxide on carbon nanofiber-supported cobalt catalysts for Fischer-Tropsch synthesis*. Journal of catalysis, 237(1), (2006), 152-161.

[143] Takenaka, S., Ishida, M., Serizawa, M., Tanabe, E., and Otsuka, K. *Formation of carbon nanofibers and carbon nanotubes through methane decomposition over supported cobalt catalysts*. The Journal of Physical Chemistry B, 108 (31), (2004), 11464-11472.

[144] Tu, J. P., Zhu, L. P., Hou, K., and Guo, S. Y. *Synthesis and frictional properties of array film of amorphous carbon nanofibers on anodic aluminum oxide*. Carbon, 41 (6), (2003), 1257-1263.

[145] Hiramatsu, M., and Hori, M. *Fabrication of carbon nanowalls using novel plasma processing*. Japanese journal of applied physics, 45 (6), (2006), 5522.

[146] Mori, T., Hiramatsu, M., Yamakawa, K., Takeda, K., and Hori, M. *Fabrication of carbon nanowalls using electron beam excited plasma-enhanced chemical vapor deposition*. Diamond and Related Materials, 17 (7), (2008), 1513-1517.

[147] Qiaoqin, Y., Chijin, X., and Hirose, A. *Plasma-enhanced deposition*

of nano-structured carbon films. Plasma Science and Technology, 7 (1), (2005), 2660.

[148] Mackay, A. L., Terrones, H., and Fowler, P. W. *Hypothetical graphite structures with negative gaussian curvature*. Philosophical Transactions of the Royal Society of London A: Mathematical, Physical and Engineering Sciences 343, no. 1667 (1993): 113-127.

[149] Yang, L., Park, C. H., Son, Y. W., Cohen, M. L., and Louie, S. G. *Quasiparticle energies and band gaps in graphene nanoribbons*. Physical Review Letters, 99(18), (2007), 186801.

[150] Giovannetti, G., Khomyakov, P. A., Brocks, G., Kelly, P. J., and van den Brink, J. *Substrate-induced band gap in graphene on hexagonal boron nitride: Ab initio density functional calculations*. Physical Review B, 76 (7), (2007), 073103.

[151] Van Lier, G., Van Alsenoy, C., Van Doren, V., and Geerlings, P. *Ab initio study of the elastic properties of single-walled carbon nanotubes and graphene*. Chemical Physics Letters, 326 (1), (2000), 181-185.

[152] Min, H., Sahu, B., Banerjee, S. K., and MacDonald, A. H. *Ab-initio theory of gate induced gaps in graphene bilayers*. Physical Review B, 75 (15), (2007), 155115.

[153] Hu, J., Ruan, X., and Chen, Y. P. *Thermal conductivity and thermal rectification in graphene nanoribbons: a molecular dynamics study*. Nano Letters, 9 (7), (2009), 2730-2735.

[154] Evans, W. J., Hu, L., and Keblinski, P. *Thermal conductivity of graphene ribbons from equilibrium molecular dynamics: Effect of ribbon width, edge roughness, and hydrogen termination*. Applied Physics Letters, 96 (20), (2010), 203112.

[155] Guo, X., Wang, J. B., and Zhang, H. W. *Mechanical properties of single-walled carbon nanotubes based on higher order Cauchy□Born rule*. International Journal of Solids and Structures, 43 (5), (2006), 1276-1290.

[156] Scarpa, F., Adhikari, S., and Phani, A. S. *Effective elastic mechanical properties of single layer graphene sheets*. Nanotechnology, 20 (6), (2009), 065709.

[157] Sfyris, D., Koukaras, E. N., Pugno, N., and Galiotis, C. *Graphene as a hexagonal 2-lattice: Evaluation of the in-plane material constants for the linear theory. A multiscale approach*. Journal of Applied Physics, 118(7), (2015), 075301.

[158] Yan, J., Zhang, Y., Kim, P., and Pinczuk, A. *Electric field effect tuning of electron-phonon coupling in graphene*. Physical review letters, 98 (16), (2007), 166802.

[159] Akturk, A., and Goldsman, N. *Electron transport and full-band electron-phonon interactions in graphene*. Journal of Applied Physics, 103 (5), (2008), 053702.

[160] Basko, D. M., Piscanec, S., and Ferrari, A. C. *Electron-electron interactions and doping dependence of the two-phonon Raman intensity in graphene*. Physical Review B, 80 (16), (2009), 165413.

[161] Spector, H. N. *Interaction of acoustic waves and conduction electrons*. Solid state physics 19 (1967): 291-361.

[162] Mikoshiba, N. *Acoustoelectric Effect in Metals*. Journal of the Physical Society of Japan 1412 (1959): 1691-1695.

[163] Mikoshiba, N. *Magnetic Field Dependence of the Acoustoelectric Effect*. Journal of Applied Physics 343 (1963): 510-515.

[164] Tolpygo K. B. and Uritskii Z., *On the theory of electron mobility*, Eksp. Teor. Fiz. 30 (1956), 929.

[165] Weinreich, G. *Acoustodynamic effects in semiconductors*. Physical Review 104, no. 2 (1956): 321.

[166] Hutson, A. R., and Donald L. White. *Elastic wave propagation in piezoelectric semiconductors*. Journal of Applied Physics 33, no. 1 (1962): 40-47.

[167] Pomerantz, M. *Amplification of Microwave Phonons in Germanium*. Physical Review Letters 13, no. 9 (1964): 308.

[168] Mensah, S. Y., Allotey, F. K. A., Mensah, N. G., Akrobotu, H., and Nkrumah, G. *The influence of external electric field on acoustoelectric effect in a superlattice*. Superlattices and Microstructures, 37 (2), (2005), 87-97.

[169] Mensah, S. Y., F. K. Allotey, S. K. Adjepong, and N. G. Mensah. *Photostimulated attenuation of hypersound in superlattices*. Superlattices and microstructures 22, no. 4, (1997): 453-457.

[170] Vyazovsky, M. V.; Syrodoev, G. A. *Generation of Acoustic Phonons in Semiconductor Superlattice in the Case of an Intraband Absorption of Electromagnetic Wave*, Radiophysics and Quantum Electronics, Vol. 48 Issue 5, (2005), p390.

[171] Bau, N. Q. and Hieu, N. V. *The Influence of the Electromagnetic Wave on the Quantum Acoustomagnetoelectric Field in a Quantum Well with a Parabolic Potential*. PIERS Proceedings, Guangzhou, China, (2014), 25-28.

[172] Shmelev, G. M., Chaikovskii, I. A., Pavlovich, V. V., and Epshtein, E. M. *Electron-Phonon Interaction in a Superlattice*. physica status solidi (b) 80, no. 2 (1977): 697-701.

[173] Grinberg, A. A., and Kramer, N. I. *Acoustomagnetic effect in piezoelectric semiconductors*. In Soviet Physics Doklady, vol. 9, p. 552. 1965.

[174] Yamada, T. *Acoustomagnetoelectric effect in Bismuth*. Journal of the Physical Society of Japan 20, no. 8 (1965): 1424-1437.

[175] Epshtein, E. M., and Yu V. Gulyaev. *AE effect in Cds pole semiconductor*. Sov. Phys. Solid State 9 (1967): 288.

[176] Kaganov, M. I., Mevlyut, Sh T., and Suslov, I. M. *The acoustoelectric current in a metal for an arbitrary conduction-electron dispersion law*. Sov. Phys. JETP, 52, no. 1 (1980): 189-191.

[177] Margulis, A. D., and Margulis, Vl A. *The quantum*

acoustomagnetoelectric effect due to Rayleigh sound waves. Journal of Physics: Condensed Matter 6, no. 31 (1994): 6139.

[178] Mensah, S. Y., and Kangah, G. K. *Amplification of acoustic waves due to an external temperature gradient in superlattices*. Journal of Physics: Condensed Matter, 3 (22), (1991), 4105.

[179] Lanzillotti-Kimura, N. D., Fainstein, A., Huynh, A., Perrin, B., Jusserand, B., Miard, A., and Lemaitre, A. *Coherent generation of acoustic phonons in an optical microcavity*. Physical review letters, 99 (21), (2007), 217405.

[180] Krauss, T. D., and Wise, F. W. *Coherent acoustic phonons in a semiconductor quantum dot*. Physical review letters, 79 (25), (1997), 5102.

[181] Esaki, L., and Tsu, R. *Superlattice and negative differential conductivity in semiconductors*. IBM Journal of Research and Development, 14 (1), (1970), 61-65.

[182] Tsu, R., and Esaki, L. *Tunneling in a finite superlattice*. Applied Physics Letters, 22 (11), (1973), 562-564.

[183] Gudiksen, M. S., Lauhon, L. J., Wang, J., Smith, D. C., and Lieber, C. M. *Growth of nanowire superlattice structures for nanoscale photonics and electronics*. Nature, 415 (6872), (2002), 617-620.

[184] Canham, L. T. *Silicon quantum wire array fabrication by electrochemical and chemical dissolution of wafers*. Applied Physics Letters, 57 (10), (1990), 1046-1048.

[185] Lehmann, V., and Gosele, U. *Porous silicon formation: a quantum wire effect*. Applied Physics Letters, 58 (8), (1991), 856-858.

[186] Kapon, E., Hwang, D. M., and Bhat, R. *Stimulated emission in semiconductor quantum wire heterostructures*. Physical Review Letters, 63 (4), (1989), 430.

[187] Wu, J. J., and Liu, S. C. *Low-temperature growth of well-aligned ZnO nanorods by chemical vapor deposition*. Advanced Materials, 14 (3), (2002), 215.

[188] Vayssieres, L. *Growth of arrayed nanorods and nanowires of ZnO from aqueous solutions*. Advanced Materials, 15 (5), (2003), 464-466.

[189] Bernevig, B. A., Hughes, T. L., and Zhang, S. C. *Quantum spin Hall effect and topological phase transition in HgTe quantum wells*. Science, 314 (5806), (2006), 1757-1761.

[190] Konig, M., Wiedmann, S., Brune, C., Roth, A., Buhmann, H., Molenkamp, L. W., and Zhang, S. C. *Quantum spin Hall insulator state in HgTe quantum wells*. Science, 318 (5851), (2007), 766-770.

[191] Chen, G. *Nanoscale energy transport and conversion*, (2005).

[192] Adachi, S. *GaAs, AlAs, and Al_xGa_xAs: Material parameters for use in research and device applications*. Journal of Applied Physics, 58 (3), (1985), R1-R29.

[193] Bannov, N., Aristov, V., Mitin, V., and Stroscio, M. A. *Electron relaxation times due to the deformation-potential interaction of electrons*

with confined acoustic phonons in a free-standing quantum well. Physical Review B, 51 (15), (1995), 9930.

[194] Steigmeier, E. F., and Abeles, B. *Scattering of phonons by electrons in germanium-silicon alloys*. Physical Review, 136 (4A), (1964), A1149.

[195] Girardeau, M. *Relationship between systems of impenetrable bosons and fermions in one dimension*. Journal of Mathematical Physics, 1 (6), (1960), 516-523.

[196] Jochim, S., Bartenstein, M., Altmeyer, A., Hendl, G., Riedl, S., Chin, C., and Grimm, R. *Bose-Einstein condensation of molecules*. Science, 302 (5653), (2003), 2101-2103.

[197] Ent, R., Ullrich, T. and Venugopalan, R. *The Glue that Binds Us*. Scientific American, 312(5), (2015), 42-49.

[198] Kaplan, I. G. *Is the Pauli exclusive principle an independent quantum mechanical postulate*. International journal of quantum chemistry, 89(4), (2002), 268-276.

[199] Yamaguchi, Y. *A composite theory of elementary particles*. Progress of Theoretical Physics Supplement, 11, (1959), 1-36.

[200] Harari, H. *A schematic model of quarks and leptons*. Phys. Lett., 86, (1979), 83.

[201] Scalapino, D. J. *The electron-phonon interaction and strong-coupling superconductors*, Vol. 1, (1969), 449-560.

[202] Engelsberg, S., and Schrieffer, J. R. *Coupled electron-phonon system*. Physical Review, 131 (3), (1963), 993.

[203] Hengsberger, M., Purdie, D., Segovia, P., Garnier, M., and Baer, Y. *Photoemission study of a strongly coupled electron-phonon system*. Physical review letters, 83 (3), (1999), 592.

[204] Lei, X. L., and Ting, C. S. *Green's-function approach to nonlinear electronic transport for an electron-impurity-phonon system in a strong electric field*. Physical Review B, 32 (2), (1985), 1112.

[205] Frohlich, H. *On the theory of superconductivity: the one-dimensional case*. In Proceedings of the Royal Society of London A: Mathematical, Physical and Engineering Sciences. Vol. 223, No. 1154, pp. (1954), 296-305.

[206] Schwan, H. P., and Foster, K. R. *RF-field interactions with biological systems: electrical properties and biophysical mechanisms*. Proceedings of the IEEE, 68 (1), (1980), 104-113.

[207] Doi, M. *Second quantization representation for classical many-particle system*. Journal of Physics A: Mathematical and General, 9 (9), (1976), 1465.

[208] Cook, J. M. *The mathematics of second quantization*. Transactions of the American Mathematical Society, (1953), 222-245.

[209] Gross, E. K. U., Ullrich, C. A., and Gossmann, U. J. *Density functional*

theory of time-dependent systems. In Density Functional Theory, (1995), 149-171.

[210] Baym, G. A. *Lectures on quantum mechanics*,(1969).

[211] Kittel, C. *Introduction to solid state physics*. Wiley, (2005).

[212] Hone, J., Batlogg, B., Benes, Z., Johnson, A. T., and Fischer, J. E. *Quantized phonon spectrum of single-wall carbon nanotubes*. Science, 289 (5485), (2000), 1730-1733.

[213] Gross, E. K., and Runge, E. *Many-particle theory*, (1986).

[214] Haken, H. *Quantum field theory of solids, an introduction*, (1976).

[215] Aoki, H., and Suezawa, H. *Landau quantization of electrons on a sphere*. Physical Review A, 46 (3), (1992), R1163.

[216] Scriba, J., Wixforth, A., Kotthaus, J. P., Bolognesi, C. R., Nguyen, C., Tuttle, G., and Kroemer, H. *The effect of Landau quantization on cyclotron resonance in a non-parabolic quantum wells*. Semiconductor Science and Technology, 8 (1S), (1993), S133.

[217] Furtado, C., Rosas, A., and Azevedo, S. *Landau quantization and curvature effects in a two-dimensional quantum dot*. EPL (Europhysics Letters), 79 (5), (2007), 57001.

[218] Zaslavsky, A., Tsui, D. C., Santos, M., and Shayegan, M. *Magnetotunneling in double-barrier heterostructures*. Physical Review B, 40 (14), (1989), 9829.

[219] Moyal, J. E. *Quantum mechanics as a statistical theory*. In Mathematical Proceedings of the Cambridge Philosophical Society (Vol. 45, No. 01, pp. 99-124),(1949), Cambridge University Press.

[220] Van Hove, L. *The approach to equilibrium in quantum statistics: A perturbation treatment to general order*. Physica, 23 (1), (1957), 441-480.

[221] Ford, G. W., and Kac, M. *On the quantum Langevin equation*. Journal of statistical physics, 46 (5-6), (1987), 803-810.

[222] Esteve, J. G. *Origin of the anomalies: The modified Heisenberg equation*. Physical Review D, 66 (12),(2002), 125013.

[223] Cresser, J. D. *A Heisenberg equation-of-motion derivation of stochastic Schrodinger equations for non-Markovian open systems*. LASER PHYSICS-LAWRENCE-, 10 (1), (2000), 337-347.

[224] Runge, E., and Gross, E. K. *Density-functional theory for time-dependent systems*. Physical Review Letters, 52 (12), (1984), 997.

[225] Shirley, J. H. *Solution of the Schrodinger equation with a Hamiltonian periodic in time*. Physical Review, 138 (4B), (1965), B979.

[226] Lazzeri, M., Piscanec, S., Mauri, F., Ferrari, A. C., and Robertson, J. *Electron transport and hot phonons in carbon nanotubes*. Physical review letters, 95 (23), (2005), 236802.

[227] Baroni, S., De Gironcoli, S., Dal Corso, A., and Giannozzi, P. *Phonons and related crystal properties from density-functional perturbation theory*. Reviews of Modern Physics, 73 (2), (2001), 515.

[228] Kosloff, D., and Kosloff, R. *A Fourier method solution for the time dependent Schrodinger equation as a tool in molecular dynamics*. Journal of Computational Physics, 52 (1), (1983), 35-53.

[229] Haug, H., and Jauho, A. P. *Quantum kinetics in transport and optics of semiconductors*. (Vol. 2). M. Cardona (Ed.). Berlin: Springer, (2008).

[230] Reggiani, L., Lugli, P., and Jauho, A. P. *Quantum kinetic equation for electronic transport in nondegenerate semiconductors*. Physical Review B, 36 (12), (1987), 6602.

[231] Datta, S. *A simple kinetic equation for steady-state quantum transport*. Journal of Physics: Condensed Matter, 2 (40), (1990), 8023.

[232] Wolfe,C. M., Holonyak Jr., N., and Stillman, G. E. *Physical Properties of Semiconduc- tors*. Englewood Cliffs, New Jersey: Prentice Hall, 1st ed, (1989).

[233] Jena, Debdeep. *Polarization induced electron populations in III-V nitride semiconductors transport, growth, and device applications*. PhD diss., University of California Santa Barbara, (2003).

[234] Gokhale, V. J., and Rais-Zadeh, M. *Phonon-electron interactions in piezoelectric semiconductor bulk acoustic wave resonators*. Scientific reports, 4, (2014).

[235] Rais-Zadeh, M., Gokhale, V. J., Ansari, A., Faucher, M., Th□ron, D., Cordier, Y., and Buchaillot, L. *Gallium nitride as an electromechanical*

material. Microelectromechanical Systems. Journal of, 23 (6), (2014), 1252-1271.

[236] Pokatilov, E. P., Nika, D. L., and Balandin, A. A. *Acoustic phonon engineering in coated cylindrical nanowires*. Superlattices and Microstructures, 38 (3), (2005), 168-183.

[237] Pokatilov, E. P., Nika, D. L., and Balandin, A. A. *Phonon spectrum and group velocities in AlN/GaN/AlN and related heterostructures*. Superlattices and microstructures, 33 (3), (2003), 155-171.

[238] Ridley, B. K., and Watkins, T. B. *The possibility of negative resistance effects in semiconductors*. Proceedings of the Physical Society, 78 (2), (1961), 293.

[239] Zemon, S., Zucker, J., Wasko, J. H.,Conwell, E. M., and Ganguly, A. K. *Parametric amplification of ultrasonic waves in CdS.* Applied Physics Letters 12, no. 11 (1968): 378-380.

[240] Hutson, A. R. *Acousto-electric explanation of non-ohmic behavior in piezoelectric semiconductors and bismuth*. Physical Review Letters, 9 (7), (1962), 296.

[241] Smith, R. W. *Current saturation in piezoelectric semiconductors*. Physical Review Letters, 9 (3),(1962), 87.

[242] Krauss, T. D., and Wise, F. W. *Coherent acoustic phonons in a semiconductor quantum dot*. Physical review letters, 79 (25), (1997), 5102.

[243] Mawardi, O. K. *Acoustic cerenkov Effect*. The Journal of the Acoustical Society of America, 31 (6), (1959), 839-840.

[244] Komirenko, S. M., Kim, K. W., Demidenko, A. A., Kochelap, V. A. and Stroscio, M. A. *Generation and amplification of sub-THz coherent acoustic phonons under the drift of two-dimensional electrons.* Physical Review B 62, no. 11 (2000): 7459.

[245] Jones, D. S. *Acoustic and electromagnetic waves*. Oxford/New York, Clarendon Press/Oxford University Press, (1986), 764.

[246] Zhao, X. F., Zhang, J., Chen, S. M. and Xu, W. *Cerenkov acoustic-phonon emission generated electrically from a polar semiconductor*, J. Applied Physics (2009), 105.

[247] Heinonen, O., Taylor, P. L., and Girvin, S. M. *Electron-phonon interactions and the breakdown of the dissipationless quantum hall effect.* Physical Review B 30, no. 6 (1984): 3016.

[248] Wahlstrand, J. K., Stevens, T. E., Kuhl, J. and Merlin, R. *Coherent phonon□polaritons and subluminal Cherenkov radiation.* Physica B: Condensed Matter 316 (2002): 55-61.

[249] Sun, C. K., Chern, G. W., Lin, K. H., and Huang, Y. K., Observation of large acoustic gain in coherent acoustic phonon oscillators. Chinese Journal of Physics, 41 (6), (2003) 643-651.

[250] Pavlovich, V. V., and E. M. Epshtein. *Conductivity of a superlattice*

semiconductor in strong electric fields. Soviet Physics semiconductors 10, no. 10 (1976): 1196-1197.

[251] Blanter, Y. M., Kaganov, M. I., Pantsulaya, A. V., and Varlamov, A. A. *The theory of electronic topological transitions*. Physics Reports, 245 (4), (1994). 159-257.

[252] Afonin, V. V., and Gal'Perin, Y. M. *Acoustoelectric effect and phonon-drag electron thermoelectric power under weak localization conditions*. Semiconductors, 27, (1993), 61-65.

[253] Spector, H. N. *Amplification of acoustic waves through interaction with conduction electrons*. Physical Review 127, no. 4 (1962): 1084.

[254] Mensah, S. Y., Allotey, F. K. A., Mensah, N. G., and Nkrumah, G. *Differential thermopower of a CNT chiral carbon nanotube*. Journal of Physics: Condensed Matter, 13 (24), (2001), 5653.

[255] Mikoshiba, N. *Acoustoelectric Effect in Metals.* Journal of the Physical Society of Japan 1412 (1959): 1691-1695.

[256] Maao, F. A., and Yu Galperin. *Acoustoelectric effects in quantum constrictions.* Physical Review B 56, no. 7 (1997): 4028.

[257] Tolpygo, K. B., and I. B. Levinson. *Fifth All-Union conference on the theory of semiconductors.* Physics-Uspekhi 6, no. 6 (1964): 825-833.

[258] Weinreich, G., Sanders Jr, T. M., and White, H. G. *Acoustoelectric effect in n-type germanium*. Physical Review, 114 (1), (1959), 33.

[259] McFee, J. H. *Ultrasonic Amplification and Non-Ohmic Behavior in CdS and ZnO*. Journal of Applied Physics, 34 (5), (1963), 1548-1553.

[260] Mensah, N. G. *Acoustomagnetoelectric effect in a degenerate semi conductor with nonparabolic energy dispersion law*. arXiv:1002.3351, (2010).

[261] Mensah, S. Y., Mensah, N. G., Elloh, V. W., Banini, G. K., Sam, F., and Allotey, F. K. A. *Propagation of ultrasonic waves in bulk gallium nitride (GaN) semiconductor in the presence of high-frequency electric field*. Physica E: Low-dimensional Systems and Nanostructures, 28 (4), (2005), 500-506.

[262] Colvard, C., Merlin, R., Klein, M. V., and Gossard, A. C. *Observation of folded acoustic phonons in a semiconductor superlattice*. Physical Review Letters, 45 (4), (1980), 298.

[263] Miller, R. C., Kleinman, D. A., and Gossard, A. C. *Energy-gap discontinuities and effective masses for GaAs, Al_xGa_x As quantum wells*. Physical Review B, 29(12), (1984), 7085.

[264] Fletcher, N. E., Ebbecke, J., Janssen, T. J. B. M., Ahlers, F. J., Pepper, M., Beere, H. E., and Ritchie, D. A. *Quantized acoustoelectric current transport through a static quantum dot using a surface acoustic wave*. Physical Review B, 68 (24), (2003), 245310.

[265] Yoon, J., Ru, C. Q., and Mioduchowski, A. *Sound wave propagation in multiwall carbon nanotubes*. Journal of Applied Physics, 93 (8),(2003), 4801-4806.

[266] Dompreh, K. A., Mensah, N. G., Mensah, S. Y., Sam, F., and Twum, A. K. *Acoustoelectric Effect in degenerate Carbon Nanotube*. arXiv preprint arXiv:1504.05484, (2015).

[267] Fleming, W. J., and Rowe, J. E. *Acoustoelectric effects in indium antimonide*. Journal of Applied Physics, 42(5), (1971), 2041-2047.

[268] Miseikis, V., Cunningham,J. E., Saeed, K., ORorke, R., andDavies. A. G., *Acoustically induced current flow in graphene*. Applied Physics Letters 100, no. 13 (2012): 133105.

[269] Nunes O. A. C. and Fonseca A. L. A. *Amplification of hippersound in graphene under external direct current electric field*. Journal of Applied Physics 112, 043707, (2012).

[270] Bandhu, L., L. M. Lawton, and G. R. Nash. *Macroscopic acoustoelectric charge transport in graphene*. Applied Physics Letters 103.13, (2013): 133101.

[271] Dompreh, Kwadwo A., Natalia G. Mensah, and Samuel Y. Mensah. *Amplification of Hypersound in Graphene with degenerate energy dispersion*. arXiv preprint arXiv:1503.07360, (2015).

[272] Bandhu, L.,Lawton, L. M. and Nash G. R. *Macroscopic acoustoelectric charge transport in graphene*, App. Phys. Lett. 103, (2013), 133101.

[273] Lin, Y-M., Dimitrakopoulos, C., Jenkins, K. A., Farmer, D. B. Chiu, H. Y., Grill, A., and Ph Avouris. *100-GHz transistors from wafer-scale epitaxial graphene*. Science 327, no. 5966 (2010): 662-662.

[274] Xu, Wen, Youpin G., Liwei L., Hua Q., and Yanli Shi. *Can graphene make better HgCdTe infrared detectors?*. Nanoscale research letters 6, no. 1 (2011): 1-4.

[275] Ryzhii, V., Satou, A. and Otsuji, T. *Plasma waves in two-dimensional electron-hole system in gated graphene heterostructures*. Journal of applied physics 101, no. 2 (2007): 024509.

[276] Beardsley, R.P., Akimov, A.V., Henini, M. and Kent, A.J. *Coherent terahertz sound amplification and spectral line narrowing in a stark ladder superlattice*. Physical review letters, 104 (8), (2010) p.085501.

[277] Grudinin, I.S., Lee, H., Painter, O. and Vahala, K.J. *Phonon laser action in a tunable two-level system*. Physical review letters, 104 (8), (2010), p.083901.

[278] Souto, E., Nunes, O. A. C., Agrello, D. A., and Fonseca, A. L. A. *Spin wave amplification in antiferromagnetic semiconductors stimulated by infrared laser field*. Physics Letters A, 286 (5), (2001), 353-356.

[279] Zhao, C. X., Xu, W., and Peeters, F. M. *Cerenkov emission of terahertz acoustic -phonons from graphene*. Applied Phys. Lett. 102, (2013), 222101.

[280] Insepov, Z., Emelin, E., Kononenko, O., Roshchupkin, D.V., Tnyshtykbayev, K.B., Baigarin, K.A. Surface Acoustic Wave Amplification by DC-Voltage Supplied to Graphene Film. arXiv:1410.4712, (2014).

[281] Pekar, S. I. *Electron-Phonon Interaction Proportional to the External Applied Field and Sound Amplification in Semiconductors*. Soviet Physics JETP, 2, (1966), 22.

[282] Klimov, V. I., McBranch, D. W., Leatherdale, C. A., and Bawendi, M. G. *Electron and hole relaxation pathways in semiconductor quantum dots*. Physical Review B, 60 (19), (1999), 13740.

[283] Mensah, S. Y., Allotey, F. K. A., and Adjepong, S. K. *Acoutomagnetoelectric effect in a superlattice*, J. Phys. Condens. Matter 8, (1996), 1235-1239.

[284] Josse, F.J. and Shana, Z.A. *Piezoelectric resonant sensor using the acoustoelectric effect*. U.S. Patent 5, 455, (1995), 475.

[285] Shilton, J. M., Mace, D. R., Talyanskii, V. I., Galperin, Y., Simmons, M. Y., Pepper, M., and Ritchie, D. A. *On the acoustoelectric current in a one-dimensional channel*. Journal of Physics: Condensed Matter, 8 (24), (1996), L337.

[286] Shilton, J.M., Talyanskii, V.I., Pepper, M., Ritchie, D.A., Frost, J.E.F., Ford, C.J.B., Smith, C.G. and Jones, G.A.C. *High-frequency single-electron transport in a quasi-one-dimensional GaAs channel induced by surface acoustic waves*. Journal of Physics: Condensed Matter, 8 (38), (1996), p.L531.

[287] Cunningham, J., V. I. Talyanskii, J. M. Shilton, M. Pepper, M. Y. Simmons, and D. A. Ritchie. *Single-electron acoustic charge transport by*

two counterpropagating surface acoustic wave beams. Physical Review B 60, no. 7, (1999): 4850.

[288] Shilton, J. M., Talyanskii, V. I., Pepper, M., Ritchie, D. A., Frost, J. E. F., Ford, C. J. B., Smith, C. G. and Jones, G. A. C. *High-frequency single-electron transport in a quasi-one-dimensional GaAs channel induced by surface acoustic waves*. Journal of Physics: Condensed Matter, 8 (38),(1996) p.L531.

[289] Bobylev, A.V., Maao, F.A., Hansen, A. and Hauge, E.H. *Two-dimensional magnetotransport according to the classical Lorentz model*. Physical review letters, 75(2), (1995), p.197.

[290] Grinberg, A.A. and Kramer, N.I. *Acoustomagnetic effect in piezoelectric semiconductors*. In Soviet Physics Doklady, Vol. 9,1965, p. 552.

[291] Zemon, S. and Zucker, J. *Parametric amplification and frequency shifts in the acoustoelectric effect*. IBM Journal of Research and Development, 13(5), (1969), pp.494-498.

[292] Epshtein, E.M. *Planar hall effect in ferromagnets*. Physics of the Solid State, 44 (7), (2002) pp.1327-1329.

[293] Akhiezer, A.I., Kaganov, M.I. and Liubarskii, G. I. *Ultrasonic absorption in metals*. Soviet Physics (JETP), 5 (4), (1957) pp.685-688.

[294] Margulis, A.D. and Margulis, V. A. *Effect of spin injection on the conduction-electron spin resonance at a ferromagnet-semiconductor contact*. Physica B: Condensed Matter, 193(2), (1994), pp.179-187.

[295] Mensah, S.Y. and Kangah, G.K. *Amplification of acoustic waves due to an external temperature gradient in superlattices*. Journal of Physics: Condensed Matter, 3(22), (1991), p.4105.

[296] Mensah, S. Y., Allotey, F. K. A., Mensah, N. G. and International Centre for Theoretical Physics, Trieste (Italy);. *Nonlinear acoustoelectric effect in semiconductor superlattice*, (1999).

[297] Suzuura, H., and Ando, T. *Phonons and electron-phonon scattering in carbon nanotubes*. Physical review B, 65(23), (2002), 235412.

[298] Levinson, Y., Entin-Wohlman, O., and Wolfle, P. *Acoustoelectric current and pumping in a ballistic quantum point contact*. Physical review letters, 85 (3), (2000), 634.

[299] Shmelev, G. M., Nguyen Quoc Anh, Tsurkan, G. I., and Mensah S. Y. *currentless Amplification of hypersound in a planar configuration by inelastic scattering of electrons*, phys. stat. sol. (b), 121, K209, (1984).

[300] Ahmadi, M. T., Johari, Z., Amin, A. N., Fallapour, A. H., Ismail, R. *Graphene Nanoribbon Conductance Model in Parabolic Band Structure*. J. of Nanomaterials, 753738, (2010).

[301] Mensah, S. Y. and Allotey, F. K. A.*AE effect in semiconductor SL*. J. Phys: Condens.Matter., Vol. 6, (1994), 6783.

[302] Mensah, S. Y. and F. K. A. Allotey. *Nonlinear AE effect in semiconductor SL* J. Phys.: Condens. Matter. Vol. 12, (2000), 5225.

[303] Bau, Nguyen Quang, Nguyen Van Hieu, and Nguyen Vu Nhan. *The quantum acoustomagnetoelectric field in a quantum well with a parabolic potential*. Superlattices and Microstructures 52, no. 5 (2012): 921-930.

[304] Nghia, N. V., Bau, N. Q., Vuong, D. Q. *Calculation of the Acoustomagnetoelectric Field in Rectangular Quantum Wire with an Infinite Potential in the Presence of an External Magnetic Field*. PIERS Proceedings, Kuala Lumpur, MALAYSIA , (2012), 772 - 777.

[305] Kasumov, A., Kociak, M., Ferrier, M., Deblock, R., Gueron, S., Reulet, B., and Bouchiat, H. *Quantum transport through carbon nanotubes: Proximity-induced and intrinsic superconductivity*. Physical Review B, 68 (21), (2003), 214521.

[306] Grinberg, A.A. and Kramer, N.I. *Acousto-magnetic effect in Piezoelectric semiconductors*. Doklady Akademi Nauk SSSR, 157(1), (1964), p.79.

[307] Yamada, T. *Acoustomagnetoelectric Effect in Bismuth*. Journal of the Physical Society of Japan, 20(8), (1965), 1424-1437.

[308] Shmelev, G. M., Nguyen Quoc Anh, Tsurkan, G. I., and Mensah S. Y. *currentless Amplification of hypersound in a planar configuration by inelastic scattering of electrons*. phys. stat. sol. (b) 121, (1984), 209,

[309] Bau, N. Q., and Hieu, N. V. *The Influence of the Electromagnetic Wave on the Quantum Acoustomagnetoelectric Field in a Quantum Well with a Parabolic Potential*. (2014).

[310] Shmelev, G. M., Tsurkan, G. I., and Anh, N. Q. *Photostimulated planar*

acoustomagnetoelectric effect in semiconductors, Phys. Stat. Sol., Vol. 121, No. 1, 97 (1984), 102.

[311] Kogami, M. and Tanaka, S. *Acoustomagnetoelectric and acoustoelectric effects in n-InSb at low temperatures*. Journal of the Physical Society of Japan, 30(3), (1971), pp.775-784.

[312] Kogami, M. and Tanaka, S. *Acoustomagnetoelectric and acoustoelectric effects in n-InSb at low temperatures*. Journal of the Physical Society of Japan, 30(3), (19710, pp.775-784.

[313] Dompreh, K. A., Mensah, S. Y., Abukari, S. S., Sam, F., and Mensah, N. G. *Amplification of acoustic waves in Armchair graphene nanoribbon in the presence of external electric and magnetic field*. arXiv:cond-mat.1401436, (2014).

[314] Parmenter, R. H. *The acousto-electric effect*. Physical Review, 89 (5), (1953), 990.

[315] Hutson, A. R., McFee, J. H., and White, D. L. *Ultrasonic amplification in CdS*. Physical Review Letters, 7 (6),(1961), 237.

[316] Weinreich, G., Sanders Jr, T. M., and White, H. G. *Acoustoelectric effect in n-type germanium*. Physical Review, 114 (1), (1959), 33.

[317] Gulayev, Yu V. *Acousto-electric effect and amplification of sound waves in semiconductors at large sound intensities.* Physics Letters A 30.4, (1969): 260-261.

[318] Ridley, B. K. *Nonlinear amplification of sound in a piezoelectric semiconductor.* Journal of Physics C: Solid State Physics 3.4, (1970): 935.

[319] Gurevich, V. L., Katilius, R., and Laikhtman, B. D. *Nonlinear Amplification and Automodulation of Sound in Piezoelectric Semiconductors*. Physical Review Letters 21.24, (1968): 1632.

[320] Gokhale, V. J., Yu Sui, and Mina Rais-Zadeh. *Novel uncooled detector based on gallium nitride micromechanical resonators.* SPIE Defense, Security, and Sensing. International Society for Optics and Photonics, 2012.

[321] Fleming, W. J., and J. E. Rowe. *Acoustoelectric effects in indium antimonide*. Journal of Applied Physics 42.5, (1971): 2041-2047.

[322] Govorov, A. O. *Nonlinear acoustoelectric transport in a two-dimensional electron system*. Physical Review B 62.4, (2000): 2659.

[323] Mensah, S. Y., Allotey, F. K. A., Mensah,N. G., Elloh,V. W. *Amplification of acoustic phonons in a degenerate semiconductor superlattice*. Physica E, Vol. 19 (3), (2003).

[324] Mensah, S.Y., Allotey, F.K.A., Mensah, N.G., Akrobotu, H. and Nkrumah, G., *The influence of external electric field on acoustoelectric effect in a superlattice*. Superlattices and Microstructures, 37(2), (2005), pp.87-97.

[325] Ruvinskii, M. A., and B. M. Ruvinskii. *On the Hypersonic Absorption*

in Straight-line Graphene Ribbons. PHYSICS AND CHEMISTRY OF SOLID STATE 14, no. 4 (2013): 709-716.

[326] Dompreh, K. A., Mensah, N. G., Mensah, S. Y., Abukari, S. S., Sam, F., and Edziah, R. *Hypersound Absorption of Acoustic Phonons in a degenerate Carbon Nanotube*. arXiv preprint arXiv:1502.07636, (2015).

[327] Ridley, B. K. *Nonlinear amplification of sound in a piezoelectric semiconductor*. Journal of Physics C: Solid State Physics, 3(4), (1970), 935.

[328] Cunningham, J. *Acoustoelectric current in submicron-separated quantum wires*. Applied Physics Letters 86.15, (2005): 2105.

[329] Couto, O.D.D., Lazic, S., Iikawa, F., Stotz, J.A.H., Jahn, U., Hey, R. and Santos, P.V., 2009. *Photon anti-bunching in acoustically pumped quantum dots*. Nature Photonics, 3 (11), pp.645-648.

[330] Hermelin, S., Takada, S., Yamamoto, M., Tarucha, S., Wieck, A.D., Saminadayar, L., Bauerle, C. and Meunier, T., 2011. *Electrons surfing on a sound wave as a platform for quantum optics with flying electrons*. Nature, 477 (7365), (2011), pp.435-438.

[331] Hernandez-Minguez, A., Moller, M., Breuer, S., Pfuller, C., Somaschini, C., Lazic, S., Brandt, O., Garcia-Cristobal, A., de Lima Jr, M.M., Cantarero, A. and Geelhaar, L. *Acoustically driven photon antibunching in nanowires*. Nano letters, 12(1), 2011, pp.252-258.

[332] Abergel, D. S. L., *Properties of graphene: a theoretical perspective.* Advances in Physics 59.4, (2010): 261-482.

[333] Poole, T., Bandhu, L., and Nash, G. R. *Acoustoelectric photoresponse in graphene*. Applied Physics Letters, 106 (13), (2015), 133107.

[334] Dompreh, K. A., Mensah, S. Y., Mensah, N. G., Abukari, S. S., Allotey, F. K., and Nkrumah-Buandoh, G. K. *Amplification of acoustic phonons in superlattice*. arXiv preprint arXiv:1101.1854, (2011).

[335] Dresselhaus, M.S. , Dresselhaus, G. and Jorio, A. *Unusual proterties and Structure of Carbon Nannotubes*. Annual Review of Materials Research, Vol. 34: 247-278, (2004).

[336] Saito, R., Dresselhaus, G. , Dresselhaus, M. *Physical Properties of Carbon Nanotubes*. (Imperial College Press, London), (1998).

[337] Mensah, S. Y., Allotey, F. K. A., Mensah, N. G., and Nkrumah. G. *Differential thermopower of a CNT chiral carbon nanotube*. Journal of Physics: Condensed Matter 13, no. 24 (2001): 5653.

[338] Mensah, S. Y., Allotey, F. K. A., Mensah, N. G., and Nkrumah. G. *Giant electrical power factor in single-walled chiral carbon nanotube*. Superlattices and microstructures 33, no. 3 (2003): 173-180.

[339] Mensah, S. Y., Twum, A.,Mensah, N. G., Dompreh, K. A., Abukari, S. S., and Nkrumah-Buandoh, G. *Effect of laser on thermopower of chiral carbon nanotube*. arXiv preprint arXiv:1104.1913 (2011).

[340] Mensah, N. G., Nkrumah, G., Mensah, S. Y., and Allotey, F. K. A. *Temperature dependence of the thermal conductivity in chiral carbon nanotubes*. Physics Letters A 329, no. 4 (2004): 369-378.

[341] Dresselhaus, M.S. and Eklund, P.C. *Phonons in carbon nanotubes*. Advances in Physics, 49(6), (2000), pp.705-814.

[342] LeRoy, B.J., Lemay, S.G., Kong, J., Dekker, C. *Electrical generation and absorption of phonons in carbon nanotubes*. Nature, (2004).

[343] Kim, J. H., Nugraha, A. R. T., Booshehri, L. G., Haroz, E. H., Sato, K., Sanders, G. D., Yee, K. J., Lim, Y. S., Stanton, C. J., Saito, R., and Kono, J. *Coherent phonons in carbon nanotubes and graphene*. Chem. Phys. 413, (2013), 55-80 .

[344] Small, J.P., Shi, L. and Kim, P. *Mesoscopic thermal and thermoelectric measurements of individual carbon nanotubes*. Solid State Communications, 127 (2), (2003), pp.181-186.

[345] Kane, C.L., Mele, E.J., Lee, R.S., Fischer, J.E., Petit, P., Dai, H., Thess, A., Smalley, R.E., Verschueren, A.R.M., Tans, S.J. and Dekker, C. *Temperature-dependent resistivity of single-wall carbon nanotubes*. EPL (Europhysics Letters), 41(6), (1998), p.683.

[346] Sanders,G. D., Nugraha, A. R. T., Sato, K., Kim, J.-H., Kono, J., Saito, R., and Stanton, C. J. Theory of coherent phonons in carbon nanotubes and graphene nanoribbons, J. Phys. Condens. Matter 25, 144201, (2013).

[347] Abukari, S. S., Mensah, S. Y., Mensah, N. G., Adu, K. W., Rabiu, M.,

Dompreh, K. A., and Twum, A. *Generation and Amplification of Terahertz Radiation in Carbon Nanotubes*. arXiv preprint arXiv:1202.4618, (2012).

[348] Entin-Wohlman, O., Levinson, Y. and Galperin, Y. M. *Acoustoelectric effect in a finite-length ballistic quantum channel*. Physical Review B, 62 (11), (2000), p.7283.

[349] Zhukovskii, V. C., Krevchik, V. D., Semenov, M. B., and Razumov, A. V. *The nonlinear optical properties of nanotubes with spiral defects in a longitudinal magnetic field*. Moscow University Physics Bulletin, 69, (1), (2014), 72-81.

[350] Weinreich, G., *Acoustodynamic effects in semiconductors*. Physical Review, 104(2), (1956), p.321.

APPENDIX

Numerical Analysis

To solve the equations (142), (148), (154), (160), (171) and (178), a high level programming language (MATLAB) was used. Here, the algorithms for Graphene Nanoribbon (GNR), Graphene, and Carbon Nanotubes (CNT) are presented.

Graphene Nanoribbon

The numerical calculations for GNR are as follows. This code is used for plotting the 3D graph of the Γ/Γ_0 versus the electric field by varying the width N of the GNR. This is a function code which requires an input of the electric field and the width.

function $[n, E0] = Nanoribbon(n, E)$;

$Eg = 0.5 * 1.6 * 10e-19./hbar$; the energy gap

$p = 2$; the sub-band index,

$w = 5 * 10e-9$; the width of the Nanoribbon

$B = 2 * pi. * (p./(n+1) - 0.67)./(a * sqrt(3))$;

B is the quantized wave vector with π being the

$alpha = wq./Eg$;

$k = (2 * B.^2 * alpha./(q) - (0.5 * q))$;

$g = -exp(eta.^2). * 2. * 10e5. * FD - int - approx(eta.^2, -1/2). * E0. * pi^2. * tau.^2. * k$;

$x1 = (1 - g./(4. * v));$

$p = 3; w = 5 * 10e - 9;$

$B = pi * (p/(w + a * sqrt(3)) - 2./(a * sqrt(3)));$

$B = 2 * pi. * (p./(n+1) - 0.67)./(a * sqrt(3));$

$alpha = wq./Eg;$

$k = (2 * B.^2 * alpha./(q) - (0.5 * q));$

$g = -exp(eta.^2). * 2. * 10e5. * FD - int - approx(eta.^2, -1/2). * E0. * pi^2. *$

$tau.^2. * k;$

$x2 = (1 - g./(4. * v));$

$p = 4; w = 5 * 10e - 9;$

$B = 2 * pi. * (p./(n+1) - 0.67)./(a * sqrt(3));$

$alpha = wq./Eg;$

$k = (2 * B.^2 * alpha./(q) - (0.5 * q));$

$x3 = (1 - g./(4. * v));$

$p = 6; w = 5 * 10e - 9;$

$B = 2 * pi. * (p./(n+1) - 0.67)./(a * sqrt(3));$

$alpha = wq./Eg;$

$k = (2 * B.^2 * alpha./(q) - (0.5 * q));$

$g = -exp(eta.^2). * 2. * 10e5. * FD - int - approx(eta.^2, -1/2). * E0. * pi^2. *$

$tau.^2. * k;$

$x4 = (1 - g./(4. * v));$

$p = 7; w = 5 * 10e - 9;$

$B = 2 * pi. * (p./(n+1) - 0.67)./(a * sqrt(3));$

$alpha = wq./Eg;$

$k = (2 * B.^2 * alpha./(q) - (0.5 * q));$

$g = -exp(eta.^2). * 2. * 10e5. * FD - int - approx(eta.^2, -1/2). * E0. * pi^2. *$

$tau.^2. * k;$

$x5 = (1 - g./(4. * v));$

plot($E0$,$x1$,'$--m$',$E0$,$x2$,'$--r$',$E0$,$x3$,'$--b$', $E0$,$x4$,'$--k$',$E0$,

$x5$,'$--c$','LineWidth',1.5,'MarkerSize',10)

,... 'MarkerEdgeColor','b','MarkerFaceColor',[0.50.50.4]);

title('Currentless Amplification', 'color', axis$_color$);

$xlabel('Electric field(E)\mathrm{Vm}^{-1}$') ylabel('$\Gamma_\perp/\Gamma_0$')

Analyzing the Bandgap of the Graphene Nanoribbon

To analyse the Bandgap of GNR as a function of the electric field and Γ/Γ_0, a $3D$ graph was plotted . The code below is a function with E and Eg as inputs.

$[E0, Eg] = meshgrid((E), (Eg));$

$m = 1; i = 1;$

$alpha = (2.23 * 0.25 * 1.6 * 10e - 19)./(B.^2);$ alpha

$n = 15;$ width of the nanoribbon

$p = 1; p = 2 * m + i;$

$w = 23 * 10 - 9;$

$B = 2 * pi. * (p./(n+1) - 0.67)./(a * sqrt(3));$ B is the quantized wave vector with pi being the

$H = wq./Eg;$

$k = (2. * hbar^2 * B * wq)./(q * hbar * Eg) - hbar * q/2;$

$alpha = hbar * wq./Eg;$

$alpha = wq./Eg;$

$k = (2 * B.^2 * alpha./(q) - (0.5 * q));$

$g = exp(eta^2). * e. * 10e6. * FD - int - approx(eta, -1/2). * E0. * pi. * tau.^2. * k;$

$x = (1 - g./(0.32 * 20 * 10e4 * 16. * v));$

$p = 2;$w =23*10-9;

B = 2*pi.*(p./(n+1) - 0.67)./(a*sqrt(3));

alpha = wq./Eg;

k = (2*B.$^2 * alpha./(q) - (0.5 * q));$

$g = exp(eta^2). * e. * 10e6. * FD - int - approx(eta, -1/2). * E0. * pi. * tau.^2. * k;$

$x = (1 - g./(0.32 * 16. * v));$

$x2 = real(x);$

plot(Eg, x,'$--r'$,Eg,$x1$,'$--b'$,Eg,$x2$,'$--g'$,Eg,$x3$,'–k','Linewidth',1.5)

$surf(E0, Eg./10e15, x./10e4)$

xlabel(' E (V/cm)')ylabel(' $E_g(eV)'$)$zlabel('\Gamma/\Gamma_0')$

Numerical Fermi-Dirac integrals

This code is that of the Fermi-Dirac integral in the equations.

$Functiony = FD - int - approx(eta, j)$

Analytic approximations for Fermi-Dirac integrals of order $j > -1/2$

if $j < -1/2$

error('The order should be equal to or larger than $-1/2$.')

else

x = eta;

switch j

case 0

y = $log(1 + exp(x))$; analytic expression

case $1/2$

$mu = x.^4 + 50 + 33.6 * x. * (1 - 0.68 * exp(-0.17 * (x+1).^2))$;

$xi = 3 * sqrt(pi)./(4 * mu.^(3/8))$;

$y = (exp(-x) + xi).^-1$;

case $3/2$

$a = 14.9$;

$b = 2.64$;

$c = 9/4$;

$y = ((j+1) * 2^(j+1)./(b + x + (abs(x-b).^c + a).^(1/c)).^(j+1)...$

$+exp(-x)./gamma(j+1)).^-1./gamma(j+1)$;

otherwise

$a = (1 + 15/4 * (j+1) + 1/40 * (j+1)^2)^(1/2)$;

$b = 1.8 + 0.61 * j$;

```
c = 2 + (2 - sqrt(2)) * 2.^(-j);
y = ((j+1) * 2.^(j+1))./(b + x + (abs(x-b).^c + a^c).^(1/c)).^(j+1)...
+exp(-x)./gamma(j+1)).^-1./gamma(j+1);
end
end
```

This code is a $3D$ code for analysing Γ/Γ_0 as against the η and the electric field $E0$.

$[E0, eta] = meshgrid(E0, eta);$

$\tau = 10e-12;$

$h = 0.2 * 10e3;$ magnetic field

$\omega_h = 8 * 10e13;$ cyclotron freq

$\eta = \omega_{\hbar.*h.*\tau};$

$\eta = (0 : 0.02 : 2.3)/(2);$

$v = 5 * 10e5;$ the velocity of sound

$q = 2.5 * 10e6;$ acoustic wave number

$\omega_q = 10e11;$ frequency of the sound

$a = 1.42 * 10e-9;$ the lattice constant

$m = 6;$ m is an integer,

$e_g = 0.25 * 1.6 * 10e-19;$ the energy gap

$m = 2; i = 1;$

$wh = 2;$ cyclotron freq

$E0 = 0.5;$

$n = 9;$ width of the nanoribbon

$p = 1; w = 5 * 10e-9;$

$B = pi * (p/(w + a * sqrt(3)) - 2./(a * sqrt(3))); alpha = wq./Eg;$

$k = (2 * B.^2 * alpha./(q) - (0.5 * q));$

$FD =$

$3 * pi./16. * FD-int-approx(eta.^2, 3/2). * FD-int-approx(eta.^2, -1/2)$

$./(\text{FD-int-approx}(\text{eta}^2, -1/2)) - FD-int-approx(eta^2, 0);$

$g = -exp(eta.^2).*FD.*E0.*sqrt(pi).*k;$

$x1 = (1 - g./(4.*v));$

$plot(eta.^2, x1, 'g', 'LineWidth', 1.5)$

$xlabel('\phi')$

$ylabel('\Gamma/\Gamma_0')$

Acoustomagneto electric field

To analyse the acoustomagnetoelectric effect in Eqn. (154), the numerical calculations are as follows

$[\mathrm{E0}, eta] = meshgrid(n, eta)$

$h = 0.2 * 10e3$; magnetic field

$w_h = 0.5 * 10e10$; cyclotron freq

$\eta = w_h .* h .* tau$;

$v = 5 * 10e5$; the velocity of sound

$q = 2.5 * 10e6$; acoustic wave number

$\omega_q = 5 * 10e9$; frequency of the sound

$a = 1.42 * 10e-9$; the lattice constant

$m = 6$; m is an integer

alpha = $(0 : 0.01 : 1)$;

$t = 2.7$; the overlapp integral (eV)

$n = 7$; width of the nanoribbon

$p = 3; w = 5 * 10e-9$;

$eg = 0.25 * 1.6 * 10e-19$; the energy gap

$B = 2 * pi. * (p./(n+1) - 0.67)./(a * sqrt(3))$;

B is the quantized wave vector with pi being the subband index

$H = (0 : 0.02 : 10) * 108/100$;

$Eg = B * a * t * e./hbar$;

$B = pi * (p/(w + a * sqrt(3)) - 2./(a * sqrt(3)))$;

$alpha = wq./Eg$;

$c = (1)./abs(sqrt(1 - alpha.^2))$;

$$k = (2 * B.^2 * alpha./(q) - (0.5 * q));$$

$$Ey = 3 * Eg. * eta. * wq./(8 * 1000 * v^3);$$

$$F = FD - int - approx(eta.^2, -1/2). * FD_int_approx(eta.^2, -1/2) - FD - int - approx(eta.^2, 0). * FD_int_approx(eta.^2, -1/2);$$

$$F1 = 0.4219 * sqrt(pi^3) * (FD - int - approx(eta.^2, -1/2)).^2 + (7 * pi * FD - int - approx(eta.^2, 0)).^2. * eta.^2;$$

$$E = Ey. * F./(F1). * c;$$

$$plot(alpha, E, 'b', 'LineWidth', 1.5)$$

For the acoustomagnetoelectric field against the alpha

$[E0, eta] = meshgrid(E0, eta);$

$t = 2.7$; the overlapp integral (eV)

$n = 7$; width of the nanoribbon

$p = 6; w = 5 * 10e - 9;$

$B = 2 * pi. * (p./(n+1) - 0.67)./(a * sqrt(3));$

B is the quantized wave vector with pi being the

$H = (0 : 0.02 : 10) * 108/100;$

$Eg = B * a * t * e./hbar;$

$B = pi * (p/(w + a * sqrt(3)) - 2./(a * sqrt(3)));$

$alpha = wq./Eg;$

$c = (1)./abs(sqrt(1 - alpha.^2));$

$k = (2 * B.^2 * alpha./(q) - (0.5 * q));$

$Ey = 3 * Eg. * eta. * wq./(8 * 1000 * v^3);$

$F = FD - int - approx(eta.^2, -1/2). * FD - int - approx(eta.^2, -1/2) -$

$FD - int - approx(eta.^2, 0). * FD_i nt_a pprox(eta.^2, -1/2);$

$F1 = 0.4219 * sqrt(pi^3) * (FD - int - approx(eta.^2, -1/2)).^2 + (7 * pi * FD -$

$int - approx(eta.^2, 0)).^2. * eta.^2;$

$E = Ey. * F./(F1). * 1./abs(sqrt(1 - alpha.^2));$

$plot(eta, E, 'r', 'LineWidth', 1.5)$

The parameters used in the numerical calculations for the $3D$

$[E0, eta] = meshgrid((0:0.02:2),(0:0.02:2));$

$eta = 2*(0.001:0.002:0.035);$

$v = 5*10e5$; the velocity of sound

$q = 2.5*10e6$; acoustic wave number

$wq = 5*10e9$; frequency of the sound

$a = 1.42*10e-9$; the lattice constant

$m = 6$; m is an integer,

$alpha = 0.2;$

$eg = 0.25*1.6*10e-19$; the energy gap

$hbar = 6.626*10e-34$; the planck constant

$e = 1.6*10e-19;$

$tau = 10e-12;$

$t = 2.7$; the overlapp integral (eV)

$n = 7$; width of the nanoribbon

$p = 6; w = 5*10e-9;$

$hbar = 1.05*10e-34$; Planck's constant (eV-s)

$m = 2; i = 1; wh = 2;$

B = 2*pi.*(p./(n+1) - 0.67)./(a*sqrt(3));

B is the quantized wave vector with pi being the

$H = (0:0.02:10)*108/100;$

$Eg = B*a*t*e./hbar;$

$alpha = wq./Eg;$

$c = (1)./abs(sqrt(1-alpha.^2));$

$$k = (2 * B.^2 * alpha./(q) - (0.5 * q));$$

$$Ey = 3 * Eg. * eta. * wq./(8 * 1000 * v^3);$$

$$F = FD - int - approx(eta.^2, -1/2). * FD - int - approx(eta.^2, -1/2) -$$

$$FD - int - approx(eta.^2, 0). * FD_i nt_a pprox(eta.^2, -1/2);$$

$$F1 = 0.4219 * sqrt(pi^3) * (FD - int - approx(eta.^2, -1/2)).^2 + (7 * pi * FD -$$

$$int - approx(eta.^2, 0)).^2. * eta.^2;$$

$$E = Ey. * F./(F1). * 1./abs(sqrt(1 - alpha.^2));$$

$$plot(eta, E, 'r', 'LineWidth', 1.5)$$

Hypersound Absorption in Carbon Nanotube

To analyse Eqn.(160) the following code was used

$gamma = 0.1$; tight-bingding overlapp intergral(eV)

$delta = 9$; deformation potential (eV)

$b = 1.42 * 10e - 9$; lattice Constant

$p_0 = 10e4$; Fermi wavevector

$q = 2 * 10e6$; Acoustic wave vector (cm^-1)

$wq = 2 * (0.1 : 0.01 : 3) * 10e10$;

$rho = 6.5 * 10e - 11$; density (g/cm^2)

$s = 10e3$; velocity of sound (m/s)

$T = 10$; Temperature

$theta = 83$;

$E_0 = 2 * gamma$;

$mu = 10$;

$Vd = 0.94$;

$X = 1 - Vd$;

$y = n * A. * (hbar. * q) * (delta.^2) * (K * T) * 10e16./(pi * rho * s. * (10e6)^4)$;

$beta = 1/(K * T)$;

y2 =(2-beta*hbar*wq.*X).*(1 - exp(-beta*hbar*wq.*X));

y3 = y2;

$plot$(wq,y3, 'r','LineWidth',1.5)

$xlabel('\omega_q(s^{-1})')$

$ylabel('R_q(s^{-1})')$

Acoustoelectric effect in Graphene

The numerical analysis of Eqn.(171) is as follows

$p_0 = 10^4$; Fermi wavevector

$q = 2 * 10e6$; Acoustic wave vector (cm^-1)

$q = 10^8$; acoustic wave vector(m^-1)

$A = 2$; Area of the sample in (m)

$wq = 2 * (0.1 : 0.01 : 15) * 10^12$;

$rho = 6.5e - 8$; density (g/cm^2)

$s = 10^3$; velocity of sound (m/s)

$T = 50$; Temperature

$E_0 = 3.57 * 10e10$;

$theta = 85$;

$E_0 = 2 * gamma$;

$E = 0.2 * 10e3$; Electric field (Vcm$^-1$)

mu = 10;

y =n* A.*(hbar.*q)*(delta.^{2}) $* (K * T) * 10e16./(pi * rho * s.* (10e6)^4)$;

$beta = 1/(K * T)$;

$y2 = (2 - beta * hbar * wq).* (1 - exp(-beta * hbar * wq))$;

$y3 = -y2$;

$plot(wq, y3, '-g', 'LineWidth', 1.5)$

$xlabel('\omega_q(s^{-1})')$

$ylabel('j/j_0')$

For Eqn. (178), the numerical analysis is as follows

$A = 2$; Area of the sample in (cm)

$wq = 0.1. * 10e12$; acoustic wave frequency

$rho = 6.5 * 10e - 8$; density (g/cm^2)

$s = 10e5$; velocity of sound (m/s)

$T = 10$; Temperature

$theta = 83$;

$E_0 = 2 * gamma$;

$E = 35 * 10e3$; Electric field $(\mathrm{Vm}^{-}1)$

x =(-1:0.01:2.5);

y = n* A.*(hbar.*q)*(delta.^{2}) $* (K * T) * 10e16./(pi * rho * s. * (10e6)^4)$;

$beta = 1/(K * T)$;

$y2 = (2 - beta * hbar * wq * X). * (1 - exp(-beta * hbar * wq. * X))$;

$y3 = y2$;

$plot(X, y3./y, ' r')$